

EFFECTS OF PROCESSING ON THE
COMPOSITION OF BOROSILICATE GELS

by

Michael Anthony Reichwein

A.S., Thames Valley State Technical College, 1979
B.S., University of Connecticut, 1981

A MASTER'S THESIS

submitted in partial fulfillment of the
requirements for the degree

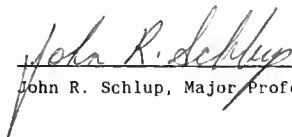
MASTER OF SCIENCE

College of Engineering
Department of Chemical Engineering

KANSAS STATE UNIVERSITY
Manhattan, Kansas

1989

Approved by:


John R. Schlup, Major Professor

LD
2608
.74
CHE
984
R45
C.2

TABLE OF CONTENTS

ALL208 315638

	<u>Page</u>
ACKNOWLEDGEMENTS	vii
LIST OF FIGURES.	viii
LIST OF TABLES	xi
I. INTRODUCTION	1
Background	1
Prior Related Work	7
Problem Statement.	11
II. REVIEW OF INSTRUMENTAL NEUTRON ACTIVATION ANALYSIS (INAA)	14
A. General Background.	14
B. Theoretical Development and Calculation of Corrected Peak Area.	16
C. Irradiation Facility.	20
D. Detector Analyzer System.	22
E. Energy Calibration.	25
F. Data Collection in General.	25
G. Preparation of Standards.	29
III. INAA PROCEDURE DEVELOPMENT	32
A. Reactions Involving Silicon	32
B. Sample Preparation.	34
C. Irradiation of Standards.	34
D. Irradiation of Samples.	35
E. Post-irradiation Handling and Counting.	35
F. Determination of Peak Areas	37
G. Data Reduction.	37

	<u>Page</u>
H. Modification of Irradiation Procedure	39
IV. VERIFICATION AND CALIBRATION OF INAA TECHNIQUE.	41
A. Determination of Aluminum, Phosphorus, or Magnesium Present in Vials, Reagents and Standards	41
B. Calibration Lines	42
B.1. Calibration Lines For First Irradiation Procedure	42
B.1A. Experimental	42
B.1B. Results.	43
B.2. Calibration Lines For Modified Irradiation Procedure.	43
C. Verification of Technique	43
C.1. Experimental.	43
C.2. Results	52
D. Discussion.	52
E. Conclusions	56
V. REVIEW OF LYOGEL CHEMISTRY	58
A. Introduction.	58
B. General Aspects of Gel Synthesis.	63
C. Borosilicate Lyogel Synthesis	66
O. Tetravalent Boron	69
VI. INAA OF $\text{SiO}_2 \cdot x\text{B}_2\text{O}_3$ LYOGELS.	74
A. Introduction.	74
B. Experimental.	75
C. $\text{SiO}_2 \cdot x\text{B}_2\text{O}_3$ and NaCl Composition Results	75

	<u>Page</u>
D. Discussion	B5
E. Conclusions	91
VII. PROCESSING OF BOROSILICATE LYOGELS: INAA OF SAMPLES FROM GELATION AND POST-GELATION STAGES.	92
A. Introduction.	92
B. INAA Sample Preparation and Procedure	92
C. Results from INAA	94
D. Discussion.	96
E. Conclusions	99
VIII. FREEZE DRYING EXPERIMENT.	101
A. Experimental.	101
B. Results From Freeze Drying Experiment	105
C. Discussion.	105
D. Conclusions	108
IX. PREPARATION OF $\text{SiO}_2 \cdot x\text{B}_2\text{O}_3$ LYOGELS VIA CO-PRECIPIATION.	109
A. Background.	109
B. Experimental.	112
B.1. Procedure for $\text{SiO}_2 \cdot x\text{B}_2\text{O}_3$ Lyogel Synthesis Via Co-precipitation.	112
B.2. INAA Sample Preparation and Procedure	114
C. Results	114
D. Discussion.	115
E. Conclusions	119
X. CONCLUSIONS.	121

	<u>Page</u>
XI. FUTURE WORK: CLDSING THE MATERIAL BALANCE.	123
A. Introduction.	123
B. Suggested Chemical Analyses	129
C. Material Balance Around Reaction Flask.	130
D. Material Balance Around Sample Vial	130
E. Material Balance Around Dryer For an Unrinsed Lyogel. .132	132
F. Material Balance Around Rinsing Tank.	134
G. Material Balance Around Dryer For a Rinsed Lyogel . . .136	136
H. Material Balance Around Swelling Solution Tank.13B	13B
I. Material Balance Around Dryer For a Swelled Lyogel. . .14D	14D
J. Data Acquisition.	142
K. Modification of INAA Method	144
APPENDIX A: DERIVATION DF MODEL USED FDR INSTRUMENTAL NEUTRDN ACTIVATIDN ANALYSIS.	146
APPENDIX B: EXAMPLE DF DATA REDUCTIDN	153
A. Calculation of P_a^C For Known Sample Composition.	153
B. Calculation of the Mass of Species "i" in a Sample of Unknown Composition	154
C. Calculation of Lyogel Composition	155
APPENDIX C: EXAMPLE DF MAXIMUM EXPERIMENTAL ERROR CALCULATIDN . .157	157
A. Calculation of Probable Error For P_C^a	157
B. Calculation of Probable Error For Slope and Intercept .15B	15B
C. Calculation of the Maximum Experimental Error of \hat{M}_i . .161	161

	<u>Page</u>
D. Calculation of the Maximum Experimental Error For the Mass of B_2O_3 In a Sample of Unknown Composition.163
APPENDIX D: COMPOUNDS OF BORON AND BOROSILICATE CHEMISTRY.166
APPENDIX E: DERIVATION OF COMPONENT MATERIAL BALANCES173
A. Material Balance Around Reaction Flask.173
B. Material Balance Around Sample Vial176
C. Material Balance Around Dryer For An Unrinsed Lyogel.177
D. Material Balance Around Rinsing Tank.179
E. Material Balance Around Dryer For a Rinsed Lyogel181
F. Material Balance Around Swelling Solution Tank.183
G. Material Balance Around Dryer For a Swelled Lyogel.185
REFERENCES187

ACKNOWLEDGEMENTS

I wish to thank the Department of Chemical Engineering, the National Science Foundation, and the Kansas State University Engineering Experiment Station for financial support provided during the completion of this work.

I would also like to thank Professor John Schlup for his support, guidance, concern for my well-being, and most of all for his boundless patience throughout this research. Also, gratitude is extended to Professors Larry Glasgow, John Matthews, and Gale Simons for their comments and suggestions.

I wish to express thanks to the following. The Tate Neutron Activation Analysis Laboratory, the Kansas State Analysis Laboratory, the Kansas State University Reactor Facility, and nuclear reactor operators Jeffery Daniels and David Whitfill. Many thanks are given to Dr. Jack Higginbotham, Chief Nuclear Reactor Operator, for his help with neutron activation analysis and for the software he provided to make calculations easier. Also, I wish to thank Mary Alexander, Susan Rolfs, Peggy Hanes, and Michelle and Janet Vinduska for patiently enduring all the rewrites and typing the final draft of my thesis.

A special thanks is given to my mother, Jeannette, for her enthusiastic encouragement and unending support. Finally, I am very thankful to my many friends, especially Medhat Morcos, Nabil Taha, Sanjay Prasad, Mounir El-Aasar, Mousa Attom, Gail and Faye Tayyem, Chris and Filio Christodoulou, and Sajan Thomas for their friendship and support.

LIST OF FIGURES

<u>Figure</u>	<u>Page</u>
1.1 Schematic of the Sol-Gel Process for Preparing Glasses and Ceramics.	23
1.2 Main Steps in Sol-Gel Methods.	4
1.3 Schematic Diagram Comparing the Approach of Previous Studies to the Approach Used in This Research	10
2.1 Schematic Diagram of the Instrumental Neutron Activation Analysis Process.	15
2.2 Location of the Rotary Specimen Rack, RSR, with Respect to the Reactor Core	21
2.3 Location of the Rotary Specimen Rack, RSR, Loading Tube in the Reactor.	23
2.4 Gamma-ray Detection System	24
2.5 Plexiglass Rack for Sample Positioning During Counting	28
2.6 Positions of Counting Rack, Sample, Detector and Associated Electronics	30
3.1 Nuclear Reaction Diagram Showing the Possible Modes of Production of A1-28	33
3.2 Spectrum Background Parameters For Peak Area Calculation	38
3.3 Location of Cadmium Filter, Core Element F7, in the Rotary Specimen Rack, RSR.	40
4.1 Calibration Line Relating Mass of SiO ₂ To Corrected Peak Area (First Irradiation Procedure)	44
4.2 Calibration Line Relating Mass of Sodium to Corrected Peak Area (First Irradiation Procedure).	45

<u>Figure</u>	<u>Page</u>
4.3 Calibration Line Relating Mass of Chlorine to Corrected Peak Area (First Irradiation Procedure)46
4.4 Calibration Line Relating Mass of SiO ₂ to Corrected Peak Area (Modified Irradiation Procedure)48
4.5 Calibration Line Relating Mass of Sodium to Corrected Peak Area (Modified Irradiation Procedure)49
4.6 Calibration Line Relating Mass of Chlorine to Corrected Peak Area (Modified Irradiation Procedure).50
5.1 Schematic Representation of Charge Effect In a Colloidal Sol .	.60
5.2 Transition from a Precipitate to a Dried Colloidal Gel60
5.3 Polymer Solutions Exhibit Two Methods of Gelation.62
5.4 Formation of Boron Oxide and a Clear Solution Containing Network-Forming Species by the Hydrolysis of Boron Alkoxides.	.70
5.5 Change in Connectivity of a Boric Oxide Network Produced by Introduction of Cations72
6.1 Solvent Content of SiO ₂ ·xB ₂ O ₃ Lyogels as a Function of Electrolyte Concentration74
6.2 Gamma-ray Spectrum of SiO ₂ Lyogel Swelled in 0.0 N NaCl Solution and Oried at 110°C76
6.3 Gamma-ray Spectrum of SiO ₂ Lyogel Swelled in 1.0 N NaCl Solution and Oried at 110°C77

<u>Figure</u>	<u>Page</u>
6.4 Gamma-ray Spectrum of SiO_2 Lyogel Swelled in 2.0 N NaCl Solution and Dried at 110°C7B
6.5 Gamma-ray Spectrum of $\text{SiO}_2 \cdot 2\text{B}_2\text{O}_3$ Lyogel Swelled in 0.0 N NaCl Solution and Dried at 110°C79
6.6 Gamma-ray Spectrum of $\text{SiO}_2 \cdot 2\text{B}_2\text{O}_3$ Lyogel Swelled in 1.0 N NaCl Solution and Oried at 110°C80
6.7 Gamma-ray Spectrum of $\text{SiO}_2 \cdot 2\text{B}_2\text{O}_3$ Lyogel Swelled in 2.0 N NaCl Solution and Dried at 110°C81
6.8 Solvent Content of $\text{SiO}_2 \cdot x\text{B}_2\text{O}_3$ Lyogels as a Function of Electrolyte Concentration and Also Composition Results from INAA.B6
6.9 B/Si Cation Ratio Obtained from INAA Versus B/Si Cation Ratio (As Batched).B7
7.1 Schematic Diagram of Overall Synthetic Procedure for Synthesizing and Processing Borosilicate Lyogels.93
7.2 Effects of Processing on the Composition of a Lyogel Batched with a B/Si Cation Ratio of 297
9.1 Regions of Precipitate and Clear Solution Formation in the Alkoxide Mixture $\text{Si}(\text{OC}_2\text{H}_5)_4/\text{B}(\text{OCH}_3)_3$ As a Function of Water Content	110
9.2 Formation of $\text{SiO}_2 \cdot n\text{B}_2\text{O}_3$ Precipitate and a Clear Gel Containing Polymerizing Species by the Hydrolysis of a Borosilicate Intermediate	11B
11.1 Schematic of Traditional Lyogel Synthesis and Processing Steps	124
11.2 Schematic of Post-Gelation Lyogel Processing Steps	125

LIST OF TABLES

<u>Table</u>	<u>Page</u>
1.1 Advantages and Disadvantages of the Sol-Gel Method over Conventional Melting for Glass	8
2.1 Settings for Canberra 8180 Multichannel Analyzer During Energy Calibration and All Counting.	26
2.2 Gamma-Ray Energies Used for the Energy Calibration of the Canberra 8180 Multichannel Analyzer.	27
4.1 Determination of Aluminum, Phosphorus, or Magnesium Present in Reagents and Standards.	41
4.2 Calibration Lines Relating Mass of Isotope to Corrected Peak Area (First irradiation procedure).	47
4.3 Calibration Lines Relating Mass of Isotope to Corrected Peak Area (First irradiation procedure).	51
4.4 Standards Checked to Verify Method Developed in This Work . .	53
5.1A Chemical Compositions of Borosilicate Glasses	64
5.1B Analyzed Compositions (wt %) for Three Preparations of a Sample Containing (wt %): SiO ₂ (71.1), B ₂ O ₃ (18.3), Al ₂ O ₃ (7.1), and BaO(3.6)	64
6.1 INAA Compositions of Borosilicate Lyogels Synthesized by Angell.	82
6.2A Chemical Compositions of Borosilicate Glasses	89
6.2B Chemical Compositions of Unrinsed Borosilicate Lyogels (This Work).	89
7.1 INAA Composition of Residue from Top of Sealed Vial	94
7.2 INAA Composition of Unrinsed Lyogels.	95
7.3 Comparison Between Unrinsed and Rinsed and Swelled Lyogels. .	96
8.4 Freeze Drying-Oven Drying Comparison Experiment	103

<u>Table</u>	<u>Page</u>
8.5 Comparison Between Freeze-Oried Lyogels and Oven- Dried Lyogels (batched as $\text{SiO}_2 \cdot x\text{B}_2\text{O}_3$)	106
9.1 INAA Results for Precipitate and $\text{SiO}_2 \cdot x\text{B}_2\text{O}_3$ Lyogels	115
11.1 Summary of Available Oata and Data to be Acquired to Close the Material Balance for the Entire Synthetic Process.	126
11.2 Summary of Component Material Balances Around Reaction Flask and Recommended Techniques.	131
11.3 Summary of Component Material Balances Around Sample Vial and Recommended Analytical Techniques.	133
11.4 Summary of Component Material Balances Around Dryer For An Unrinsed Lyogel and Recommended Analytical Techniques.	135
11.5 Summary of Component Material Balances Around Rinsing Tank and Recommended Analytical Techniques.	137
11.6 Summary of Component Material Balances Around Oryer For A Rinsed Lyogel and Recommended Analytical Techniques.	139
11.7 Summary of Component Material Balances Around Swelling Tank and Recommended Analytical Techniques	141
11.8 Summary of Component Material Balances Around Dryer For A Swelled Lyogel and Recommended Analytical Techniques	143

CHAPTER I. INTRODUCTION

Background

The sol-gel process was developed in the early 1960's by a research group at the British Atomic Energy Research Establishment at Harwell, England [1]. It has been used for making protective films for heat engine materials [2], for the preparation of microspheres (500-1000 μ m in diameter) for uranium carbide fuels used in nuclear reactors [3], for making catalysts and catalyst supports [4,5] and for making anti-reflective coatings [6]. The sol-gel process for making glasses and ceramics is presently an area of intense research activity [7]. While many sol-gel procedures are available for preparing materials ranging from thin films of glass to monolithic ceramic bodies, the factors controlling the properties of the final product are only partially understood. In particular, the colloidal phenomena associated with sol-gel systems have only recently been systematically investigated [8,31,6B,69].

Sol-gel processing has been studied intensely because it provides a way to "grow" ceramic polymers in solution at room temperature, shape them by casting, film formation, or fiber drawing, and consolidate them to dense glasses or polycrystalline ceramics at temperatures often less than half the conventional processing temperature (Figure 1.1) [7]. There are several advantages to low temperature processing. For example, energy requirements are reduced as are impurities (due to containerless processing and the use of higher purity distillable precursors). More importantly, low

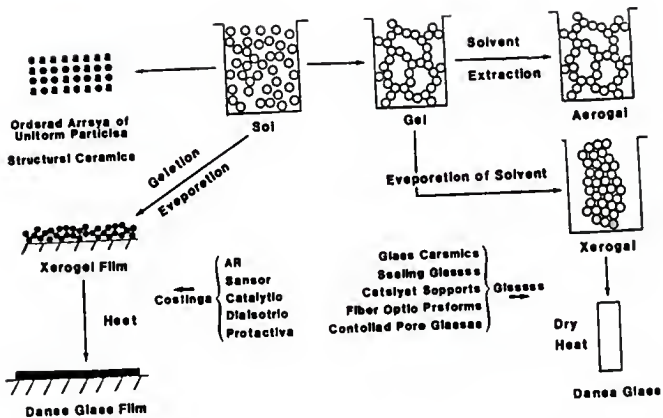


Figure 1.1. Schematic of the sol-gel process for preparing glasses and ceramics [7].

temperature processing allows the synthesis of thermodynamically unstable materials which typically are difficult to obtain by conventional high temperature processing [7]. Examples of these materials include the avoidance of phase separation [9] and crystallization [10] in binary silicate glasses, the synthesis of high surface area substrates and films [11], and the formation of thermodynamically unstable oxynitride glasses [12].

Before proceeding further several terms need to be defined. The term "gel" will be used to describe coherent fluid/solid colloidal systems having at least two components. All of the components are dispersed continuously throughout the system. Colloids are small particles with at least one dimension on the order of a few microns or less. Soils are liquid colloidal dispersions in which settling of the colloidal particles does not occur on a practical time scale. Gels form when the colloid (dispersed phase) combines with the fluid (continuous phase) to produce a network. The gel, as a whole, has mechanical properties similar to those of an elastomeric solid. The dispersion medium will be referred to as the "solvent". The term "lyogel" will be used specifically for those gel systems which have a high concentration of solvent. Syneresis is the spontaneous exudation of solvent and is the opposite of swelling.

Sol-gel methods involve three main parts: gel synthesis, post-gelation and sintering (Figure 1.2) [13]. Gel synthesis may proceed via two different routes, producing either polymeric gels or colloidal gels. The colloidal route begins with the preparation of the sol. As solvent evaporates, a point is reached when interaction between the

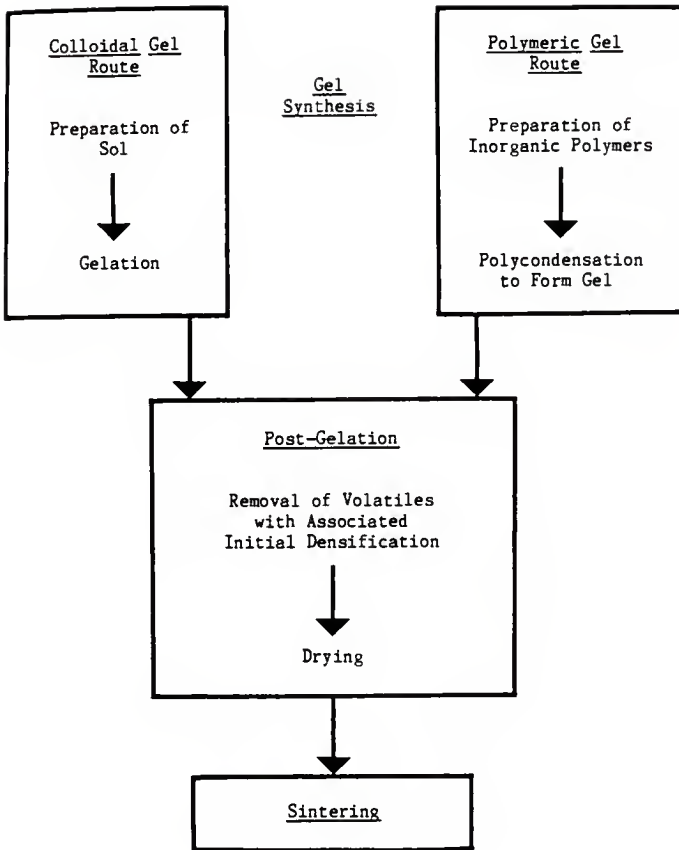
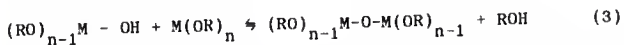
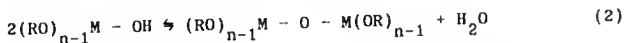


Figure 1.2. Main steps in sol-gel methods [8].

double layer associated with each particle prevents translatory movement. The occurrence of this non-fluid state indicates a gel has formed.

The polymeric path begins with the preparation of a solution of inorganic monomers. The most common process employs metal alkoxides of network forming elements $M(OR)_x$, where M is Si, B, Ti, Al, etc. and R is often an alkyl group) as monomeric precursors [7]. In alcohol/water solutions the alkoxide groups, undergoing hydrolysis, are replaced by hydroxyl groups (Reaction 1). Usually an acid or base is used as a catalyst for these hydrolysis reactions. Subsequently the hydroxyl groups are involved in condensation reactions that produce polymeric solution species comprised of -M-O-M- linkages (Reactions 2 and 3) [7].



It should be noted that, while Reactions 1-3 in the forward direction are usually used to describe the sol-gel process, these reactions are reversible. The reverse reaction rates depend on pH, temperature, water and solvent concentrations, as well as the connectivity of M within the polymer [14,15].

Polymer systems can be broken down into two distinct types. In the first type, Type I as per Yoldas [36], the polymer species are formed by initial polymerization to form oligomers. Evaporation of solvent leads to physical entanglement of the oligomers and a gel is

formed. In the second type, Type II [36], gelation occurs when two polymer species randomly collide and, via hydrolysis and dehydration reactions, are joined to form one longer polymer. As this polycondensation continues, the polymers crosslink to form a network which spans the entire solution volume [7]. At the gel point, physical properties such as the viscosity and the elastic modulus increase abruptly. The solid network prevents the liquid from rapidly escaping and the liquid prevents the network from spontaneously collapsing [16]. Gelation is of interest in materials technology because it provides a path for net shape processing. The sudden rise in viscosity "freezes-in" shapes obtained by casting, film deposition, or fiber drawing [7].

In the post-gelation step, the gel is rinsed to remove volatile components. Professor John Schlup's research group at Kansas State University is the only group to incorporate a rinsing step into the post-gelation stage for borosilicate lyogels (8, 31, 68, 69). Although there is a small volume change associated with rinsing, the purpose of this step is to wash away unreacted monomers and initiators as well as solvent and reaction by-products. The rinsed gel is then dried to remove the rinsing solution (which may be water). Usually it is dried either by slow evaporation in a convection oven (to minimize the internal stresses caused by the volume changes on drying and to minimize capillary forces in the gel pores), by supercritical fluid extraction in an autoclave, or by freeze drying. The dried gels are called xerogels and aerogels, respectively (Figure 1.1). Solvent evaporation results in shrinkage primarily due to surface tension,

which exerts a hydrostatic compressive stress on the gel proportional to the curvature of the liquid-vapor meniscus [7]. As the drying gel shrinks, condensation reactions continue as reactive terminal groups meet, causing the gel to become more restricted and stiffer. The pores are only partially filled with water and liquid-vapor interfaces develop within pores. When the gel is rigid enough to withstand the compressive capillary stresses that accompany drying, further water evaporation creates interconnected porosity, or "mud cracking", within the gel. Supercritical fluid extraction and freeze drying eliminates liquid-vapor interfaces, which greatly reduces the drying shrinkage [17]. The final step in the sol-gel method for preparing ceramics is sintering.

Since the final products have better homogeneity and purity, sol-gel methods are suitable for making specialty ceramics. However, with the high cost of raw materials, it is unlikely that these techniques can be competitive for conventional glass products such as containers, flat glass and common fibers. A list of advantages and disadvantages of the sol-gel methods is given in Table 1.1 [18]. Sol-gel methods are viable when the advantages gained from the techniques are required and the resulting high value-added product can be made at a profit.

Prior Related Research

The major disadvantage of the sol-gel method is the large uncontrolled shrinkage of the gel during the drying and sintering processes [18]. For many previous studies when the final product developed cracks, the synthesis conditions were changed by varying

Table 1.1. Advantages and Disadvantages of the Sol-Gel Method over Conventional Melting for Glass [18].

Advantages

1. Better homogeneity from raw materials.
 2. Better purity from raw materials.
 3. Lower temperature of preparation:
 - (a) save energy;
 - (b) minimize evaporation losses;
 - (c) minimize air pollution;
 - (d) no reactions with containers, thus higher purity;
 - (e) bypass phase separation;
 - (f) bypass crystallization.
 4. New noncrystalline solids outside the range of normal glass formation.
 5. New crystalline phases from new noncrystalline solids.
 6. Better glass products from special properties of gel.
 7. Special products such as films.
-

Disadvantages

1. High cost of raw materials.
 2. Large shrinkage during processing.
 3. Residual fine pores.
 4. Residual hydroxyl groups.
 5. Residual carbon.
 6. Health hazards of organic solutions.
 7. Long processing times.
-

reactant concentrations, solvents or other parameters. Few attempts were made to change the gel once it was formed. The research presented in this thesis is a continuation of the work done by Angell [8] in attempting to separate the effects due to gel synthesis from effects due to swelling or syneresis in the post-gelation step (Figure 1.3 [8]). The goal was to reduce the problems associated with the drying process by first minimizing the gel volume in the wet state. This was accomplished by placing the gels in solutions which might induce syneresis, and thus shrinkage of the gel.

When placed in an electrolyte solution a charged surface, such as a borosilicate gel, will attract counterions and repel co-ions. Thus electrolyte in the solvent reduces the effective surface charge of the borosilicate network. As the effective surface charge of the borosilicate network is reduced, the distance between neighboring segments of the network is decreased. The result is that the gel volume is reduced.

The experiments were conducted on borosilicate gels using a synthesis procedure similar to those reported by Nogami and Moriya [19] and by Yoldas [20], and which subsequently was modified by Angell [8]. No post-gelation studies involving borosilicate gels had been published previous to the work by Angell. The gel synthesis procedure used was repeated as precisely as possible in order to minimize the differences in the gels due to synthesis parameters. Thus, any changes in the gel volumes following rinsing (and the swelling or syneresis produced) were attributed to these operations.

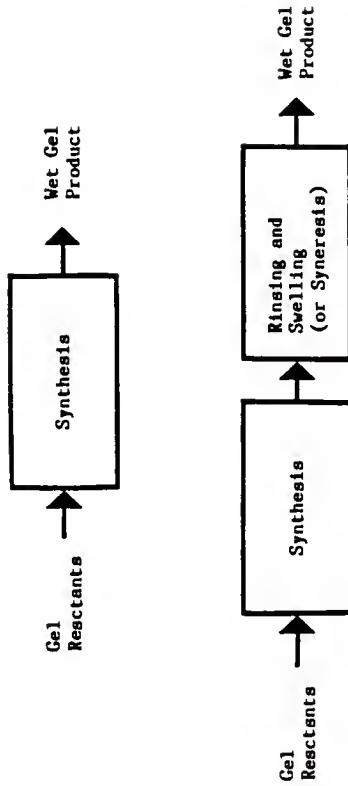


Figure 1.3. Schematic diagram comparing the approach of previous studies to the approach used in this research [8].

Problem Statement

Most of the research presented in this thesis was in response to questions that arose from the results given by Angell [8]. In particular, these results showed that some of the swelling behavior between lyogels were identical, even though the lyogels had different as-batched compositions. This suggests that the actual composition of the lyogel might be different from the as-batched composition. Further, upon exploration of the borosilicate lyogel chemistry in solution, it was found that there should be differences between the as-batched composition and the actual composition of the lyogel after swelling.

Various techniques for borosilicate analysis were considered. Instrumental neutron activation analysis, INAA, was selected because it is a very sensitive and accurate analytical technique for determining the mass of an element present in an unknown sample. Also, INAA is nondestructive, requires a small sample mass, and requires little sample preparation. Although INAA has been used extensively in many fields of research, a procedure for the analysis of borosilicate materials containing sodium chloride using INAA was not found. Thus, an INAA procedure was developed which provided silicon, sodium, and chlorine mass compositions for the borosilicate lyogels under investigation.

The subsequent chapters of this thesis fall into three categories, namely, INAA, lyogel and borosilicate chemistry, and proposed future work. Firstly, INAA background and theory will be introduced, then the INAA technique developed will be described, and

then verification of this technique will be discussed. Secondly, lyogel and borosilicate chemistry will be examined, and INAA results of dried borosilicate lyogels will be presented. Lastly, material balances for the entire synthetic process will be derived. Experiments, including suggested analytical techniques, to obtain a closed material balance will be proposed.

INSTRUMENTAL NEUTRON ACTIVATION ANALYSIS (INAA)

II. Review of INAA

III. INAA Procedure Development

IV. Verification and Calibration of INAA Technique

CHAPTER II

REVIEW OF INSTRUMENTAL NEUTRON ACTIVATION ANALYSIS (INAA)

A. General Background

Instrumental Neutron Activation Analysis, INAA, is a very sensitive and accurate analytical technique for determining the mass of an element present in an unknown sample. Figure 2.1 illustrates the INAA process which usually involves irradiating an unknown sample with thermal neutrons. Neutrons are available at several energy levels. Thermal neutrons are neutrons in thermal equilibrium with their environment and have low energies (0.025 eV at 20°C) [29]. Epithermal neutrons have energies greater than thermal neutrons. Fast neutrons have energies greater than 1.9 MeV [29]. In this work, thermal neutrons, as well as fast neutrons, were utilized.

INAA with thermal neutrons utilizes the neutron-gamma ray reaction designated as (n, γ) . Neutrons are captured by the nucleus of the parent atom, thus producing a new nuclide with a mass number one unit greater than the parent nuclide. The new nuclide, or daughter product, is often radioactive and decays by emitting beta and/or gamma rays. By measuring the emission rate of gamma rays having specific energies and using an understanding of the activation reactions involved, both qualitative and quantitative analysis of the parent element is possible.

For example, consider INAA of copper [27]. When copper with a mass number of 63 is placed in a thermal neutron flux, copper-64 is produced by the following reaction:

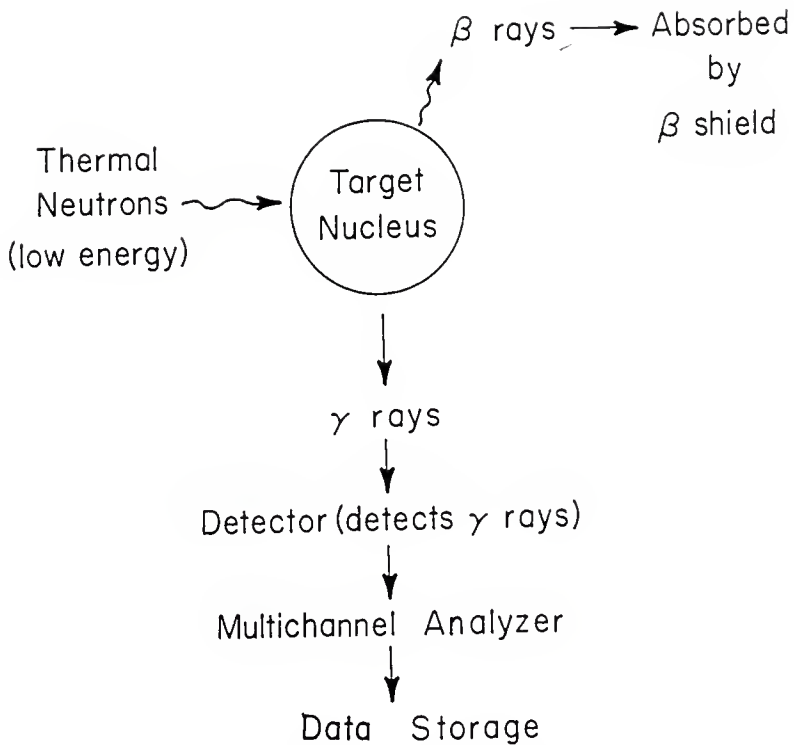


Figure 2 .1. Schematic diagram of the Instrumental Neutron Activation Analysis process.



Copper-64 is radioactive with a half-life of 12.8 hours and emits gamma rays with an energy of 1345.8 keV. The emission rate of the 1345.8 keV gamma ray is measured. Using these data, along with data obtained from a copper-63 standard, the amount of copper in the sample can be determined.

INAA has many advantages over other analytical techniques. These advantages include the following [27].

1. INAA is nondestructive.
2. Pre- or post-chemistry is not required.
Thus foreign materials are not introduced.
3. The technique is manpower efficient since minimal sample preparation is required.
4. Many elements may be determined simultaneously from a single sample and a single analyzer setting.
5. INAA is very fast once the experimental procedure has been optimized for a given type of sample.
6. Liquid, solid, or gas samples may be analyzed.
7. Only small sample masses (~0.1g) are required.
8. INAA is very sensitive for a large number of elements.

B. Theoretical Development and Calculation of Corrected Peak Area

A detailed derivation of the model employed to describe the measurement of the concentration of a given element in an unknown sample is given by Higginbotham [24]. For convenience a less detailed derivation is given in Appendix A.

The mass of the parent element in a sample can be determined by utilizing many quantities, some of which are known and others which

are measured. The peak area for the specific energy gamma-ray emitted from the daughter product is measured with a detector system. Time values are determined for each pulse height distribution (plot of the number of counts versus channel number) measured. The natural abundance, atomic number of the parent isotope, value for the daughter product gamma-ray yield, and value for the probability of decay for daughter product atoms are found in the literature. The mass, M, of the parent element is given by the following equation [24].

$$M = \frac{P_a \lambda}{A_b N_A \sigma_p \phi E_f Y \left[1 - e^{-\lambda t_r} \right] \left[e^{\lambda(t_r - t_s)} - e^{-\lambda(t_r - t_e)} \right]} \quad (1)$$

where:

P_a = the peak area

A = the atomic weight of the isotope or isotopic atomic weight

λ = the probability of decay for daughter product atoms

A_b = the natural abundance of the parent isotope

N_A = Avagadro's number

σ_p = the absorption cross-section of the parent isotope

ϕ = the flux of neutrons striking the target nucleus

E_f = the absolute efficiency of the detector (i.e., the number of counts recorded in a certain channel divided by the number of counts actually occurring)

Y = the gamma-ray yield (i.e., the number of gamma rays of each energy per disintegration)

t_r = the irradiation time

t_s = the time the detector system begins to count the number of gamma-ray detector interactions

t_e = the time the detector system stops collecting.

Eq. (1) applies to both the standards and the fluence monitors. The fluence monitors are metal wires of known mass wrapped separately around the sample and the standards containers. Thus, Eq. (1) for the standard becomes

$$s^M = \frac{s^P a K_1}{s^{\phi} \left[1 - e^{-\lambda s^t r} \right] \left[e^{\lambda (s^t r - s^t s)} - e^{-\lambda (s^t r - s^t e)} \right]} \quad (2)$$

$$\text{where } K_1 = \frac{s^{\lambda}}{s^A N_A \left[s^{\sigma P} \right]_s E_f Y} = \text{constant}$$

$\lambda = (\ln 2)/(\text{half-life of daughter product}).$

Similarly, Eq. (1) is applied to the fluence monitors (wires) of the standards.

$$s^M = \frac{s^P a K_2}{s^{\phi} \left[1 - e^{-\lambda_w (s^t r)} \right] \left[e^{\lambda_w (s^t r - s^t s)} - e^{-\lambda_w (s^t r - s^t e)} \right]} \quad (3)$$

$$\text{where } K_2 = \frac{s^{\lambda_w}}{s^A N_A \left[s^{\phi} \right]_s E_f Y} = \text{constant}$$

$\lambda_w = (\ln 2)/(\text{half-life of wire}).$

Rearranging Eq. (3) to solve for s^{ϕ} , Eq. (4) below is obtained.

$$s^{\phi} = \frac{s^P a K_2}{s^M \left[1 - e^{-\lambda_w (s^t r)} \right] \left[e^{\lambda_w (s^t r - s^t s)} - e^{-\lambda_w (s^t r - s^t e)} \right]} \quad (4)$$

Since the wire is placed in the same location on each vial irradiated, it is assumed that $s\phi = \frac{w}{s}\phi$.

Substituting Eq. (4) into Eq. (2) yields

$$s^M = \frac{P_a K_1^M \left[1 - e^{-\lambda_w (s^w t_r)} \right] \left[e^{\lambda_w (s^w t_r - w^w t_s)} - e^{\lambda_w (s^w t_r - w^w t_e)} \right]}{P_a K_2 \left[1 - e^{-\lambda_s t_r} \right] \left[e^{\lambda (s^t r - t_s)} - e^{\lambda (s^t r - t_e)} \right]} \quad (5)$$

For constant irradiation times and for homogeneous standards having the same counting geometry, a constant equal to the slope of the mass line for the standard can be obtained.

$$\frac{K_1 \left[1 - e^{-\lambda_w (s^w t_r)} \right]}{K_2 \left[1 - e^{-\lambda_s t_r} \right]} = X = \text{constant} = \text{slope of the mass line for the standard}$$

Letting the remainder of the right hand side of Eq. (5) be denoted as the corrected peak area, P_a^C , then

$$s^M = X P_a^C, \quad (6)$$

$$\text{where } P_a^C = \frac{P_a \left[e^{\lambda_w (s^w t_r - w^w t_s)} - e^{\lambda_w (s^w t_r - w^w t_e)} \right]}{P_a \left[e^{\lambda (s^t r - t_s)} - e^{\lambda (s^t r - t_e)} \right]}$$

X = slope of the mass line for the standard.

A plot of s^M versus P_a^C should be linear with an intercept of zero. Once the standard line has been established for a given element it can be used to determine the mass of that element in a given sample of unknown composition. The irradiation time for the samples must be the same as for the standard. Also, the samples should be homogeneous, should have the same geometry during counting as the standard, and should have the same gross activity as the standard to allow equality between the system dead times so that

$$s^E_f = [E_f]_{\text{sample}}. \quad (7)$$

By substituting the sample values into the expression for P_a^C , $[P_a^C]_{\text{sample}}$ can be calculated. Substituting this quantity into Eq. (6) yields the mass of the desired element in the sample.

C. Irradiation Facility [24]

The neutron irradiation of samples utilizes the Rotary Specimen Rack, or RSR, of the TRIGA Mark II nuclear reactor at Kansas State University [3]. The maximum steady-state thermal flux is 1×10^{13} neutrons/cm²-sec and the maximum thermal fluence per pulse is 4×10^{14} neutrons/cm².

The Rotary Specimen Rack, RSR, is a circular aluminum ring supporting 40 cylindrical sample irradiation containers. The rack assembly is encased in a watertight, air-filled aluminum housing embedded in the graphite reflector surrounding the reactor core

(Figure 2.2). The samples are loaded by placing the sample vials into a second plastic vial attached to a nylon cord. This assembly is lowered through a tube into the desired irradiation position (Figure 2.3).

D. Detector Analyzer System [24,25,26]

The daughter products formed emit gamma rays at characteristic energies. The detection system counts the number of gamma rays arriving at the detector at each energy. The detection system is shown in Figure 2.4. It consists of a solid state Ge(Li) drifted detector connected to a multichannel analyzer (MCA). When gamma rays interact with the detector, a voltage is generated proportional to the energy of the incident gamma ray and is sent to the analog-to-digital converter (ADC). The digital data is stored in the MCA memory in one of 4096 channels. A plot of the number of counts versus channel number is defined as the pulse height distribution.

E. Energy Calibration

An energy calibration is performed to relate the gamma ray energy to the channel number. To determine accurately the energies of the peaks in the gamma ray spectrum, the Canberra 8180-Ge(Li) system must be calibrated by measuring the spectrum of known gamma ray emitters. The Canberra 8180 generates a linear energy calibration equation by fitting a line through the gamma ray energy as a function of peak channel.

The multichannel analyzer settings shown in Table 2.1 were used. A spectrum is obtained using a ^{137}Cs and a ^{60}Co source. These spectra

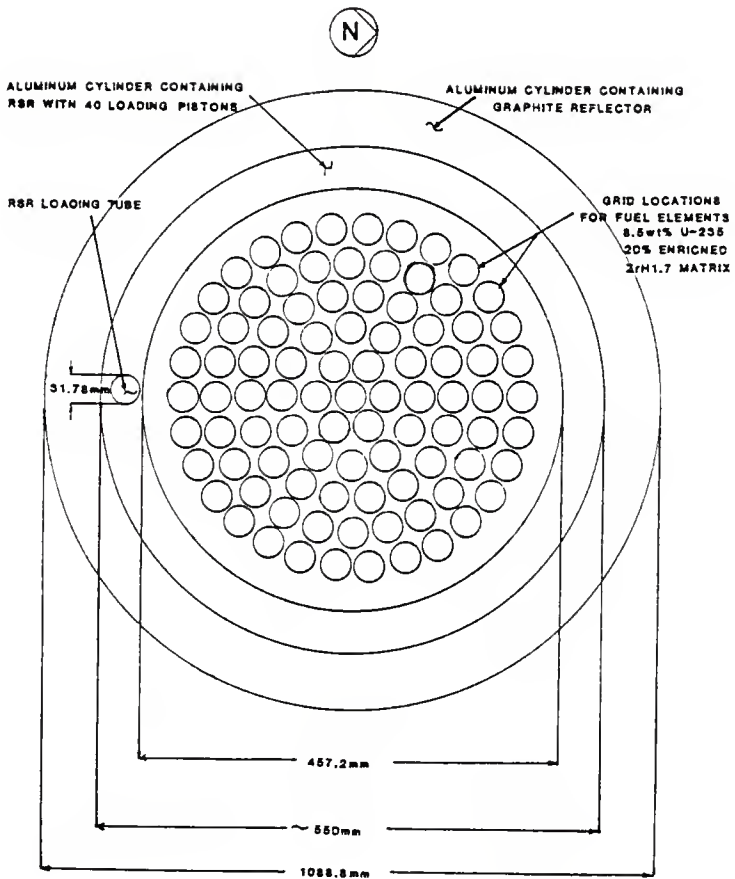


Figure 2.2. Location of the Rotary Specimen Rack, RSR, with respect to the reactor core [24].

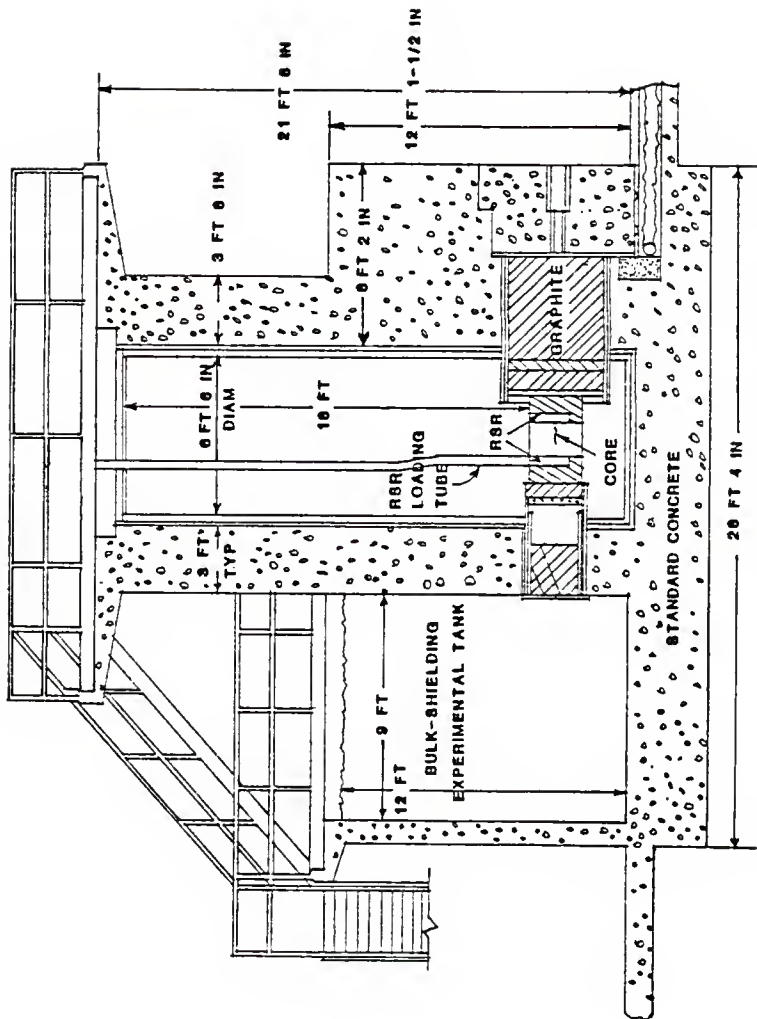


Figure 2.3. Location of the Rotary Specimen Rack, RSR, loading tube in the reactor [24].

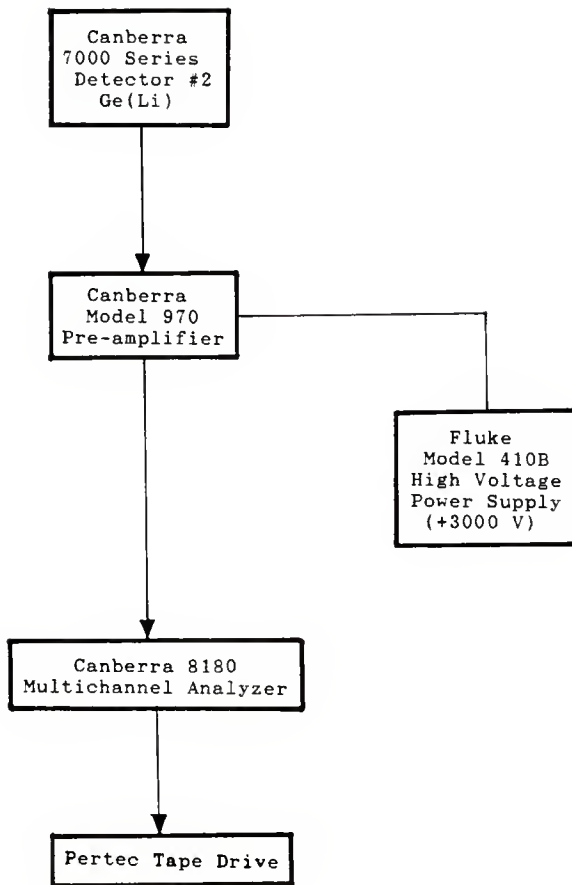


Figure 2.4. Gamma-ray detection system.

Table 2.1. Settings for Canberra 8180 Multichannel Analyzer
During Energy Calibration and All Counting.

<u>Function</u>	<u>Setting</u>
Preset count	OFF
Preset time	LIVE
Function	PHA N=9, M=5
I/O device	TAPE OUT
Data	ADD
Control	MANUAL
Memory Control Transfer	1/1
Coarse gain	100
Fine gain	7.30
Time constant	2 μ s
Baseline Restorer	LOW
Pile-up Rejector	OUT
LLD	0.4
ULD	10.1
Conv. gain	4096
Baseline	4.87
Gate	OFF
Digital Offset	all levers down

Table 2.2. Gamma Ray Energies Used for the Energy Calibration of the Canberra 8180 Multichannel Analyzer [21].

<u>Isotope</u>	<u>Gamma Ray Energy (keV)</u>
^{137}Cs	661.6
^{60}Co	1173.2
^{60}Co	1332.5

provide three reference peaks. The channel numbers associated with these energies are used to establish a linear relationship between energy and channel number. A region of interest is established around each of the peaks listed in Table 2.2 and their energies are entered into the Canberra 8180 MCA. The analyzer is now calibrated and ready for data collection.

F. Data Collection in General

Data collection for a particular sample starts with the placement of the sample near the detector. The location in the detector must be constant for each sample and standard because variation in the counting geometry will lead to differences in the absolute efficiency of the detector. Such variations violate the assumption of equivalent counting geometries in Eq. (7). A Plexiglass rack placed on top of the detector casing is used to hold samples at specific locations and distances above the detector, as shown in Figure 2.5. Polyethylene disks and Plexiglass plates may be placed between the sample and the detector to minimize exposure of the detector to beta particles. The detector is attached to a Dewar containing liquid nitrogen (Figure 2.6). The liquid nitrogen cools the detector to prevent thermal migration of lithium from the detector. The location of the detector pre-amplifier, which contains the high voltage connection for the detector and for the signal output, is shown as well. The energy spectrum is stored on magnetic tape for later data analysis [24].

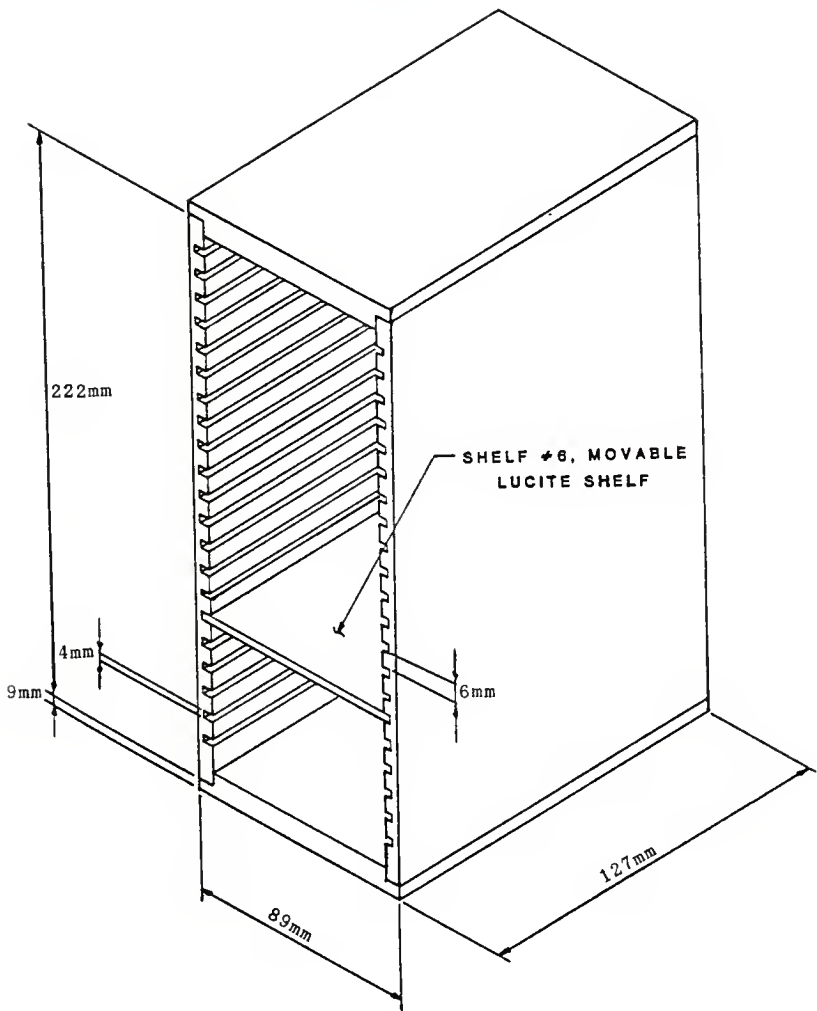


Figure 2.5. Plexiglass rack for sample positioning during counting(modified from Ref. 24).

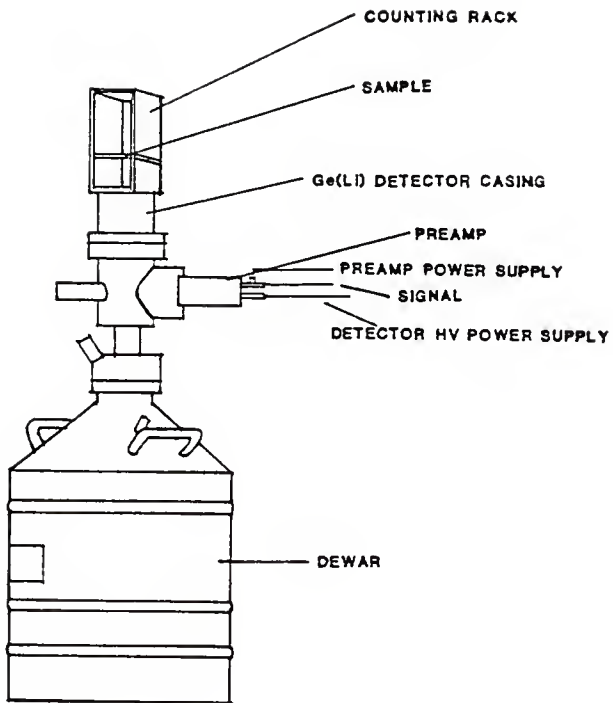


Figure 2.6. Positions of counting rack, sample, detector and associated electronics [24].

G. Preparation of Standards

NaCl and SiO₂ were used to prepare standards. The maximum mass of NaCl used was 0.107g and that of SiO₂ was 0.131g. A polyethylene vial with a cap was used to encapsulate each standard. For each standard the vial was cleaned by rinsing with warm tap water, deionized water, and ethanol, in that order. The vials then were air dried. All handling of the vials was done using surgical gloves. The vials then were weighed to an accuracy of $\pm 0.001g$.

NaCl and SiO₂ were transferred to the vial using a stainless steel spatula and a plastic funnel. The vial was filled until the desired makeup was obtained. Care was taken so that no sample contacted the outside or top edge of the vial. The cap was closed, sealing the vial. A 0.127 mm diameter tungsten wire was wrapped around the top of the vial and the ends of the wire were twisted together. Excess wire was removed. The total mass was determined; and, the mass of the wire was obtained by difference.

The vial was placed in a polyethylene bag to prevent contamination of the exterior of the vial. The opening of the bag was twisted and taped. A label was affixed over the tape.

In addition, standards containing a known amount of boron were prepared to check the validity of the INAA technique being developed. Boron readily reacts with neutrons, but the boron nuclides produced are short-lived (a half-life of 0.23 minutes). Thus, special techniques are required if boron analysis is to be obtained. Boron is difficult to determine with high sensitivity or freedom from

interference [22]. Various samples containing NaCl, SiO₂ and H₃BO₃ were prepared as described previously, except that an electric soldering iron was used to seal the cap to the vial. The vial was sealed to prevent any H₃BO₃ from escaping due to volatilization. Care is required so as not to penetrate the vial. The compositions of all reagents, some empty vials, NaCl, and SiO₂ were obtained via INAA as well.

A. Reactions Involving Silicon

Most INAA studies have emphasized activation produced by thermal neutrons [29]. As discussed in the Introduction, the silicon content of various borosilicate lyogels was desired.

^{28}Si undergoes an (n,p) reaction with fast neutrons to produce ^{28}Al during neutron activation analysis. This is the most suitable isotope for analysis of silicon in silicate materials.

However, other neutron reactions also produce ^{28}Al : $^{27}\text{Al}(n,\gamma)^{28}\text{Al}$, $^{31}\text{P}(n,\alpha)^{28}\text{Al}$, and the second-order reaction $^{26}\text{Mg}(n,\gamma)^{27}\text{Mg} \rightarrow ^{27}\text{Al}(n,\gamma)^{28}\text{Al}$ (Figure 3.1) [29]. Koch [30] found that this second-order reaction can present significant problems in the analysis of ^{28}Al when Mg is present in a sample. Interference from phosphorus is serious, with the sensitivity of the (n, α) reaction of ^{31}P being about half of that for the ^{28}Si reaction [22]. The interference from aluminum is much less significant, with its activation being two orders of magnitude less sensitive than for the equivalent amount of phosphorus [22]. Typically ^{27}Al would be the primary impurity of interest for the borosilicate lyogels investigated. No phosphorous or magnesium is anticipated based on the compositions of the reagents.

Therefore, a technique to measure gamma rays emitted from the decay of ^{28}Al produced by fast neutrons reacting with ^{28}Si is needed.

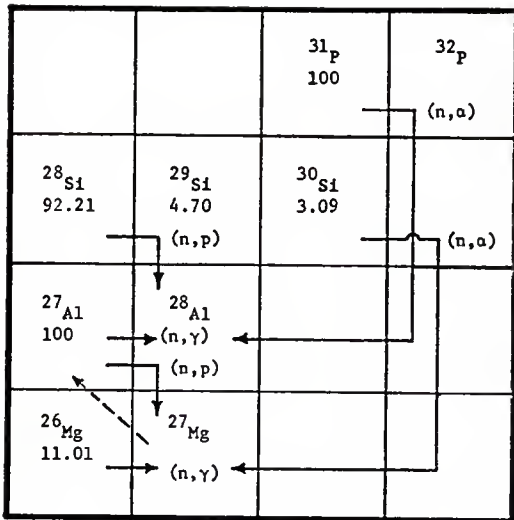


Figure 3.1. Nuclear Reaction Diagram showing the possible modes of production of Al-28. Isotopic abundances, in percent, are below the nuclide identifications. Reactions are identified in parentheses. The dashed line represents the beta decay of Mg-27 to Al-27 [29].

²⁸Al emits a 1.78 MeV gamma ray which is suitable for INAA. Fast-neutron reactions usually have such small cross-sections that they can be neglected. However, use of a thermal-neutron filter can be used to exploit the fast-neutron activation reactions. Cadmium filters commonly have been used in reactor flux measurements to separate thermal from epithermal neutron flux [29, 33, 34, 35]. The cadmium filter technique enhances the (n,p) reaction while reducing thermal-neutron activation by reducing the number of thermal neutrons interacting with a sample that is to be irradiated [29]. Thus, a cadmium filter was used to change the energy spectrum of neutrons being used to activate samples.

B. Sample preparation

Samples were prepared for INAA analysis in the same manner as the standards. The mass of sample used ranged from 0.100g to 0.125g.

C. Irradiation of Standards

The TRIGA Mark II Reactor was brought to a steady state power of 225 kW. The standard was placed inside a reactor loading vial lined with 0.020 inch thick cylindrical cadmium foil and the assembly was attached to a "fishing pole" loading device. The standard was inserted into the Rotary Specimen Rack, RSR2, and irradiated for various time intervals to determine an optimum irradiation time. This was defined as the irradiation time giving a satisfactory counting time. An irradiation time of 6 minutes was adequate.

Upon removal of the standard from RSR2 a timer was started. This start time was used in subsequent calculations. Since more standards were to be irradiated, the time the standard was removed from RSR2 was recorded for each sample. These data were used for wire decay calculations. Reagents, NaCl, SiO₂ and empty vials were irradiated in the same manner.

D. Irradiation of Samples

Samples of unknown composition were irradiated for 6 minutes as per the standards.

E. Post-irradiation Handling and Counting

Since one of the radionuclides of interest was ²⁸Al (a half-life of 2.241 minutes), only one standard could be irradiated and counted at a time. Approximately 2 minutes elapsed between the end of an irradiation procedure and the beginning of the first gamma ray measurement. Thus there was not enough time to count more than one standard before the ²⁸Al intensity was reduced to background levels.

The tungsten wire ring was removed from the vial, put into the labeled polyethylene sample bag, and placed in a lead container for counting at a later time. A 3-5/8 inch diameter polyethylene disk, 18/32 inch thick, was placed on top of the detector. The irradiated standard was placed upright, above the detector center, on the first shelf of the rack shown in Figure 2.5 of Chapter II.

The analyzer dead time was not greater than 15% for any of the measurements. Dead time of the analyzer is that percentage of time the analyzer is unable to count interactions in the detector. By trial-and-error it was determined that the first shelf of the rack yielded satisfactory data.

Each standard was counted until at least 10,000 counts for each peak were obtained. When the Na and Cl peaks had at least 10,000 counts and ^{28}Al was present in a small quantity, the maximum counting time was 20 minutes. After this time ^{28}Al is reduced to insignificant levels and essentially no ^{28}Al interactions with the detector occur. When the sample counting had been completed, the elapsed time was recorded. After each standard had been counted, the spectrum was stored on magnetic tape.

After the data on each standard had been acquired, the tungsten wire ring is placed above the detector center, with the polyethylene disk in place, on the first shelf of the rack and counted. The counting continued until at least 30,000 counts associated with the ^{187}W peak at 685.8 keV had been obtained. The elapsed time was recorded after the 30,000 counts had been measured. The spectrum of the wire was then stored on magnetic tape after measurement.

Samples of unknown composition were handled and counted in the same manner as the standards. Again, all spectra were stored on magnetic tape after measurement.

F. Determination of Peak Areas [24,25,26,2B]

The peak areas are calculated from the detector-gamma-ray interactions measured. Each interaction of a gamma ray with the detector results in a count being recorded in a specific channel for the energy associated with that gamma ray. As these data are accumulated, the pulse height distribution as a function of channel number is obtained (Figure 3.2). The background level for each peak is determined by averaging K points on either side of the peak to determine average background levels. Then a straight line is drawn between these averaged values. The peak area is computed as follows.

$$P_a = \text{Integral} - \text{Background} \quad (1)$$

where: P_a = peak area

$$\text{Integral} = \sum_{i=A}^B X_i, \text{ where } X_i \text{ is the number of counts in the } i\text{th channel.}$$

$$\text{Background} = \frac{(B-A+1)}{2K} \left[\sum_{j=A}^{A+K-1} X_j + \sum_{m=B-K+1}^B X_m \right]$$

Substituting into Eq. (1) gives the peak area, P_a .

$$P_a = \sum_{i=A}^B X_i - \frac{(B-A+1)}{2K} \left[\sum_{j=A}^{A+K-1} X_j + \sum_{m=B-K+1}^B X_m \right] \quad (2)$$

G. Data Reduction

After a spectrum had been recorded, the regions about the peaks corresponding to the elements to be measured were set. The peak area

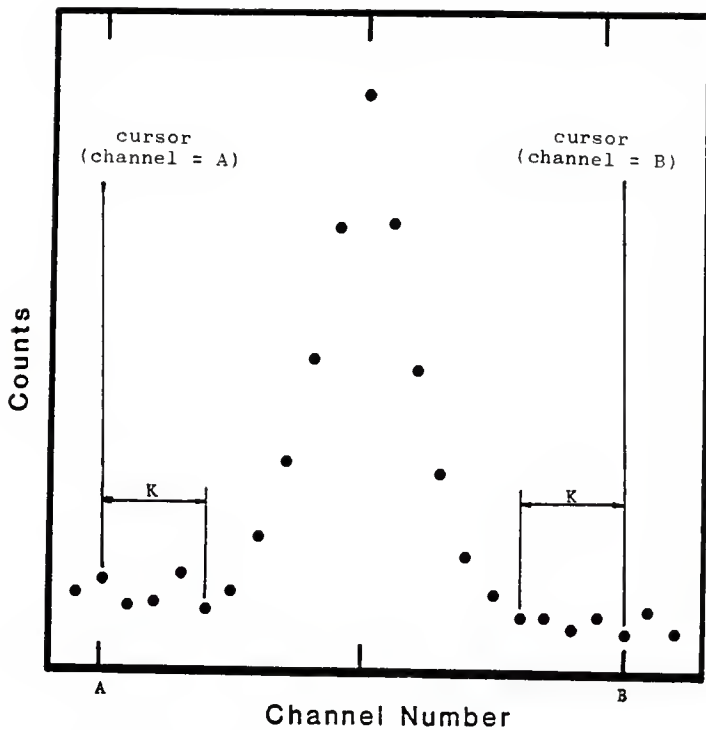


Figure 3.2. Spectrum background parameters for peak area calculation (modified from Ref.24).

and peak area error were calculated. For example, if aluminum is being analyzed, the gamma ray energy emission at 1778.7 keV is located. A region of interest about this peak is established by locating the ends of the tails of the peak and using these points as the right cursor and the left cursor positions as shown in Figure 3.2. An example analysis and calculation is presented in Appendix B.

H. Modification of Irradiation Procedure

During the course of this research, the emission from the irradiated cylindrical cadmium filter briefly exposed the sample handler to several hundred mr/hr. Although the cumulative exposure was well within the limits for a standard operator at any nuclear facility, a higher level of protection was desired. Thus, the irradiation procedure was modified as described below.

The sample was placed inside a reactor loading vial in which the top was lined with 0.020-inch thick cadmium foil. This assembly was inserted into core element F7, which has a cadmium filter (Figure 3.3). Under these conditions the sample handler was exposed to about 100 mr/hr for a very brief period of time. This is a significant improvement in radiation protection.

Standards and samples were irradiated for 1 minute at 225kW. Post-irradiation handling procedures were performed as described previously in Sections A.4 to B.2. This modified procedure required new calibration curves.

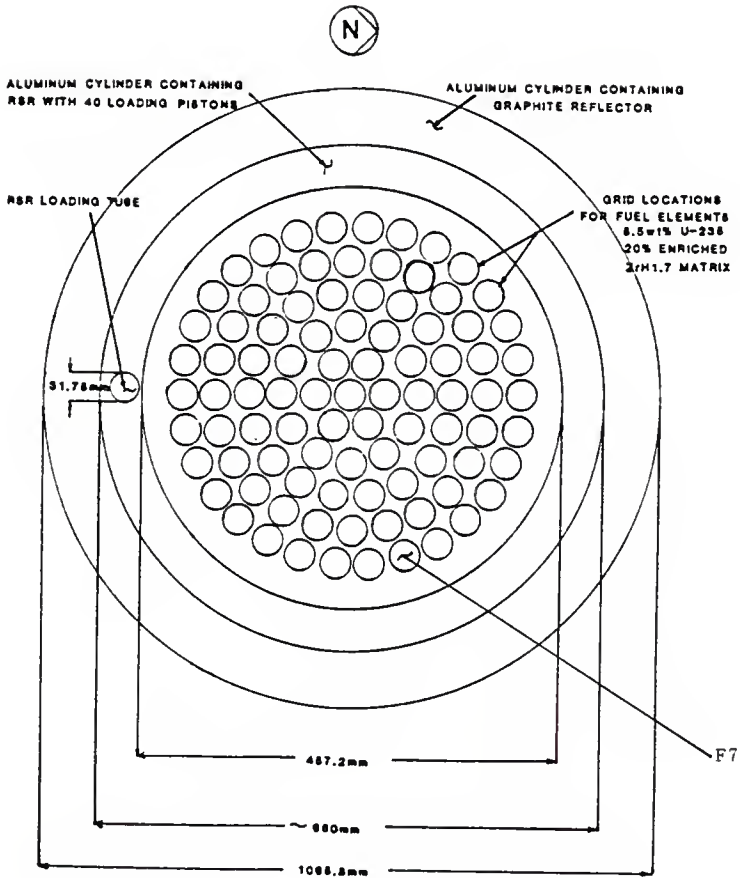


Figure 3.3. Location of cadmium filter, core element F7, in the Rotary Specimen Rack, RSR (modified from Ref.24).

CHAPTER IV. VERIFICATION AND CALIBRATION OF INAA TECHNIQUE

A. Determination of Aluminum, Phosphorus or Magnesium Present in Vials, Reagents and Standards

Chemical reagents and empty (blank) vials were irradiated at 225 kW for 6 minutes and counted as described in Chapter III. They were analyzed for aluminum, phosphorus and magnesium. No trace amounts, at the parts per million level, were found to be present. Detailed results are given in Table 4.1.

Table 4.1. Determination of Aluminum, Phosphorus or Magnesium Present in Vials, Reagents and Standards.

Substance	Mass of Element (μg)*		
	Aluminum	Phosphorus	Magnesium
Vial	< 0.1	< 70	< 5
0.15M HCl	< 0.1	< 70	< 5
TEOS	**	< 70	< 5
$\text{B}(\text{OCH}_3)_3$	< 0.1	< 70	< 5
SiO_2	**	< 70	< 5
NaCl	< 0.1	< 70	< 5
H_3BO_3	< 0.1	< 70	< 5

* Detection limits found in References 22, 23, 66.

** Al proportional to the mass of silicon in sample.

B. Calibration Lines

B.1. Calibration Lines for First Irradiation Procedure

B.1.A. Experimental

NaCl and SiO₂ were used to prepare standards. The maximum mass of NaCl used was 0.107g and that of SiO₂ was 0.131g. A polyethylene vial with a cap was used to encapsulate each standard. For each standard the vial was cleaned by rinsing with warm tap water, deionized water, and ethanol, in that order. The vials then were air dried. All handling of the vials was done using surgical gloves. The vials then were weighed to an accuracy of ± 0.001g.

NaCl and SiO₂ were transferred to the vial using a stainless steel spatula and a plastic funnel. The vial was filled until the desired makeup was obtained. Care was taken so that no sample contacted the outside or top edge of the vial. The cap was closed, sealing the vial. A 0.127 mm diameter tungsten wire was wrapped around the top of the vial and the ends of the wire were twisted together. Excess wire was trimmed off using scissors. The total mass was determined; and, the mass of the wire was obtained by difference.

The vial was placed in a polyethylene bag to prevent contamination of the outside of the vial. The opening of the bag was twisted and taped. A label was affixed over the tape.

Figure 4.1 Calibration Line

Silicon Dioxide

(first irradiation procedure)

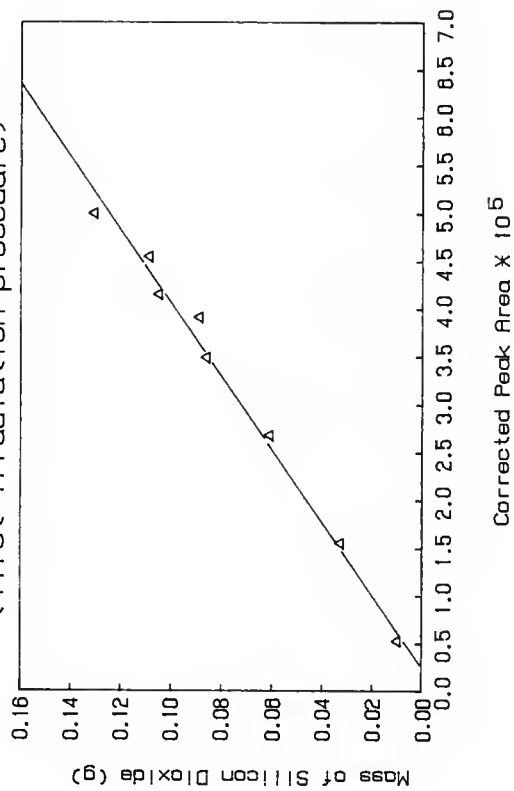


Figure 4.2 Calibration Line

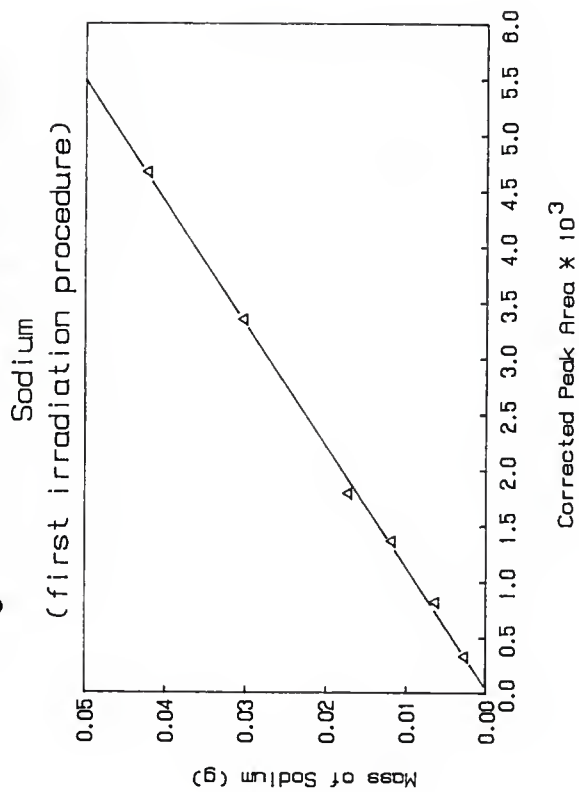


Figure 4.3 Calibration Line

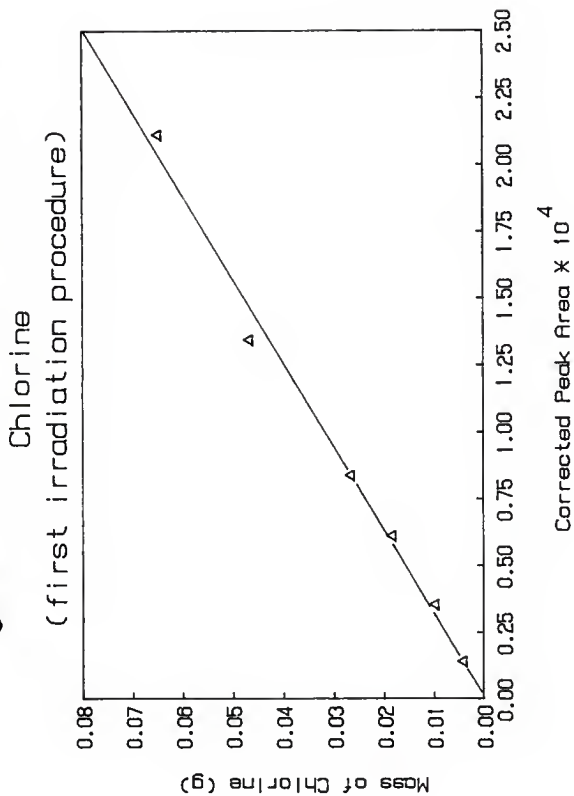


Table 4.2. Calibration Lines Relating Mass of Isotope to Corrected Peak Area (first irradiation procedure).

$$\hat{M}_{\text{SiO}_2} = 2543.88 P_a^C - 0.005315$$

(± 79.8)
 (± 0.0028)

Correlation coefficient = 0.9963

$$\Delta M_{\text{SiO}_2} = 79.79 P_a^C + 0.005586$$

$$\hat{M}_{\text{Na}} = 9.2022 P_a^C - 0.0004428$$

(± 0.154)
 (± 0.0004)

Correlation coefficient = 0.9990

$$\Delta M_{\text{Na}} = 0.1539 P_a^C + 0.0007177$$

$$\hat{M}_{\text{Cl}} = 322.85 P_a^C - 0.0006072$$

(± 11.2)
 (± 0.00125)

Correlation coefficient = 0.9955

$$\Delta M_{\text{Cl}} = 11.23 P_a^C + 0.001593$$

where: \hat{M}_i is the mass of a given element i calculated from the linear regression analysis. Slopes and intercepts are given with their most probable error.

ΔM_i is the maximum experimental error.

Figure 4.4 Calibration Line

Silicon Dioxide

(modified irradiation procedure)

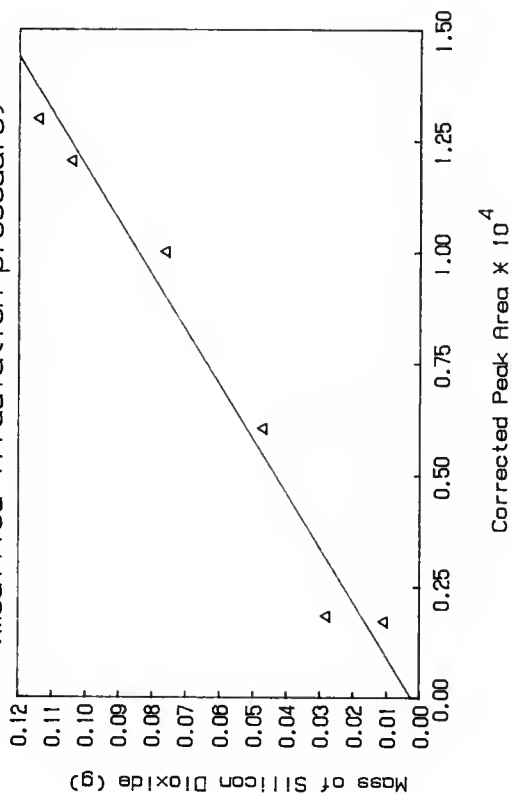


Figure 4.5 Calibration Line

Sodium

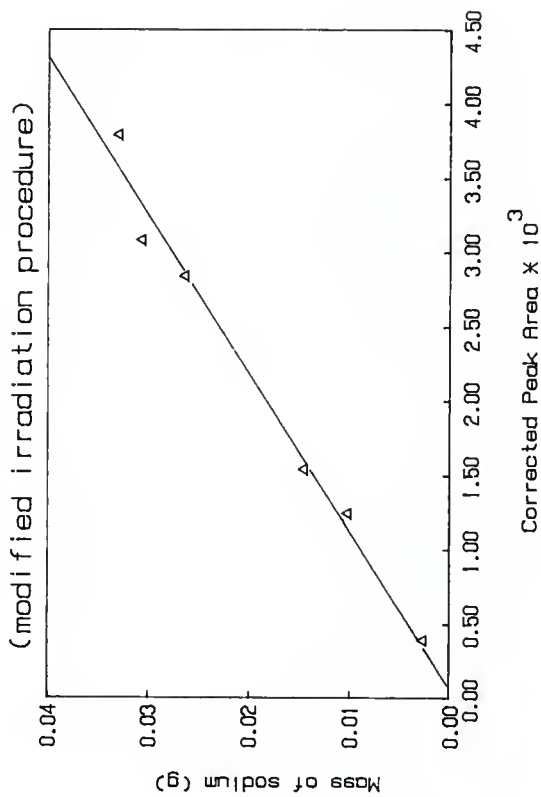


Figure 4.6 Calibration Line

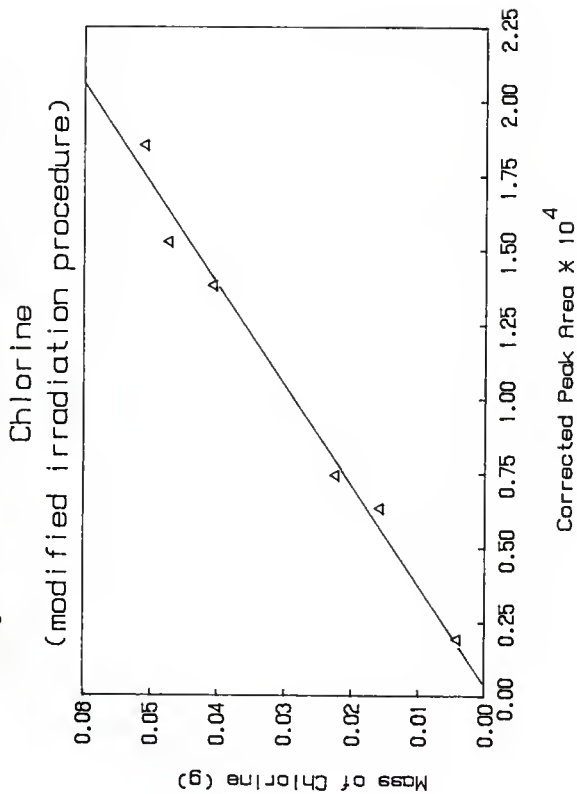


Table 4.3. Calibration Lines Relating Mass of Isotope to Corrected Peak Area (modified irradiation procedure).

$$\hat{M}_{\text{SiO}_2} = 870.078 P_a^C - 0.000846$$

$$(\pm 27.4) \quad (\pm 0.00046)$$

Correlation coefficient = 0.9880

$$\Delta M_{\text{SiO}_2} = 27.36 P_a^C + 0.0014$$

$$\hat{M}_{\text{Na}} = 9.5446 P_a^C - 0.0008782$$

$$(\pm 0.160) \quad (\pm 0.0008)$$

Correlation coefficient = 0.9928

$$\Delta M_{\text{Na}} = 0.1596 P_a^C + 0.001072$$

$$\hat{M}_{\text{Cl}} = 300.747 P_a^C - 0.001493$$

$$(\pm 10.5) \quad (\pm 0.003)$$

Correlation coefficient = 0.9930

$$\Delta M_{\text{Cl}} = 10.46 P_a^C + 0.003393$$

where: \hat{M}_i is the mass of a given element i calculated from the linear regression analysis. Slopes and intercepts are given with their most probable error.

ΔM_i is the maximum experimental error.

B.1.B. Results

The calibration lines from least squares linear regression based upon samples with known compositions, using the irradiation procedure described in Chapter III Section C, are shown in Figures 4.1-4.3 and summarized in Table 4.2. An example of the maximum experimental error calculation is given in Appendix C.

B.2. Calibration Lines For Modified Irradiation Procedure

The calibration lines from least squares linear regression based upon the samples with known compositions, using the modified irradiation procedure described in Chapter III Section H, are shown in Figures 4.4-4.6 and summarized in Table 4.3.

C. Verification of Technique

C.1. Experimental

The validity of the INAA method developed in Chapter III was verified by irradiating several samples containing known amounts of SiO_2 , NaCl and H_3BO_3 . The samples were prepared in the same manner as the standards prepared in Section B of this chapter, except that an electric soldering iron was used to seal the cap to the vial. The vial was sealed to prevent any H_3BO_3 from escaping due to volatilization. Care is required so as not to penetrate the vial. These samples with known composition were then irradiated at 225 kW for 6 minutes and counted as described in Chapter III.

C.2. Results

The results are listed in Table 4.4. The mass of H_3BO_3 was determined by subtracting the masses of SiO_2 and NaCl calculated via INAA from the sample mass. The mass of SiO_2 computed from INAA and the mass of SiO_2 as prepared agree within 2 percent for each sample, except Sample 5 which differs by 4.7 percent. The relative difference between the mass of NaCl computed from INAA and the mass of NaCl as prepared increases with increasing boron content. The relative difference for NaCl ranges from 0.0 to 17.6 percent with the actual NaCl mass being greater than or equal to that computed from INAA in all cases. For Samples 1 and 2, which had more than 5.8 weight percent boron, the actual NaCl mass was outside the computed maximum experimental range.

D. Discussion

The results in Table 4.4 indicate that the more boron present in a sample the greater the relative difference between the actual NaCl mass and the NaCl mass computed from INAA, with the actual mass always being larger. Thus, the mass of boron is affecting the activation of NaCl, but this was not anticipated.

Boron acts like a thermal neutron sink; that is, boron captures a significant number of thermal neutrons that pass through the cadmium filter [45]. So, a larger mass of boron will capture more thermal neutrons than a smaller one. Remember that it is the thermal neutrons

Table 4.4. Standards Checked to Verify Method Developed in This Work.

Sample	Actual Composition	Composition computed via INAA (± maximum experimental error)
1	0.088g SiO ₂	0.086 ± 0.009g SiO ₂
	0.033g NaCl	0.027 ± 0.003g NaCl
	0.112g H ₃ BO ₃	0.120g H ₃ BO ₃ ± 0.013g
2	0.091g SiO ₂	0.090 ± 0.009g SiO ₂
	0.038g NaCl	0.034 ± 0.003g NaCl
	0.064g H ₃ BO ₃	0.069g H ₃ BO ₃ ± 0.013g
3	0.100g SiO ₂	0.100g ± 0.009g SiO ₂
	0.020g NaCl	0.020g ± 0.003g NaCl
	0.019g H ₃ BO ₃	0.019g H ₃ BO ₃ ± 0.013g
4	0.074g SiO ₂	0.075 ± 0.008g SiO ₂
	0.106g H ₃ BO ₃	0.105g H ₃ BO ₃ ± 0.009g
5	0.102g SiO ₂	0.107 ± 0.009g SiO ₂
	0.067g H ₃ BO ₃	0.062g H ₃ BO ₃ ± 0.010g

Note: H₃BO₃ masses in the INAA column were determined by difference.

which activate NaCl. As increasing amounts of boron absorb more thermal neutrons, less NaCl is being activated.

Therefore, the NaCl mass computed from INAA would be different from the actual mass. Examination of the relevant equations will show that the mass of NaCl computed from INAA should be less than the actual mass of NaCl. Recall from Eq. (2) of Chapter II that the sample mass, s^M , is inversely proportional to ϕ_s , the flux of thermal neutrons striking the target nucleus, either Na or Cl in this case.

$$s^M = \frac{s^P a^K 1}{s^{\phi} \left[1 - e^{-\lambda_s t_r} \right] \left[e^{\lambda_s (t_s - t_r)} - e^{-\lambda_s (t_s - t_e)} \right]} \quad (11-2)$$

Further, it was assumed that ϕ_s was equal to ϕ_w , the flux of thermal neutrons striking the wire fluence monitor. Thus, under normal activation conditions, the following relationships hold.

$$s^M \propto \frac{1}{s^{\phi}} \quad (1a)$$

$$s^M \propto \frac{1}{w^{\phi}} \quad (1b)$$

where $\phi_s = \phi_w$.

However, boron absorbs thermal neutrons. This would indicate that ϕ_s would be less than ϕ_w because less neutrons are striking the Na or Cl target nucleus. Therefore $\frac{1}{s^{\phi}}$ is greater than $\frac{1}{w^{\phi}}$, indicating that the NaCl mass computed from INAA, which is based on $\frac{1}{w^{\phi}}$, should be

less than the actual mass of NaCl in the sample. The results given in Table 4.4 substantiate this argument.

It has been seen that the NaCl mass calculated from INAA will be less than the actual NaCl mass in the sample. Since the mass of boron is obtained by difference, the estimates for the mass of boron will be higher than the true mass. This can be seen in the following example.

$$\text{Boron Mass} = \text{Sample mass} - \text{SiO}_2 \text{ mass} - \text{NaCl mass} \quad (2)$$

Let sample mass = 20 g.

$$\text{SiO}_2 \text{ mass} = 10 \text{ g.}$$

$$\text{actual NaCl mass} = 5 \text{ g.}$$

$$\text{NaCl mass calculated from INAA} = 3 \text{ g.}$$

Hence,

$$\text{Actual Boron Mass} = 20 - 10 - 5 = 5 \text{ g.}$$

$$\text{Boron Mass Computed Via INAA} = 20 - 10 - 3 = 7 \text{ g.}$$

It is seen that the mass of boron computed via INAA is higher than the actual mass of boron in the sample. Therefore, all the estimates of the boron mass for samples containing NaCl will be too high using the INAA technique developed in this research.

For samples that contain NaCl, as the boron content in the sample increases, the more the estimate differs from the true value. Thus at low boron content the estimate will be close to the true value. For samples that contain less than 5.8 weight percent boron the actual boron mass is within the computed maximum experimental error range. Since boron losses occur at several steps during processing, it is anticipated that the actual boron content of the sample is rather low. This implies that the estimate of the boron content measured at this

time is close to the true value. A modified INAA method to obtain a more accurate NaCl mass estimate, and thus a more accurate estimate for the boron mass, will be discussed in Chapter XI (proposed future work).

E. Conclusions

Vials, reagents and standards were found to be free of elements that cause Al-28 interferences. The INAA method developed provides very accurate estimates for Si, Na, Cl and boron masses when the boron content is less than 2.3 weight percent. For samples containing less than 5.8 weight percent boron the actual boron content will be within the computed maximum experimental error range. It is anticipated that the actual boron content of the vast majority of samples analyzed in this research will be rather low. In these cases estimates of Si, Na, Cl and boron masses will be close to the true values.

LYOGEL ANO BOROSILICATE CHEMISTRY

V. REVIEW OF LYOGEL CHEMISTRY

VI. INAA OF $\text{SiO}_2 \cdot x\text{B}_2\text{O}_3$ LYOGELS

VII. PROCESSING OF BOROSILICATE LYOGELS: INAA OF SAMPLES FROM
GELATION AND POST-GELATION STAGES

VIII. FREEZE DRYING EXPERIMENT

IX. PREPARATION OF $\text{SiO}_2 \cdot x\text{B}_2\text{O}_3$ LYOGELS VIA CO-PRECIPITATION

X. CONCLUSIONS

A. Introduction

Gels may be separated into two types, colloidal systems and polymeric systems [36]. Although each are gels, there are fundamental differences in the gelling mechanism and nature of the gel in these systems. In colloidal systems gelation results from colloidal, or double layer, effects which also determine the interparticle distance at the gelling point. Gelling in polymeric systems occurs due to condensation polymerization. The nature and kinetics of these reactions determine the properties of the gel and the resultant inorganic polymer.

Partlow and Yoldas [36] have discussed colloidal systems. A colloidal system may be described as a dispersion of particles in a liquid medium. The diameter of the particle is usually less than 1000 Å. Each particle has a surface charge and associated electric double layer. The dispersion is caused by a mutual repulsion of similar surface charges. When particles approach each other their diffuse double layers begin to interfere. This interference causes changes in the distribution of the ions in the double layer of each particle, and the free energy of the system increases. Thus work must be performed to bring about these changes. This work manifests itself as a repulsion between the particles. Ions of indifferent and potential-determining electrolytes, such as HNO_3 , HCl , NH_4^+ and OH^- , are present in the interface at the particle surface due to alignment of charges.

Therefore, an effective net electrical field is present at a distance from the particle. This situation is shown schematically in Figure 5.1. Sol particles are represented as spheres in a box.

Initially, uncharged or weakly charged sol particles rest randomly at the bottom of the box (Figure 5.1A), similar to a precipitate. As the surface charge on these particles is increased (Figure 5.1B), a net repulsion between particles results and they can move freely within the box, provided that the particles have sufficiently little mass. In this state the system is called a sol. If the volume of the "box" is decreased, a point is reached where interaction of the electric double layers prevents translatory movement. The occurrence of this non-fluid state indicates the gelling point (Figure 5.1C). A similar state may be initiated by decreasing the solvent content, thus effectively decreasing the interparticle distance. Figure 5.2 shows the analogous transition from a precipitate (Figure 5.2A) to a sol (5.2B), to the gel (5.2C), and finally, to the dried gel (5.2D). In this case the volume of the liquid may be likened to a box within which the particles are restrained.

Partlow and Yoldas [36] have discussed polymer systems. The polymer system is one of the few gel systems where a true oxide network is formed by chemical polymerization in the liquid at or near room temperature [37,38]. Alkoxides are standard starting materials for this process, but hydrolysis of most alkoxides yields a fine oxide powder [39]. However, under appropriate conditions, these reactions can result in polymerization to form an inorganic polymer.

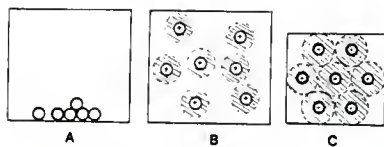


Figure 5.1. Schematic representation of charge effect in a colloidal sol [36].

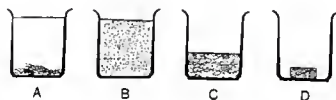


Figure 5.2. Transition from a precipitate to a dried colloidal gel [36].

Polymerization and gelation occur only when soluble polymerizable species are present in the liquid.

Because of fundamental differences in the microstructure between polymeric gels and colloidal gels they behave differently. Furthermore, there are differences among various polymer systems which can be broken down into two distinct types (Figure 5.3). In the first type, Type I as per Yoldas [36], the polymer species are formed by initial polymerization to form oligomers. Evaporation of solvent leads to physical entanglement of the oligomers and a gel is formed. In the second type, Type II [36], the chemical reactions leading to polymerization and network formation take place throughout the liquid. Active species slowly build up an inorganic network by eliminating alkyl groups from the structure by chemical reaction. If the reaction rate and behavior is such that continuity is maintained, a gel will form.

The sol-gel process for making glasses and ceramics has been studied intensively in recent years. Within the last six years, at least eight symposia have been devoted to this area of research [41-48]. Borosilicates and boron containing materials have been the focus of much research in sol-gel processing. For example, at the Fourth International Workshop on Glasses and Glass Ceramics from Gels [49] 8 percent of the papers discussed borosilicates, while 14 percent discussed boron containing materials. Most researchers have assumed that the as-batched composition is the true composition. However, Nogami and Moriya [50] and Brinker and Scherer [70] have shown

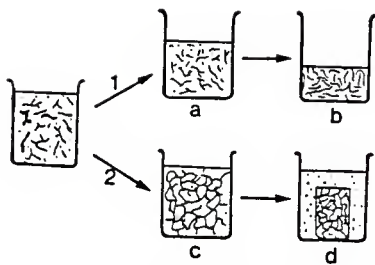


Figure 5.3. Polymer solutions exhibit two methods of gelation [36].

differences between the as-batched compositions and the actual composition (Tables 5.1A and 5.1B).

Examination of Tables 5.1A and 5.1B shows that the final product contains less boron than was batched. Exploring the borosilicate chemistry will explain these results.

B. General Aspects of Gel Synthesis

The most common sol-gel process utilizes metal alkoxides of network forming elements ($M(OR)_x$, where M is Si, B, Ti, Al, etc., and R is often an alkyl group) [7]. $M(OR)_x$ undergoes hydrolysis typically with an alcohol as the solvent. The alkoxide groups are removed stepwise by hydrolysis (generally using acid or base catalysts) and are replaced by hydroxyl groups (Reaction 1) [7]. Subsequent condensation reactions involving the hydroxyl groups yield soluble oligomeric species consisting of $-M-O-M-$ or $-M_1-O-M_2-$ linkages [Reactions (2) to (6)] [7,51].

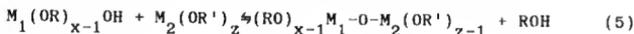
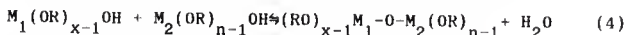
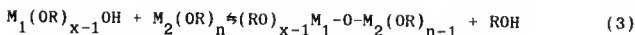
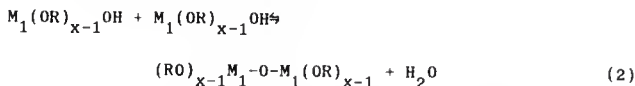
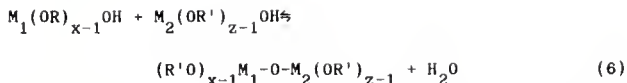


Table 5.1A. Chemical Compositions of Borosilicate Glasses [50].

As-batched Composition (mol %)	Analyzed Composition (mol %)
$\text{SiO}_2 \cdot 0.176\text{B}_2\text{O}_3$	$\text{SiO}_2 \cdot 0.17\text{B}_2\text{O}_3$
$\text{SiO}_2 \cdot 0.25\text{B}_2\text{O}_3$	$\text{SiO}_2 \cdot 0.24\text{B}_2\text{O}_3$
$\text{SiO}_2 \cdot 0.43\text{B}_2\text{O}_3$	$\text{SiO}_2 \cdot 30\text{B}_2\text{O}_3$
$\text{SiO}_2 \cdot 0.67\text{B}_2\text{O}_3$	$\text{SiO}_2 \cdot 0.42\text{B}_2\text{O}_3$
$\text{SiO}_2 \cdot \text{B}_2\text{O}_3$	$\text{SiO}_2 \cdot 0.46\text{B}_2\text{O}_3$

Table 5.1B. Chemical Compositions (wt %) For Three Preparations of the Following Batched Composition (wt %): 71.1 SiO_2 , 18.3 B_2O_3 , 7.1 Al_2O_3 , 3.6 BaO [70].

	SiO_2	B_2O_3	Al_2O_3	BaO
LpH5	80.3	6.9	9.8	3.0
MpH5	76.8	11.2	9.0	2.9
HpH12	74.4	12.9	9.6	3.0

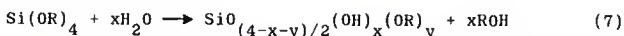


When preparing a lyogel from more than one alkoxide, one must start with an alkoxide which is slow to hydrolyze [40]. The slowest hydrolysing alkoxide is first rendered to an active polymerizing species as described previously, while the fast hydrolysing alkoxide is kept in its unreacted form so that self-polymerization cannot occur. If this procedure is not followed, inhomogeneities, such as the precipitation of boric acid, $B(OH)_3$, will result [52]. For example, if one were to initially form a self-polymerizing species from a fast hydrolysing alkoxide and try to react it with a slow hydrolysing alkoxide, the fast hydrolysing alkoxide would self-polymerize faster than the condensation reaction with the slow hydrolysing alkoxide. An inhomogeneity would result. However, if the slow hydrolysing alkoxide is partially hydrolysed first and then reacted with the unreacted fast hydrolysing alkoxide, dissimilar constituents tend to become neighbors. For example, one would expect $-M_1-O-M_2-$ rather than $-M_1-O-M_1-$. Thus better homogeneity is attained [40].

The product of these reactions generally remains liquid due to the absence of sufficient number of hydroxyl groups in solution that can react with the network and complete polymerization. After all constituents are introduced and chemical bonds are formed, excess water is added to remove remaining -OR groups. This usually causes polymerization to a gel.

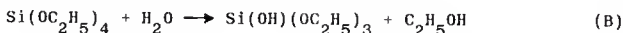
C. Borosilicate Lyogel Synthesis

Voldas [40] has described the hydrolysis of silicon alkoxides. These alkoxides, even in excess water, do not completely hydrolyse to an -OR-free complex such as $\text{SiO}_{(4-x)/2}(\text{OH})_x$. Unlike hydrolysis of boron alkoxides, -OR and OH^- radicals can co-exist in large numbers in the hydrolysed product.

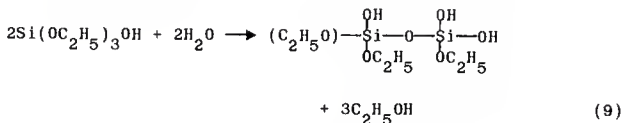


Reaction (7) is a simplified form of a series of condensation reactions involving polymerization of species containing OH^- and -OR groups to form bridging oxygens similar to those shown in Reactions (2) to (6).

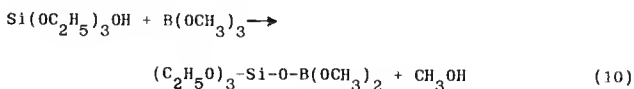
Starting with tetraethylorthosilicate as the silicon alkoxide, the hydrolysis would proceed as follows.

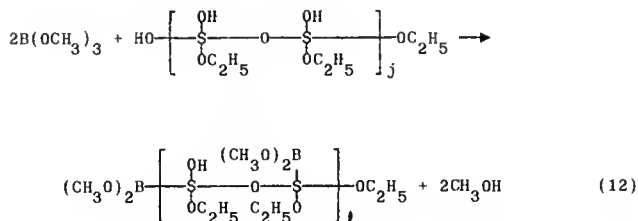
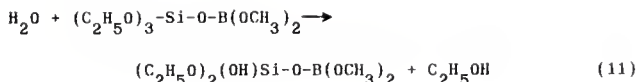


Further hydrolysis-polymerization reactions yield [52]



After the boron alkoxide, $\text{B}(\text{OCH}_3)_3$, is introduced, reactions of the following types occur [53,54].





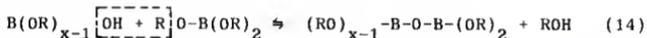
For a low concentration of $\text{B}(\text{OCH}_3)_3$, there are enough silanol groups available to react with $\text{B}(\text{OCH}_3)_3$. However, with an increasing content of $\text{B}(\text{OCH}_3)_3$ some will not react with the silanol groups. This excess $\text{B}(\text{OCH}_3)_3$ causes self-polymerization and results in the precipitation of boric acid, $\text{B}(\text{OH})_3$ [54]. (The solubility of $\text{B}(\text{OH})_3$ in alcohol is 5.56g per 100 cc of alcohol [71].) The chemical reaction is as follows [72,73].



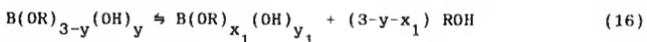
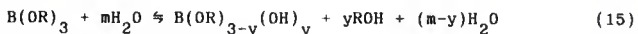
The addition of excess water removes $-\text{OCH}_3$ and $-\text{OC}_2\text{H}_5$ groups from the borosilicate network formed in Reaction (12). Continued polymerization results in a borosilicate lyogel which has the formula $\text{SiO}_2 \cdot x\text{B}_2\text{O}_3$.

When $B(OR)_3$ is mixed with water, a series of intermediate species, such as $B(OR)_2OH$, $B(OR)(OH)_2$, and $B(OH)_3$, initially form depending upon the degree of hydrolysis [40] (Reaction 1). Yoldas [40] has discussed the applicable boron chemistry. What follows is a summary of the material found in that paper.

The relative concentrations of the various boron intermediate species will depend on the availability of water and the dilution of the system. By diluting the aikoxides and the water with alcohol before mixing, it is possible to control the type and extent of initial hydrolysis in these reactions. Initial species immediately undergo a series of condensation reactions resulting in the formation of secondary species with bridging oxygens.



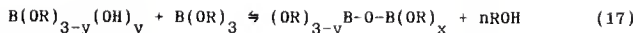
The formation of initial intermediate species and their condensation to form polymer chains can be represented by the following general equations.



where: $0 < y < 3$

$$y = \frac{1}{2}(y_1 + 3 + x_1).$$

In this system, $-OR$ and OH^- groups react with each other and form bridging oxygens, releasing alcohol until one of the groups is completely eliminated.



where: $0 < y < 3$

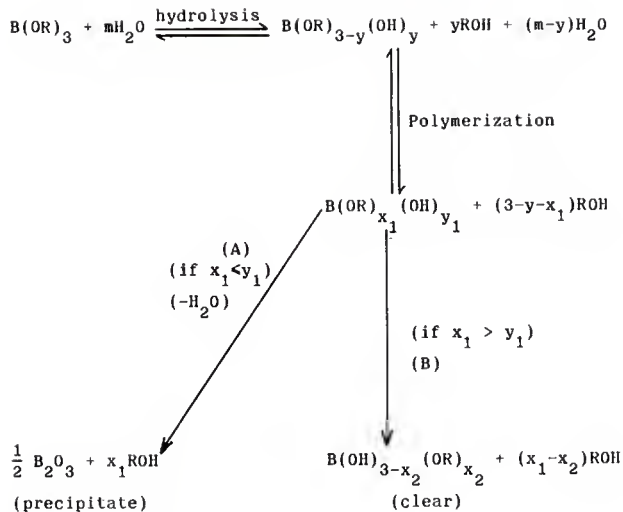
$$x + n = 3.$$

If $B(OR)_{3-y}(OH)_y$ contains sufficient hydroxyl groups (if $y > 3-y$ in Reaction 15), polymerization continues until all $-OR$ groups are removed from the network. Thus precipitation of boric oxide occurs. If there are an insufficient number of hydroxyl groups to remove all the $-OR$ groups (if $(3-y) > y$ in Reaction 15), then the polymer network contains $-OR$ groups in the structure. When this occurs the network remains soluble in alcohol and available for polymerization with constituents. A reaction scheme representing precipitation of B_2O_3 and formation of soluble and polymerizable species from boron alkoxide is shown in Figure 5.4 [40].

D. Tetravalent Boron

Nuclear magnetic resonance measurements [59], infrared [60] and Raman spectra [61] have shown that increasing the sodium content of a borate glass introduces a corresponding number of tetravalent boron atoms. Thus, the coordination of the boron with neighboring Na^+ ions changes from a three connected network to a four connected network (Figure 5.5) [62]. The resulting negative charge on the tetravalent boron atoms is balanced by the associated Na^+ ions.

Leaching studies of borosilicate glasses have shown that the stability of $=B-O-B=$ bonds toward hydrolysis increases with the sequential replacement of trigonal borons with tetrahedral borons



where: $0 < y < 3$

$$y = \frac{1}{2}(y_1 + 3 + x_1)$$

$$y_1 = 3 - 2x_2 + x_1$$

if $m > 1.5$: $x_2 < 0$ (does not exist)

if $m < 1.5$: $x_2 > 0$

Figure 5.4 Formation of boron oxide (A); and a clear solution containing network-forming species (B) by the hydrolysis of boron alkoxides (modified from Ref. 40).

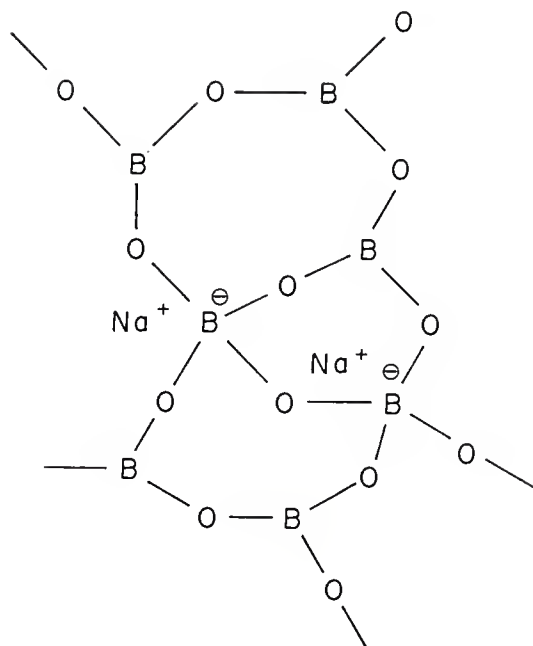
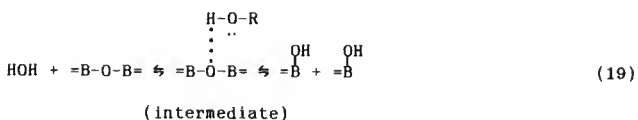
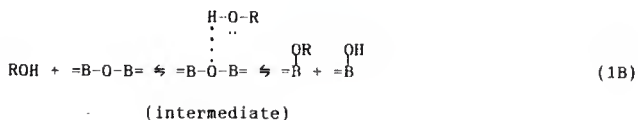
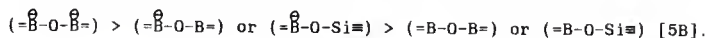


Figure 5.5. Change in connectivity of a boric oxide network produced by introduction of cations [62].

[58]. The results of that study can be explained on the basis of the stability of =B-O-B= bonds towards dissociative reactions of the type:



Because boron has no available low energy d orbitals, tetrahedrally coordinated boron cannot form the five coordinate sp^3d transition state required for S_N2 (substitutional second order nucleophilic) reactions of the type shown in Reactions (18) and (19). Tetrahedral borons involved in $\overset{\ominus}{\text{B}}-\text{O}-\overset{\ominus}{\text{B}}$ and $\overset{\ominus}{\text{B}}-\text{O}-\text{Si}\equiv$ are coordinately saturated and therefore cannot participate in these nucleophilic dissociation processes. Thus, the kinetic stability of $\overset{\ominus}{\text{B}}-\text{O}-\overset{\ominus}{\text{B}}$ and $\overset{\ominus}{\text{B}}-\text{O}-\text{Si}\equiv$ bonds would be expected to decrease in the following order:



CHAPTER VI. INAA OF $\text{SiO}_2 \cdot x\text{B}_2\text{O}_3$ LYOGELS

A. Introduction

The major disadvantage of the sol-gel method is the large uncontrolled shrinkage of the gel during the drying and sintering processes [18]. For many previous studies when the final product developed cracks, the synthesis conditions were changed by varying reactant concentrations, solvents or other parameters. Few attempts were made to change the gel once it was formed. The research presented in this thesis is a continuation of the work done by Angell [8] in attempting to separate the effects due to gel synthesis from effects due to swelling or syneresis in the post-gellation step. The goal was to reduce the problems associated with the drying process by first minimizing the gel volume in the wet state. This was accomplished by placing the gels in solutions which might induce syneresis, and thus shrinkage of the gel prior to drying.

When placed in an electrolyte solution, a charged surface, such as a borosilicate gel, will attract counterions and repel co-ions. Thus electrolyte in the solvent reduces the effective surface charge of the borosilicate network. As the effective surface charge of the borosilicate is reduced, the distance between neighboring segments of the network is decreased. The result is that the gel volume is reduced.

Most of the research presented in this thesis was in response to questions that arose from the swelling data given by Angell (Figure 6.1) [8]. It is seen that some of the swelling behavior of the

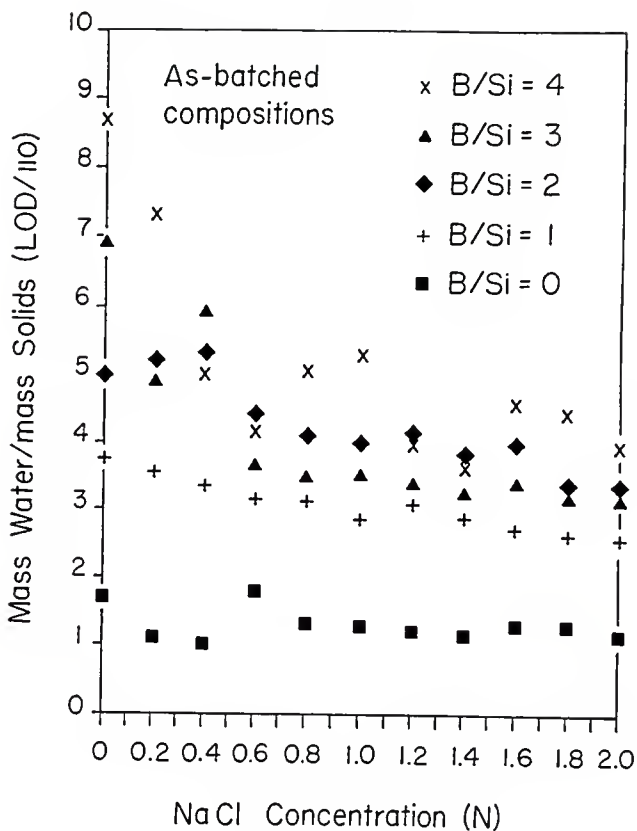


Figure 6.1. Solvent content of $\text{SiO}_2 \cdot x\text{B}_2\text{O}_3$ lyogels as a function of electrolyte concentration (modified from Ref.31).

lyogels are identical, but that the lyogels had different as-batched compositions. This suggests that the actual composition of the lyogel might be different from the as-batched composition.

B. Experimental

Borosilicate lyogels were synthesized by Angell [8]. The author and Angell subsequently placed them in NaCl solutions of varying concentrations in an attempt to induce syneresis, and thus reduce lyogel volume or solvent content. After the lyogels were swelled, they were dried at 110°C to determine the mass of solvent evaporated, as one indication of the degree of swelling. Samples were prepared, irradiated and counted as described previously in Sections A to G of Chapter III, INAA Procedure Development. Calculations using INAA data were facilitated by software provided by Higginbotham [32]. The software was debugged by the author since this was the first application for which it had been used. A sample calculation is shown in Appendix 8.

C. SiO₂·xB₂O₃ and NaCl Composition Results

Lyogel compositions were determined by the INAA procedure developed in this work. The resulting spectra for various samples are shown in Figures 6.2 to 6.7.

Complete INAA results are listed in Table 6.1. It is evident from these data that the as-batched compositions are significantly different from those computed via INAA. Boron losses are occurring during the synthesis and drying processes.

Figure 6.2
Silica
(in 0.0 N NaCl)

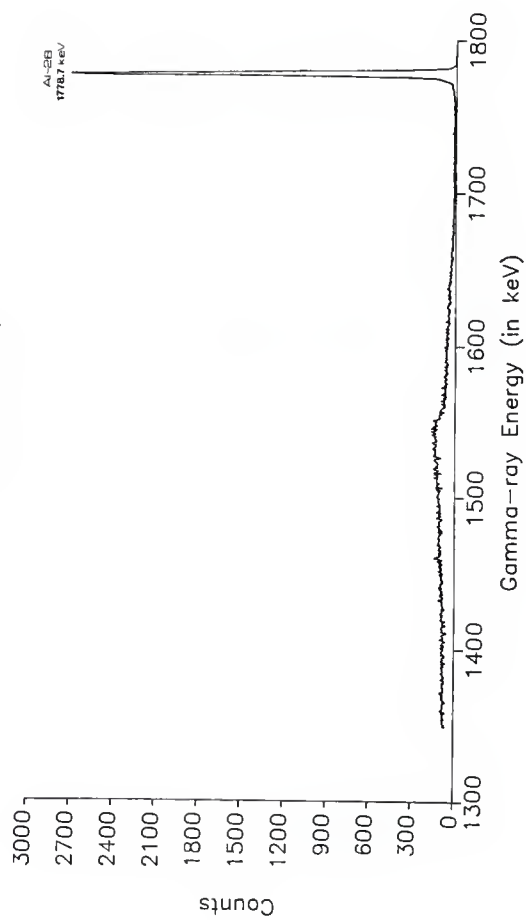


Figure 6.3
Silica
(in 1.0 N NaCl)

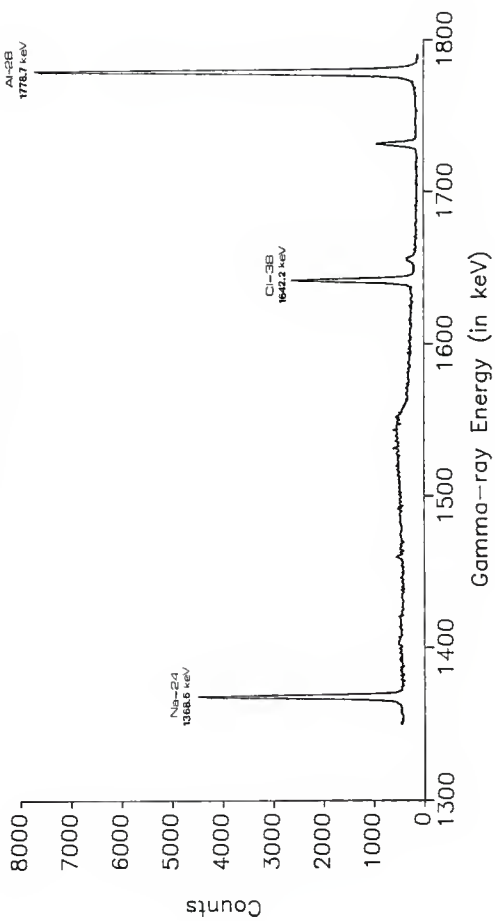


Figure 6.4
Silica
(in 2.0 N NaCl)

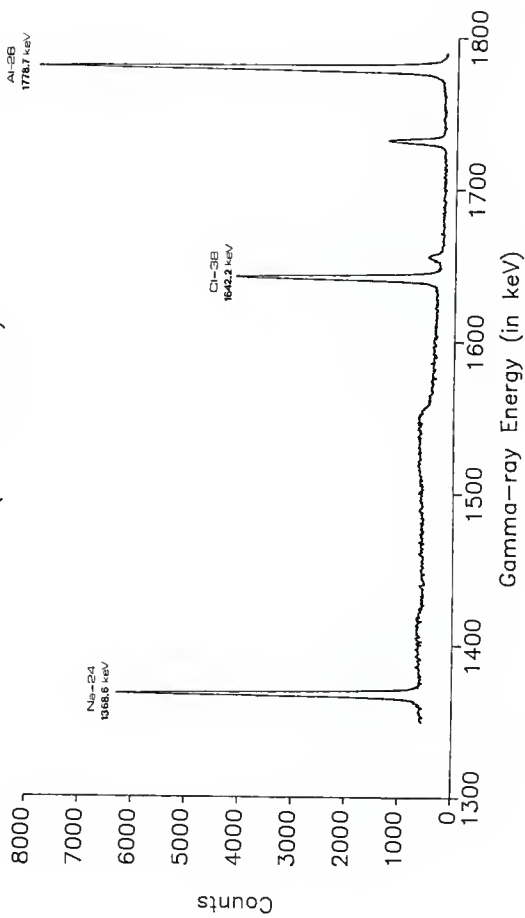


Figure 6.5
B:Si Ratio = 4
(in 0.0 N NaCl solution)

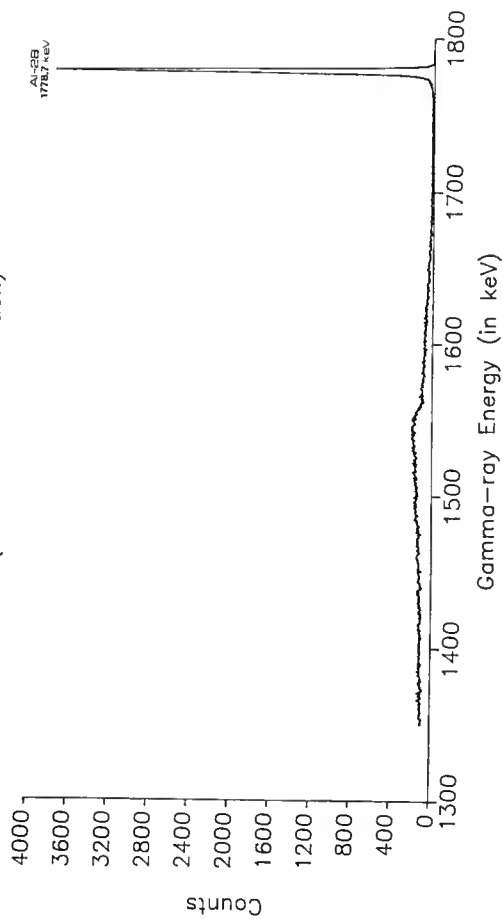


Figure 6.6
B:Si Ratio = 4
(in 1.0 N NaCl solution)

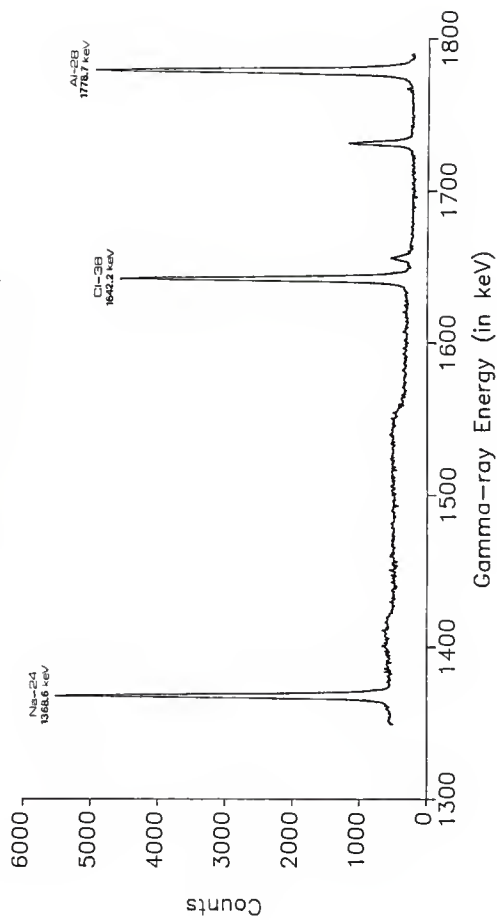


Figure 6.7
B:Si Ratio = 4
(in 2.0 N NaCl solution)

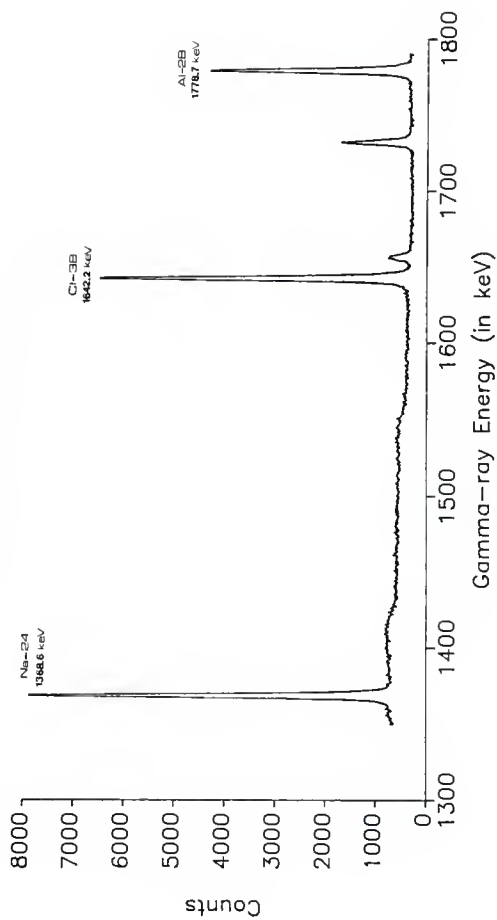


Table 8.1. INMA Composition of Borosilicate Lyogels Synthesized by Angell [8].

As-batched Composition	Constituent mass (g) (± maximum experimental error)			Composition Via INMA	
	Sample Mass (g)	0.0N	1.0N		2.0N
SiO ₂	0.0N: 0.079	0.080g SiO ₂	0.115g SiO ₂ (±0.003)	0.117g SiO ₂ (±0.003)	SiO ₂
	1.0N: 0.113	(±0.006g)	0.002g Na (±0.001)	0.005g Na (±0.001)	
	2.0N: 0.123		0.002g Cl (±0.002)	0.008g Cl (±0.002)	
SiO ₂	0.0N: 0.114	0.121g SiO ₂	0.109g SiO ₂ (±0.009)	0.095g SiO ₂ (±0.009)	SiO ₂
	1.0N: 0.114	(±0.010g)	0.005g Na (±0.001)	0.007g Na (±0.001)	
	2.0N: 0.124		0.005g Cl (±0.002)	0.011g Cl (±0.002)	
SiO ₂ ¹ B ₂ O ₃	0.0N: 0.084	0.092g SiO ₂	0.113g SiO ₂ (±0.009)	0.095g SiO ₂ (±0.009)	0.0N: SiO ₂ -0B ₂ O ₃
	1.0N: 0.124	(±0.009g)	0.006g Na (±0.001)	0.008g Na (±0.001)	1.0N: SiO ₂ -0B ₂ O ₃
	2.0N: 0.114		0.010g Cl (±0.002)	0.014g Cl (±0.002)	2.0N: SiO ₂ -0B ₂ O ₃
SiO ₂ ¹ B ₂ O ₃	0.0N: 0.116	0.120g SiO ₂	0.099g SiO ₂ (±0.009)	0.086g SiO ₂ (±0.009)	0.0N: SiO ₂ -0B ₂ O ₃
	1.0N: 0.112	(±0.010g)	0.004g Na (±0.001)	0.008g Na (±0.001)	1.0N: SiO ₂ -0.024B ₂ O ₃
	2.0N: 0.121		0.007g Cl (±0.002)	0.013g Cl (±0.002)	2.0N: SiO ₂ -0.010B ₂ O ₃
SiO ₂ ¹ B ₂ O ₃	0.0N: 0.116	0.121g SiO ₂	0.101g SiO ₂ (±0.009)	0.083g SiO ₂ (±0.008)	0.0N: SiO ₂ -0B ₂ O ₃
	1.0N: 0.111	(±0.001g)	0.006g Na (±0.001)	0.013g Na (±0.001)	1.0N: SiO ₂ -0B ₂ O ₃
	2.0N: 0.120		0.011g Cl (±0.002)	0.022g Cl (±0.002)	2.0N: SiO ₂ -0.010B ₂ O ₃
				0.001g B ₂ O ₃ (±0.013)	

Table 6.1. (cont'd)

As-batched Composition	Sample Mass (g)	Constituent mass (g) (± maximum experimental error)			Composition Via INAA
		0.0N	1.0N	2.0N	
$\text{SiO}_2\text{-B}_2\text{O}_3$ $\text{SiO}_2\text{-B}_2\text{O}_3$	0.0N: 0.114	0.112g SiO_2 (±0.009)	0.091g SiO_2 (±0.009)	0.095g SiO_2 (±0.009)	0.0N: $\text{SiO}_2\text{-OB}_2\text{O}_3$
	1.0N: 0.111		0.006g Na (±0.001)	0.012g Na (±0.001)	1.0N: $\text{SiO}_2\text{-0.052B}_2\text{O}_3$
	2.0N: 0.11B		0.009g Cl (±0.002)	0.019g Cl (±0.002)	2.0N: $\text{SiO}_2\text{-OB}_2\text{O}_3$
			0.006g B_2O_3 (±0.012)		
$\text{SiO}_2\text{-B}_2\text{O}_3$ $\text{SiO}_2\text{-B}_2\text{O}_3$	0.0N: 0.107	0.113g SiO_2 (±0.009)	0.100g SiO_2 (±0.009)	0.098g SiO_2 (±0.009)	0.0N: $\text{SiO}_2\text{-OB}_2\text{O}_3$
	1.0N: 0.116		0.005g Na (±0.001)	0.009g Na (±0.001)	1.0N: $\text{SiO}_2\text{-OB}_2\text{O}_3$
	2.0N: 0.12B		0.012g Cl (±0.002)	0.015g Cl (±0.002)	2.0N: $\text{SiO}_2\text{-0.052B}_2\text{O}_3$
			0.006g B_2O_3 (±0.013)		
$\text{SiO}_2\text{-B}_2\text{O}_3$ $\text{SiO}_2\text{-B}_2\text{O}_3$	0.0N: 0.125	0.128g SiO_2 (±0.001)	0.101g SiO_2 (±0.009)	0.068g SiO_2 (±0.008)	0.0N: $\text{SiO}_2\text{-OB}_2\text{O}_3$
	1.0N: 0.118		0.007g Na (±0.001)	0.015g Na (±0.001)	1.0N: $\text{SiO}_2\text{-OB}_2\text{O}_3$
	2.0N: 0.115		0.012g Cl (±0.002)	0.024g Cl (±0.002)	2.0N: $\text{SiO}_2\text{-0.111B}_2\text{O}_3$
			0.011g B_2O_3 (±0.012)		
$\text{SiO}_2\text{-B}_2\text{O}_3$ $\text{SiO}_2\text{-B}_2\text{O}_3$	0.0N: 0.109	0.112g SiO_2 (±0.009)	0.107g SiO_2 (±0.009)	0.079g SiO_2 (±0.008)	0.0N: $\text{SiO}_2\text{-OB}_2\text{O}_3$
	1.0N: 0.126		0.009g Na (±0.001)	0.012g Na (±0.001)	1.0N: $\text{SiO}_2\text{-OB}_2\text{O}_3$
	2.0N: 0.127		0.013g Cl (±0.002)	0.019g Cl (±0.002)	2.0N: $\text{SiO}_2\text{-0.1B}_2\text{O}_3$
			0.017g B_2O_3 (±0.012)		

Table B.1. (cont'd)

Constituent mass (g)
(± maximum experimental error)

As-batched Composition	Sample Mass (g)	0.0N	1.0N	2.0N	Composition Via INAA
$SiO_2 B_2 O_3$	0.0N: 0.113	0.106g SiO_2 (±0.009)	0.092g SiO_2 (±0.009)	0.062g SiO_2 (±0.008)	0.0N: SiO_2 -0.054B ₂ O ₃
	1.0N: 0.10B	0.007g Na (±0.001)	0.007g Na (±0.001)	0.014g Na (±0.001)	1.0N: SiO_2 -0B ₂ O ₃
	2.0N: 0.10B	0.007g B ₂ O ₃ (±0.010)	0.012g Cl (±0.002)	0.018g Cl (±0.002) 0.016g B ₂ O ₃ (±0.012)	2.0N: SiO_2 -0.223B ₂ O ₃
$SiO_2-2B_2O_3$	0.0N: 0.109	0.101g SiO_2 (±0.009)	0.084g SiO_2 (±0.008)	0.058g SiO_2 (±0.008)	0.0N: SiO_2 -0.073B ₂ O ₃
	1.0N: 0.11B	0.011g Na (±0.001)	0.011g Na (±0.001)	0.014g Na (±0.001)	1.0N: SiO_2 -0.074B ₂ O ₃
	2.0N: 0.122	0.009g B ₂ O ₃ (±0.010)	0.016g Cl (±0.002)	0.024g Cl (±0.002) 0.007g B ₂ O ₃ (±0.013) 0.026g B ₂ O ₃ (±0.012)	2.0N: SiO_2 -0.387B ₂ O ₃

Note: Mass of B₂O₃ obtained by difference.

For higher boron concentrations, a doubling of the NaCl mass in the swelling solution did not result in a doubling of the sodium and chloride retained in the processed lyogels. Figure 6.8 shows the solvent content of $\text{SiO}_2 \cdot x\text{B}_2\text{O}_3$ lyogels as a function of electrolyte concentration, the as-batched compositions, and the compositions calculated from INAA. The as-batched compositions have a significantly higher boron content than those from those calculated from INAA data. The water content of the lyogel decreases as the electrolyte content increases. The data is linear for lyogels with an as-batched boron concentration less than $\text{SiO}_2 \cdot \frac{1}{4}\text{B}_2\text{O}_3$. The data for lyogels with as-batched boron concentrations of $\text{SiO}_2 \cdot \frac{1}{2}\text{B}_2\text{O}_3$ and greater are non-linear.

The B/Si cation ratio obtained from INAA versus the B/Si cation ratio (as batched) is shown in Figure 6.9. Lyogels swelled in 2.0N NaCl solutions have much higher B/Si cation ratios than those swelled in 0.0N or 1.0N NaCl solutions. Lyogels swelled in 0.0N or 1.0N NaCl solution exhibit B/Si cation ratios which are identical within experimental error.

D. Discussion

The dried samples contain the sodium and chloride ions present in the lyogel solvent. This results in a higher solids content due to the retention of sodium and chloride ions by the lyogel upon drying. Estimates of the mass ratio of electrolyte solution to borosilicate

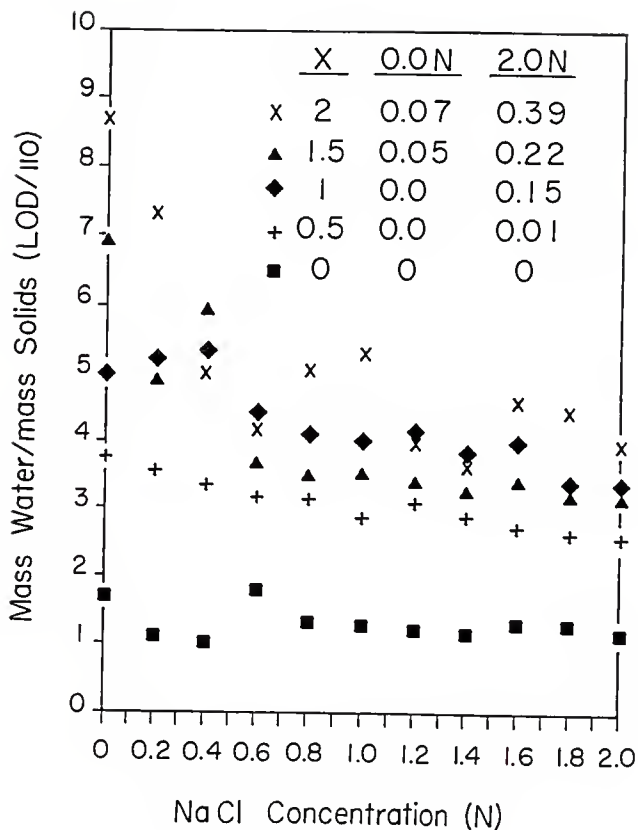


Figure 6.8. Solvent content of $\text{SiO}_2 \cdot x\text{B}_2\text{O}_3$ lyogels as a function of electrolyte concentration and also composition results from INAA (modified from Ref.31).

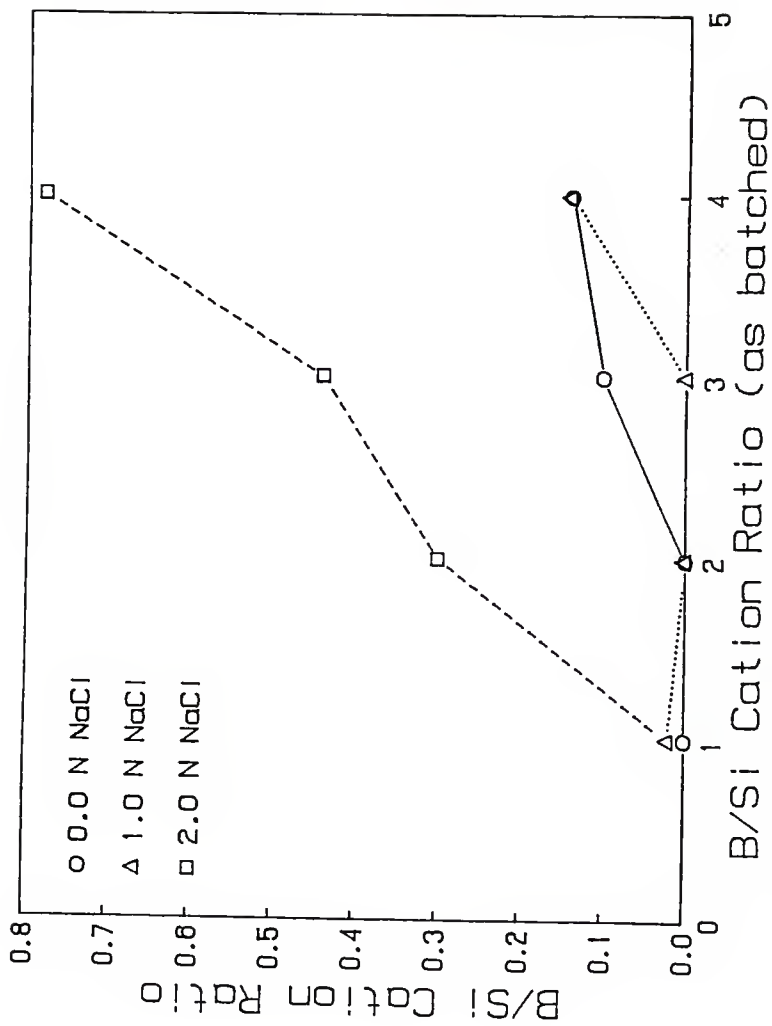


Figure 6.9. B/Si cation ratio obtained from INAA versus B/Si cation ratio (as-batched).

solids show that this corrected ratio is nearly constant with respect to electrolyte concentration for SiO_2 and $\text{SiO}_2 \cdot \frac{1}{4}\text{B}_2\text{O}_3$ lyogels. The non-linearities apparent in the data in Figure 6.8 are present in the corrected data although much less distinct [31].

The swelling behavior is controlled by the electrolyte concentration of NaCl swelling solutions. Increasing electrolyte in the lyogel solvent negates the effects of the surface charges at the liquid-solid interface of the lyogel. This causes a specific adsorption of ions and compression of the double layer. As the effective surface charge of the lyogel is reduced, the distance between neighboring segments of the network is reduced. The result is a reduction in lyogel volume and a corresponding decrease in solvent/solids mass ratio.

The as-batched compositions are significantly higher in boron content than those computed via INAA. This was expected from the data of Nogami and Moriya (Table 6.2A) [50]. The boron content of the unrinsed lyogels discussed herein also reveals such differences (Table 6.2B). However, the boron compositions dropped significantly upon rinsing the residual reactants and ethanol from the lyogels. For example, a dried lyogel having an as-batched composition of $\text{SiO}_2 \cdot \text{B}_2\text{O}_3$ was shown to have a composition of $\text{SiO}_2 \cdot 0.27\text{B}_2\text{O}_3$ prior to rinsing with water. Following equilibration for 28 days in deionized water, the boron content of the lyogel was negligible.

Table 6.2A. Chemical Compositions of Borosilicate Glasses [50].

As-batched Composition (mol %)	Analyzed Composition (mol %)
$\text{SiO}_2 \cdot 0.176\text{B}_2\text{O}_3$	$\text{SiO}_2 \cdot 0.17\text{B}_2\text{O}_3$
$\text{SiO}_2 \cdot 0.25\text{B}_2\text{O}_3$	$\text{SiO}_2 \cdot 0.24\text{B}_2\text{O}_3$
$\text{SiO}_2 \cdot 0.43\text{B}_2\text{O}_3$	$\text{SiO}_2 \cdot 0.30\text{B}_2\text{O}_3$
$\text{SiO}_2 \cdot 0.67\text{B}_2\text{O}_3$	$\text{SiO}_2 \cdot 0.42\text{B}_2\text{O}_3$
$\text{SiO}_2 \cdot \text{B}_2\text{O}_3$	$\text{SiO}_2 \cdot 0.46\text{B}_2\text{O}_3$

Table 6.2B. Chemical Compositions of Unrinsed Borosilicate Lyogels (This Work).

As-batched Composition (mol %)	Analyzed Composition (mol %)
$\text{SiO}_2 \cdot 0.25\text{B}_2\text{O}_3$	$\text{SiO}_2 \cdot 0\text{B}_2\text{O}_3$
$\text{SiO}_2 \cdot 0.75\text{B}_2\text{O}_3$	$\text{SiO}_2 \cdot 0.26\text{B}_2\text{O}_3$
$\text{SiO}_2 \cdot \text{B}_2\text{O}_3$	$\text{SiO}_2 \cdot 0.27\text{B}_2\text{O}_3$

The data above indicate that the co-polymerization reactions at the conditions used did not result in a homogeneous product. Rinsing followed by swelling followed by drying at 110°C resulted in a decreased B/Si cation ratio. Low molecular weight boron-rich species were distributed throughout a silicon-rich lyogel network, and more of the boron-rich species than the silicon-rich species is being removed by rinsing with water. Although the lyogels described above demonstrated significant differences in their swelling behavior in electrolyte solutions, the differences in the boron content of these lyogels were limited. Therefore, differences exist in the charge distribution in these networks as a consequence of the addition of boron in lyogel synthesis but cannot be explained as a direct consequence of the boron concentration of the network itself.

As the NaCl concentration in the swelling solution increased, the B/Si cation ratio increased. Depending on the pH, Na^+ addition causes boron to change from trigonal to tetrahedral coordination. As discussed previously in Section D of Chapter V, tetrahedral boron is coordinately saturated and cannot participate in nucleophilic dissociation reactions of the type presented there. Formation of =B-Na^+ species is consistent with these data.

The results of this chapter show that boron losses during synthesis and processing are significant. Chapter VII will examine further INAA results for various stages of the overall borosilicate lyogel synthetic process. Arguments will be presented to explain boron losses from borosilicate lyogels.

E. Conclusions

The swelling behavior of borosilicate lyogels is affected by the lyogel solvent properties. Additional control of the solvent content of the lyogel beyond synthesis appears to be a viable option for increasing lyogel densities prior to drying and sintering.

CHAPTER VII. PROCESSING OF BOROSILICATE LYOGELS: INAA SAMPLES FROM
GELATION AND POST-GELATION STAGES

A. Introduction

In Chapter VI it was demonstrated that the as-batched compositions of $\text{SiO}_2 \cdot x\text{B}_2\text{O}_3$ lyogels differ significantly from those determined from INAA. It is obvious that boron is lost during the synthesis and subsequent processing steps. Figure 7.1 shows the overall synthetic procedure for synthesizing and processing an $\text{SiO}_2 \cdot x\text{B}_2\text{O}_3$ lyogel. Various samples from different stages of the overall synthetic process were analyzed via INAA to determine their composition.

B. INAA Sample Preparation and Procedure

As discussed in Chapter III, irradiation vials were cleaned by rinsing with warm tap water, deionized water, and ethanol, in that order. The vials then were air dried. All handling of the vials was done using surgical gloves. The vials then were weighed to an accuracy of $\pm 0.001\text{g}$.

Approximately 0.110g of the sample was placed in the vial using a stainless steel spatula and a plastic funnel. Care was taken so that no sample contacted the outside or top of the vial. A 0.127 mm diameter tungsten wire was wrapped around the top of the vial and the ends of the wire were twisted together. Excess wire was trimmed off

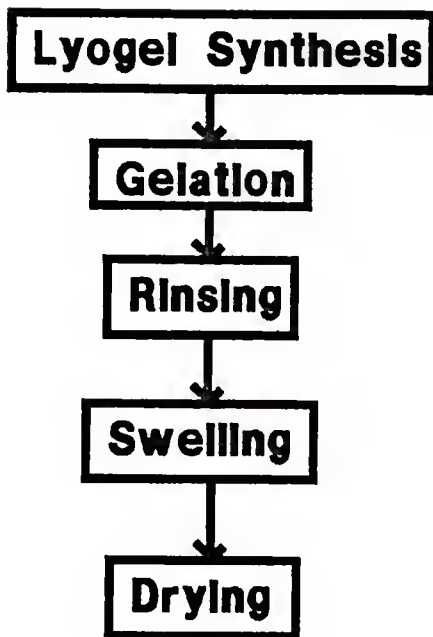


Figure 7.1. Schematic diagram of overall synthetic procedure for synthesizing and processing borosilicate lyogels.

using scissors. The total mass was determined with the mass of the wire being obtained by difference.

The vial was placed in a polyethylene bag to prevent contamination of the exterior of the vial. The opening of the bag was twisted and taped. A label was affixed over the tape. The samples were irradiated and counted as described previously in Chapter III.

C. Results From INAA

During gelation a white residue was observed around the tops of the sealed sample vials. The residue was analyzed for silicon, and it was assumed that the remaining mass was boron containing species. The INAA results are shown in Table 7.1. The residue is approximately 99 weight percent borate.

Table 7.1. INAA Composition of Residue from Top of Sealed Vial.

Sample Mass (g)	Mass of Silicon (g)	*Mass of Boron Containing Species (g)	Fraction of Boron Containing Species
0.042	0.0002 (±0.006)	0.042 (±0.007)	0.995
0.056	0.0007 (±0.006)	0.055 (±0.007)	0.998

* Mass of boron containing species obtained by difference.

Compositions of lyogels that were not rinsed and were dried at 110°C are given in Table 7.2. These show significantly lower B/Si cation ratios, ranging from 0 to 0.54, as compared to the as-batched ratios (ranging from 0.5 to 2). These losses include those resulting

Table 7.2. INAA Composition of Unrinsed and Dried Lyogels.

As-batched Composition	Sample Mass (g)	Constituent Mass (g) (± maximum experimental error)	Composition Via INAA
$\text{SiO}_2 \cdot 0.25\text{B}_2\text{O}_3$	0.113	0.118g SiO_2 (±0.001)	$\text{SiO}_2 \cdot 0\text{B}_2\text{O}_3$
$\text{SiO}_2 \cdot 0.75\text{B}_2\text{O}_3$	0.106	0.082g SiO_2 (±0.008) 0.025g B_2O_3 * (±0.009)	$\text{SiO}_2 \cdot 0.259\text{B}_2\text{O}_3$
$\text{SiO}_2 \cdot \text{B}_2\text{O}_3$	0.119	0.090g SiO_2 (±0.004) 0.029g B_2O_3 * (±0.005)	$\text{SiO}_2 \cdot 0.27\text{B}_2\text{O}_3$

*Note: Mass of B_2O_3 obtained by difference.

from reesterification to a volatile borate residue, and also any losses that might occur during synthesis and during drying.

Table 7.3 shows a comparison between unrinsed lyogels and those rinsed in water and swelled in a 1.0 N NaCl solution. Rinsing and swelling, followed by drying at 110°C, reduced the B/Si cation ratio to 0.0 if boron was present in the unrinsed lyogel.

Table 7.3. Comparison Between Unrinsed Lyogels and Rinsed and Swelled Lyogels.

	B/Si Ratio as Batched		
	(0.5)	(1.5)	(2.0)
Not Rinsed, dried at 110°C	0.0	0.52	0.30
Rinsed and Swelled dried at 110°C	0.0	0.0	0.0

Figure 7.2 summarizes the effects of processing on the composition of a lyogel batched as $\text{SiO}_2 \cdot \text{B}_2\text{O}_3$. The B/Si cation ratio is shown after gelation and drying (0.54), after rinsing and drying (0.92), and after rinsing, swelling and drying (0.0). All the B/Si cation ratios are significantly different than the as-batched B/Si cation ratio of 2.

D. Discussion

The residue composition results listed in Table 7.1 indicate that the residue is 99 weight percent borate. Borate species are reesterified as follows.

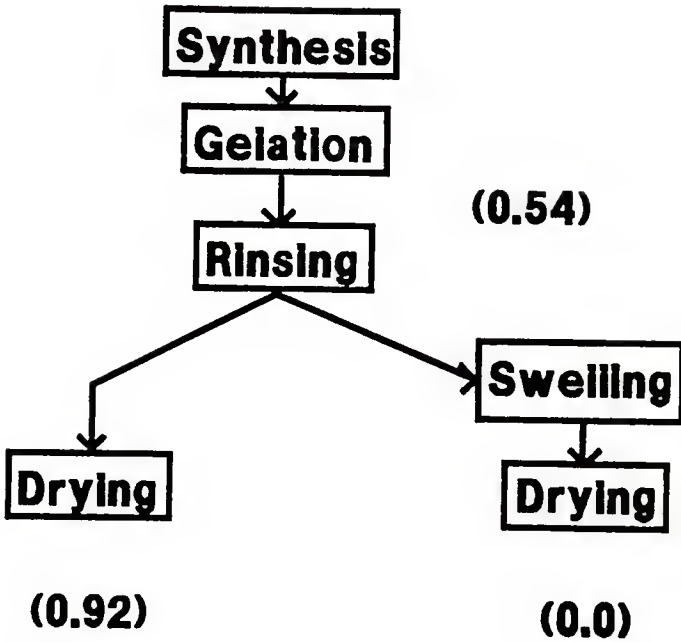
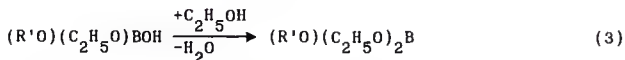
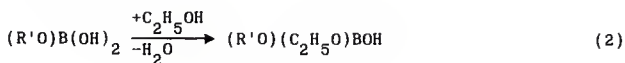


Figure 7.2. Effects of processing on the composition of a lyogel batched with a B/Si cation ratio of 2. The numbers in parentheses are B/Si cation ratios.

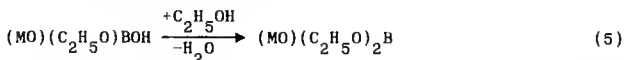
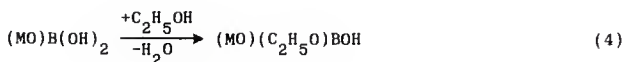


This reesterification results in the formation of volatile borate, $\text{B}(\text{OCH}_3)_3$ [55,56]. This $\text{B}(\text{OCH}_3)_3$, along with unreacted $\text{B}(\text{OCH}_3)_3$ and volatilized $\text{Si}(\text{OC}_2\text{H}_5)_4$, reacts with moisture in the air to form the silicon-boron containing residue that is about 1% silicon.

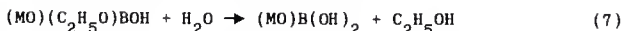
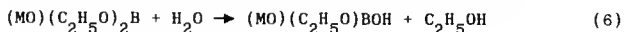
The following reactions help to explain the results presented in Table 7.3 [56].



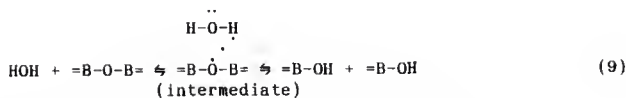
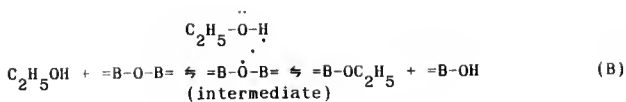
Replacing R' with a metal, M, results in the following. The lyogels were rinsed initially with ethanol.



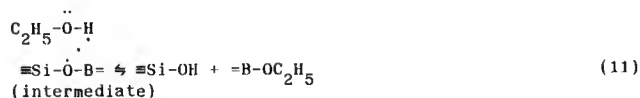
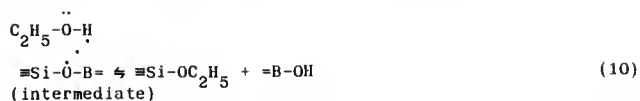
The amount of ethanol in the rinsing solution was decreased gradually by dilution with water until the rinsing solution was essentially pure water. Assuming that $(\text{C}_2\text{H}_5\text{O}-)$ is more reactive than $(\text{MO}-)$ would result in reactions of the following type.



Letting M be =B-, the results are as follows [5B].



Letting M be $\equiv \text{Si}-$, results in the following [49].



Upon rinsing, five species may be encountered. They are the borosilicate lyogel, $\equiv\text{Si}-\text{OC}_2\text{H}_5$, $\equiv\text{Si}-\text{OH}$, $=\text{B}-\text{OC}_2\text{H}_5$, and $=\text{B}-\text{OH}$. After rinsing, only the borosilicate lyogel remains in large fragments and the other four species are rinsed away with the rinsing solution.

E. Conclusions

Boron is being lost at several stages during the overall process. During gelation, reesterification and unreacted boron form a borate residue at the tops of sealed sample vials. During rinsing lower

molecular weight species are rinsed away and only the borosilicate lyogel remains. Rinsing and drying causes both boron and silicon losses from the lyogel. Rinsing, followed by swelling, followed by drying at 110⁰C results in losses of both boron and silicon from the lyogel.

CHAPTER VIII. FREEZE DRYING EXPERIMENT

An experiment was conducted to compare oven-dried lyogels to freeze-dried lyogels. An $\text{SiO}_2 \cdot \text{B}_2\text{O}_3$ lyogel was synthesized following the procedure given by [40,50,64] and modified by Angell [8].

A. Experimental

The following procedure was used to synthesize the $\text{SiO}_2 \cdot \text{B}_2\text{O}_3$ lyogel.

Apparatus:

- (1) 3-neck 500 ml flask
- (2) tapered glass stoppers
- (3) electric stirrer, variable speed
- (4) stirring blade, plastic
- (5) water bath, constant-temperature to within 0.5°C
- (6) thermometer
- (7) glass condenser with tapered glass stopper
- (8) graduated cylinder, one for each chemical used
- (9) 50 ml polypropylene beakers, polypropylene stoppers
- (10) ring stand and clamps to support electric stirrer and hold 3-neck flask
- (11) pump
- (12) small tank
- (13) hoses
- (14) 1 liter flask

(15) model 10-MR-TR Virtis Freeze-dryer

Materials:

- (1) tetraethylorthosilicate, $\text{Si}(\text{OC}_2\text{H}_5)_4$
- (2) trimethylborate, $\text{B}(\text{OCH}_3)_3$, 99%
- (3) ethanol, $\text{C}_2\text{H}_5\text{OH}$, 100%
- (4) 0.15 M HCl solution

Preparation of equipment:

- (1) Prepare a constant temperature water bath at 50°C .
- (2) Partially immerse the 3-neck 500 ml flask in the constant temperature water bath.
- (3) Mount the stirrer to the ring stand and position it so that the blade does not hit the bottom of the flask.
- (4) Mount the condenser on top of the flask and start the cooling water through the condenser.
- (5) Stopper the remaining neck of the 3-neck flask.

Procedure:

- (1) Pour 45 ml of $\text{Si}(\text{OC}_2\text{H}_5)_4$ into the flask.
- (2) Start the stirrer at about 2 revolutions per second.
- (3) Hydrolyze the $\text{Si}(\text{OC}_2\text{H}_5)_4$ by adding a mixed solution of 10 ml $\text{C}_2\text{H}_5\text{OH}$ and 5 ml of 0.15 M HCl solution.

- (4) Stopper the flask.
- (5) Continue to stir this mixture at 50°C for 1 hour.
- (6) Add 45 ml of $B(OCH_3)_3$ to the hydrolyzed solution.
- (7) Continue to stir this mixture at 50°C for 2 hours.
- (8) Add 5 ml 0.15 M HCl solution.
- (9) Continue to stir this mixture at 50°C for 1 hour.
- (10) Pour 25 ml portions of the liquid gel solution into the 50 ml polypropylene beakers.
- (11) Seal the beakers with polypropylene stoppers.
- (12) Set the beakers aside and allow gelation to proceed.
- (13) When the gels are viscous enough that they do not change shape when the 50-ml beakers are turned upside down, remove the gels for further processing.
- (14) Prepare four samples as shown in Table 8.4.

Table B.4. Freeze Drying--Oven Drying Comparison Experiment.

	Sample A	Sample B
	Unrinsed	Rinsed
Oven Dry	Sample A'	Sample B'
Freeze Dry	Sample A''	Sample B''

- (15) Sample A: Take the lyogel from one of the 50-ml beakers and split it into 2 parts (Sample A', Sample A''). Prepare for INAA as described previously in Section B of Chapter III.
- (15a) Sample A': Oven dry at 110°C until constant weight. Prepare for INAA as described previously in Section B of Chapter III.
- (15b) Sample A'': Freeze dry under a 100 millitorr vacuum at -40°C. Slowly heat the sample to 25°C while maintaining the 100 millitorr vacuum. Dry until constant weight. Prepare for INAA as described previously in Section B of Chapter III.
- (16) Sample B: Take the lyogel from another 50-ml beaker and split it into 2 parts (Sample B', Sample B'').
- (16a) Place Samples B' and B'' into a small tank with pure ethanol. Slowly pump fresh water into the tank while slowly pumping rinsing solution out of the tank. This will gradually dilute the pure ethanol to essentially pure water. Continue dilution until the effluent from the rinse tank is less than 1 percent ethanol.

(16b) Remove Sample B' from the rinsing solution and oven dry at 110°C until constant weight. Prepare for INAA as described previously in Section B of Chapter III.

(16c) Remove Sample B'' from the rinsing solution and freeze dry as described in Step 15(b) until constant weight. Prepare for INAA as described previously in Section B of Chapter III.

B. Freeze Drying Experiment Results

The results of this experiment are shown in Table 8.5. The unrinsed lyogels have virtually the same composition (B/Si cation ratio of about 0.5), as determined by INAA, regardless of the drying process employed. The rinsed and dried lyogels also have a different measured B/Si cation ratio than the as-batched ratio of 2. The measured B/Si cation ratios were 0.92 and 1.90.

C. Discussion

Once again, the as-batched composition for the unrinsed and dried lyogel, a B/Si cation ratio of 2, is significantly different from the measured B/Si cation ratio of about 0.5. This difference can be attributed to volatile borate formation during synthesis and gelation, as well as any losses that occur during the drying process. These

Table 8.5. Comparison Between Freeze-Dried Lyogels and Oven-Dried Lyogels (batched as $\text{SiO}_2 \cdot \text{B}_2\text{O}_3$).

Sample	Sample Mass (g)	SiO_2 Mass (g)	* B_2O_3 Mass (g)	Molar Composition
Not rinsed, dried at 110°C	0.119	0.090 (±0.004)	0.029 (±0.005)	$\text{SiO}_2 \cdot 0.27\text{B}_2\text{O}_3$
Not rinsed, freeze dried	0.111	0.087 (±0.004)	0.024 (±0.005)	$\text{SiO}_2 \cdot 0.23\text{B}_2\text{O}_3$
Rinsed, dried at 110°C	0.113	0.074 (+0.004)	0.039 (±0.005)	$\text{SiO}_2 \cdot 0.46\text{B}_2\text{O}_3$
Rinsed, freeze dried	0.111	0.053 (±0.003)	0.058 (±0.004)	$\text{SiO}_2 \cdot 0.95\text{B}_2\text{O}_3$

*Mass of B_2O_3 obtained by difference.

lyogels have essentially identical compositions, regardless of the drying process employed. This suggests that the mechanisms for boron or silicon losses due to drying are similar during drying at 110°C and during freeze drying.

The results for the rinsed and dried lyogels can be explained by the rinsing reactions (4) to (12) of Chapter VII. Upon rinsing, five species may be encountered. They are the borosilicate lyogel, $\equiv\text{Si-OC}_2\text{H}_5$, $\equiv\text{Si-OH}$, $=\text{B-OC}_2\text{H}_5$, and $=\text{B-OH}$. After rinsing, only the borosilicate lyogel remains in large fragments and the other four species are rinsed away with the rinsing solution. A graduate student in the author's research group, Barbara Angell, observed that a filter with a nominal cutoff molecular weight of 10,000 continually clogged during the rinsing process. This suggests that some or all of the species rinsed from the lyogel, namely $\equiv\text{Si-OC}_2\text{H}_5$, $\equiv\text{Si-OH}$, $=\text{B-OC}_2\text{H}_5$, or $=\text{B-OH}$, are oligomers and not merely ions in solution.

Also, these results show that rinsing and drying produces products of different compositions depending on the drying process employed. The unrinsed and dried lyogels have essentially identical compositions, regardless of the drying process employed. It is reasonable to assume that the unrinsed lyogels had essentially the same compositions prior to any further processing. After rinsing and drying the B/Si cation ratio for the freeze dried lyogel, 1.90, is more than double that of the lyogel dried at 110°C, 0.92. This suggests that more silicon is lost during the rinsing and freeze drying processes and/or that more complete condensation reactions occur for $\equiv\text{Si-O-B=}$ type species. More complete condensation reactions

for boron species would result in an increase in B_2O_3 and thus increase the B/Si cation ratio. Rinsing followed by freeze drying results in a B/Si cation ratio that is very close to the as-batched cation ratio of 2.

Comparing the unrinsed lyogels to those rinsed shows that the B/Si cation ratio is larger for the rinsed gels. This implies the following. Firstly, more silicon than boron may be lost during the rinsing process. Secondly, more complete condensation reactions may occur for $\equiv Si-O-B \equiv$ type species, resulting in an increase in B_2O_3 and thus increasing the B/Si cation ratio. It may be possible that both a loss of silicon and more complete boron species condensation reactions occur, or that only one of these takes place.

D. Conclusions

Rinsing followed by freeze drying results in a product composition that is very close to the as-batched composition. The unrinsed and dried lyogels have virtually the same composition. This indicates that the mechanisms for boron or silicon losses due to drying are similar during drying at $110^\circ C$ and during freeze drying. When the lyogels are rinsed and dried, the results depend on the drying process employed. Rinsing results in lower molecular weight species being rinsed away, with only the borosilicate lyogel remaining.

A. Background

The gels that have been discussed to this point have been borosilicate Type II polymeric gels [36]. The chemical reactions leading to polymerization and network formation took place throughout a liquid solution. Active species slowly built up an inorganic network by eliminating alkyl groups from the structure by chemical reaction. If the reaction rate and behavior is such that continuity was maintained, a gel formed. As described in Chapter V, Section A, the product remains in solution because of the absence of sufficient hydroxyl groups to complete polymerization. After all gel constituents were added and oligomers were formed, excess water was added to remove the remaining -OR groups. This causes the solution to polymerize further to a clear gel.

These gels are homogeneous and consist of one liquid phase. Yoldas [40] has determined regions of clear solution and precipitate when solutions having various $\text{Si}(\text{OC}_2\text{H}_5)_4/\text{B}(\text{OCH}_3)_3$ ratios were hydrolyzed with different amounts of water (Figure 9.1). No other results concerning these data are given in that paper or in others. The material presented in this chapter is an extension of the work done by Yoldas [40]. The goal was to ascertain the composition of the precipitate and the composition of the clear solution corresponding to a given point located above the line in Figure 9.1.

The hydrolysis of metal alkoxide solutions also provides insight into the mechanism of reactions taking place. Yoldas [40] has

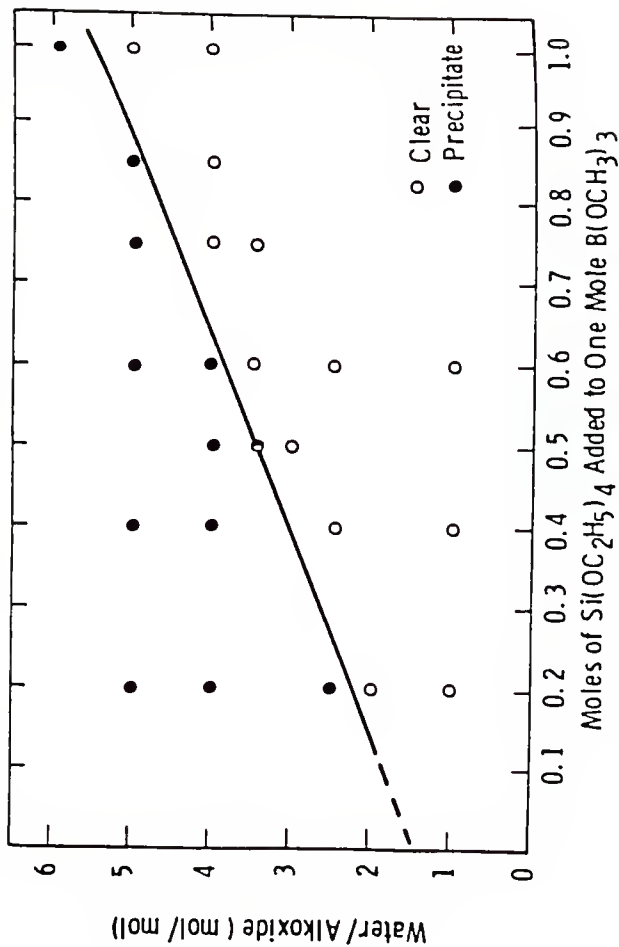


Figure 9.1. Regions of precipitate and clear solution formation in the alkoxide mixture $\text{Si}(\text{OC}_2\text{H}_5)_4/\text{B}(\text{OCH}_3)_3$ as a function of water content [40].

discussed this in detail and the following is a summary of his findings. Figure 9.1 [40] shows the regions of clear solution and precipitate when solutions having various $\text{Si}(\text{OC}_2\text{H}_5)_4/\text{B}(\text{OCH}_3)_3$ ratios were hydrolysed with different amounts of water. The line separating clear solutions from those that have precipitates is given by

$$\frac{M_{\text{H}_2\text{O}}}{M_1} = A + \frac{BM_2}{M_1} \quad (1)$$

where: $M_{\text{H}_2\text{O}}$ = moles of water

M_1 = moles $\text{B}(\text{OCH}_3)_3$

M_2 = moles of $\text{Si}(\text{OC}_2\text{H}_5)_4$

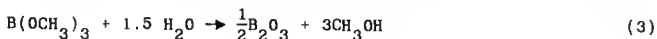
A = intercept

B = slope

If M_1 is one mole Eq. (1) becomes (see Figure 9.1)

$$M_{\text{H}_2\text{O}} = 4M_2 + 1.5 \quad (2)$$

This means that 1.5 moles of H_2O are required to condense 1 mole of $\text{B}(\text{OCH}_3)_3$, and that approximately 4 additional moles of water are required per mole of $\text{Si}(\text{OC}_2\text{H}_5)_4$ added. These numbers give information about the nature of the hydrolysis products. For example, the hydrolysis product of 1 mole of $\text{B}(\text{OCH}_3)_3$ is an oxide rather than a hydroxide [40], requiring 1.5 moles of water per mole of $\text{B}(\text{OCH}_3)_3$:



B. Experimental

B.1. Experimental Procedure for $\text{SiO}_2 \cdot x\text{B}_2\text{O}_3$ Lyogel Synthesis Via Co-precipitation

$\text{SiO}_2 \cdot x\text{B}_2\text{O}_3$ lyogels were prepared via co-precipitation according to the procedure below. All quantities of reactants were kept the same as in Section A of Chapter VIII (procedure for $\text{SiO}_2 \cdot \text{B}_2\text{O}_3$ lyogel synthesis) except that the moles H_2O /moles $\text{B}(\text{OCH}_3)_3$ ratio was changed so that a precipitate would form. This corresponds to the point 6 moles H_2O / mole $\text{B}(\text{OCH}_3)_3$ and 0.514 moles $\text{Si}(\text{OC}_2\text{H}_5)_4$ / mole $\text{B}(\text{OCH}_3)_3$ located on Figure 9.1.

Apparatus:

- (1) Test tube block heater
- (2) Test tubes and stoppers
- (3) 50-ml polypropylene beakers and polypropylene stoppers
- (4) Thermometer

Materials:

- (1) tetraethylorthosilicate, $\text{Si}(\text{OC}_2\text{H}_5)_4$
- (2) trimethyl borate, $\text{B}(\text{OCH}_3)_3$, 99%
- (3) ethanol, $\text{C}_2\text{H}_5\text{OH}$, 100%
- (4) 0.15 M HCl solution

Procedure:

- (1) Place test tube in block heater and set temperature at 50°C. Wait until temperature is constant.
- (2) Pour 4.09 ml of $\text{Si}(\text{OC}_2\text{H}_5)_4$ into test tube.
- (3) Hydrolyze the $\text{Si}(\text{OC}_2\text{H}_5)_4$ by adding 0.91 ml of $\text{C}_2\text{H}_5\text{OH}$ containing 1.93 ml of 0.15M HCl solution.
- (4) Mix well and stopper test tube.
- (5) Mix every 5 minutes.
- (6) After 1 hour, add 4.09 ml of $\text{B}(\text{OCH}_3)_3$ and mix well. Stopper test tube.
- (7) Mix every 5 minutes.
- (8) After 2 hours, add 1.93 ml of 0.15 M HCl solution to complete hydrolysis.
- (9) Mix well and stopper test tube.
- (10) Mix every 5 minutes.
- (11) After 1 hour remove solution from test tube and pour it into polypropylene beakers.
- (12) Seal the beakers with polypropylene stoppers.
- (13) Wait 18 hours.
- (14) Separate clear solution from precipitate.
- (15) Place clear solution in polypropylene beakers and seal them with stoppers. Let solution gel.
- (16) After solution has gelled, dry at 110°C until constant weight.
- (17) Rinse precipitate with pure ethanol.
- (18) Dry precipitate at 110°C until constant weight.

B.2. INAA Sample Preparation and Procedure

Irradiation vials were cleaned by rinsing with warm tap water, deionized water, and ethanol, in that order. The vials then were air dried. All handling of the vials was done using surgical gloves. The vials then were weighed to an accuracy of $\pm 0.001\text{g}$.

Approximately 0.110g of the sample was placed in the vial using a stainless steel spatula and a plastic funnel. Care was taken so that no sample contacted the outside or top of the vial. A 0.127 mm diameter tungsten wire was wrapped around the top of the vial and the ends of the wire were twisted together. Excess wire was trimmed off using scissors. The total mass was determined with the mass of the wire being obtained by difference.

The vial was placed in a polyethylene bag to prevent contamination of the outside of the vial. The opening of the bag was twisted and taped. A label was affixed over the tape. The samples were irradiated and counted as described previously in Chapter III.

C. Results

The INAA results are given in Table 9.1. They show that the clear gel solution is SiO_2 and that the precipitate is $\text{SiO}_2 \cdot x\text{B}_2\text{O}_3$. These indicate that the clear gel contained no boron (within an experimental error of 2 percent).

The precipitate is white and is more dense than the clear solution. The precipitate is soluble in water when rinsed. The coprecipitation reaction was completed within 18 hours. The clear

solution gelled, above the white precipitate, in 13 days. The clear gel exhibited syneresis.

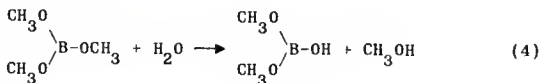
Table 9.1. INAA Results for Precipitate and $\text{SiO}_2 \cdot x\text{B}_2\text{O}_3$
Lyogel (Batched with the molar ratio of
 $\text{TEOS}:\text{H}_2\text{O}:\text{B}(\text{OCH}_3)_3$ of 0.514:6:1).

Sample	Composition Via INAA
Clear Gel Solution Sample #1	$\text{SiO}_2 \cdot 0\text{B}_2\text{O}_3$
Clear Gel Solution Sample #2	$\text{SiO}_2 \cdot 0\text{B}_2\text{O}_3$
Precipitate Sample #1	$\text{SiO}_2 \cdot 3.4\text{B}_2\text{O}_3$
Precipitate Sample #2	$\text{SiO}_2 \cdot 3.0\text{B}_2\text{O}_3$

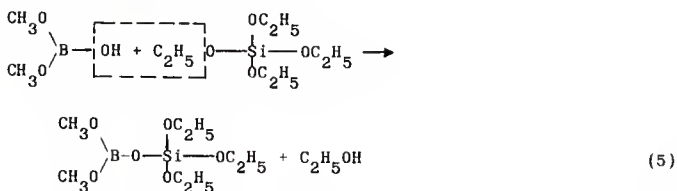
D. Discussion

Yoldas [40] has defined the regions of clear solution and precipitation (Figure 9.1). He did not present any data or results showing the composition of the precipitate or of the clear solution, nor did he present any data regarding gelation of the clear supernate.

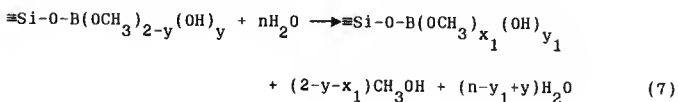
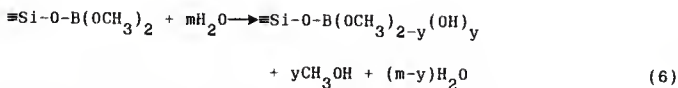
Yoldas [40] has discussed lyogel formation via co-precipitation. Much of the following is based upon the work of that paper. When $\text{B}(\text{OCH}_3)_3$ reacts with water, a series of intermediate species, such as $\text{B}(\text{OCH}_3)_2\text{OH}$, $\text{B}(\text{OCH}_3)(\text{OH})_2$ and $\text{B}(\text{OH})_3$, initially form depending upon the extent of the hydrolysis reaction. For example, one such reaction is the following.



The relative concentrations of each species will depend on the availability of water and the dilution of the system. By diluting the alkoxides and the water with alcohol before mixing, it is possible to control the product species and extent of initial hydrolysis in these reactions. Initial species immediately undergo a series of condensation reactions resulting in the formation of secondary species with bridging oxygens. For example,



The formation of initial intermediate species and their condensation to form polymer chains can be represented by the following general equations.



where: $0 < y < 2$

$$x_1 + y_1 = 2$$

In this system, $-\text{OCH}_3$ and OH^- groups cannot coexist in significant quantities. They react with each other and form bridging

oxygens, while releasing alcohol (see Reaction 5), until one of the groups is completely eliminated. Two outcomes are possible. If the species contain sufficient hydroxyl groups (if $y_1 > x_1$ in Reaction 7), polymerization continues until all $-OCH_3$ groups are removed from the network. Thus, precipitation of a silicon-boric oxide occurs. However, if there are an insufficient number of hydroxyl groups to remove all the $-OCH_3$ groups (if $x_1 > y_1$ in Reaction 7), then the polymer network contains $-OCH_3$ groups in the structure. When this occurs the network remains soluble in alcohol and available for further polymerization. A schematic representation of precipitate borosilicate and soluble and polymerizable species from a $\equiv Si-O-B(OCH_3)_2$ intermediate is shown in Figure 9.2.

The clear gel contains no boron. It is a silica lyogel and forms above the $SiO_2 \cdot nB_2O_3$ precipitate, which collects on the bottom of the sample vial. The silica lyogel shrinks as it polymerizes and undergoes condensation reactions. The increase in bridging oxygen bonds causes the gel network to contract [65]. As this shrinkage proceeds liquid is expelled from the pores, and syneresis is observed. The white $SiO_2 \cdot 3B_2O_3$ precipitate is soluble in water when rinsed. This behavior is quite different from a $SiO_2 \cdot 3B_2O_3$ lyogel, which would not dissolve upon rinsing. The lyogel would partially dissociate when rinsed but would not dissolve. So, it's possible to make two distinctly different materials, namely a precipitate and a lyogel, with the same composition and have markedly different properties.

E. Conclusions

A lyogel and a co-precipitate may be produced by increasing the water available for hydrolysis. If all other variables are held constant, it is the amount of water that is the critical parameter in determining whether a lyogel is produced or a lyogel and a co-precipitate are produced. A lyogel forms above the co-precipitate product. The lyogel is SiO_2 and the co-precipitate is $\text{SiO}_2 \cdot 3.2\text{B}_2\text{O}_3$.

CHAPTER X. CONCLUSIONS

An Instrumental Neutron Activation Analysis technique was developed to determine the composition of borosilicate lyogels. Si, Na, and Cl masses were determined and the mass of B_2O_3 was obtained by difference. It was assumed that silicon has a single valence of +4 and that boron has a single valence of +3. These results showed that the final lyogel composition has significantly less boron than the as-batched lyogel composition. Thus boron is lost from the lyogel during the overall synthetic process.

Formation of volatile boron species is one source of boron loss. The residue formed around the tops of sealed sample vials during gelation was found to be 99 percent boron containing species. Also, the results for boron or silicon losses are similar during drying at $110^{\circ}C$ and during freeze drying.

Rinsing results indicated that the B/Si cation ratio was increased after rinsing. Either more silicon than boron is lost from the lyogel during rinsing, or the condensation reactions for boron containing species are proceeding during rinsing, or both.

Rinsing followed by swelling resulted in a decreased B/Si cation ratio. This suggests that more boron than silicon is being lost from the lyogel during rinsing and swelling. As the NaCl concentration in the swelling solution increased, the B/Si cation ratio increased. Depending on the pH, Na^+ addition causes boron to change from trigonal to tetrahedral coordination. Tetrahedral boron is coordinately saturated and cannot participate in nucleophilic dissociation

reactions of the type discussed in this research. Formation of $\equiv\text{B}-\text{Na}^+$ species is consistent with these data.

In addition, a lyogel and a co-precipitate may be produced by increasing the water available for hydrolysis. If all other variables are held constant, it is the amount of water that is the critical parameter in determining whether a lyogel is produced or a lyogel and a co-precipitate are produced. A lyogel forms above the co-precipitate product. The lyogel is SiO_2 and the co-precipitate is $\text{SiO}_2 \cdot 3.2\text{B}_2\text{O}_3$.

Lastly, it has been demonstrated that there is a significant difference between the as batched, intermediate, and final lyogel compositions. This makes it difficult to obtain a product having a specified composition or reproducible properties. It is clear that each step in the overall process affects the final lyogel composition. Thus the changes that occur at each step must be understood in detail. Only then will it be possible to obtain reproducible products with specified compositions.

FUTURE WORK

XI . FUTURE WORK: CLOSING THE MATERIAL BALANCE

A. Introduction

The composition of a borosilicate lyogel has been determined after gelation and drying, and after it has been rinsed, swelled and dried. However, these data do not yield enough information to close a material balance for the process. The processing steps must be modified slightly to obtain the desired data. Figures 11.1 and 11.2 illustrate the modified overall synthetic procedure for synthesizing and processing a borosilicate, $\text{SiO}_2 \cdot x\text{B}_2\text{O}_3$, lyogel. Table 11.1 summarizes the available data and the data which must be acquired to close the material balance.

where:

$$1^M_{IN} = M_{\text{Si}(\text{OC}_2\text{H}_5)_4} + M_{\text{B}(\text{OCH}_3)_3} + M_{\text{H}_2\text{O}} + M_{\text{C}_2\text{H}_5\text{OH}}$$

$$1^M_{out} = 1^m_{\text{Si}(\text{OC}_2\text{H}_5)_4} + 1^m_{\text{B}(\text{OCH}_3)_3} + 1^m_{\text{SiO}_2} \\ + 1^m_{\text{B}_2\text{O}_3} + 1^m_{\text{H}_2\text{O}} + 1^m_{\text{C}_2\text{H}_5\text{OH}} + 1^m_{\text{CH}_3\text{OH}} + 1^m_{\text{C}}$$

$$1^Y = 1^y_{\text{Si}(\text{OC}_2\text{H}_5)_4} + 1^y_{\text{SiO}_2} + 1^y_{\text{B}(\text{OCH}_3)_3} + 1^y_{\text{B}_2\text{O}_3} \\ + 1^y_{\text{H}_2\text{O}} + 1^y_{\text{CH}_3\text{OH}} + 1^y_{\text{C}_2\text{H}_5\text{OH}} + 1^y_{\text{C}}$$

$$2^Y = 2^y_{\text{Si}(\text{OC}_2\text{H}_5)_4} + 2^y_{\text{SiO}_2} + 2^y_{\text{B}(\text{OCH}_3)_3} + 2^y_{\text{B}_2\text{O}_3} \\ + 2^y_{\text{H}_2\text{O}} + 2^y_{\text{CH}_3\text{OH}} + 2^y_{\text{C}_2\text{H}_5\text{OH}} + 2^y_{\text{C}}$$

Table 11.1. Summary of Available Data and Data to Be Acquired to Close The Material Balance For The Entire Synthetic Process (See Figures 11.1 and 11.2).

<u>Available Data</u>	<u>Data To Be Acquired</u>
1^M_{IN} , 1^M_i , 1^M_{out}	1^Y , 2^Y , 3^Y , 4^Y , 5^Y
3^M_{out}	5^M_{out}
2^M_{out} , 2^M_{IN}	7^M_{out}
4^M_{out} , 4^M_{IN}	
6^M_{out}	
8^M_{out}	
9^M_{out}	

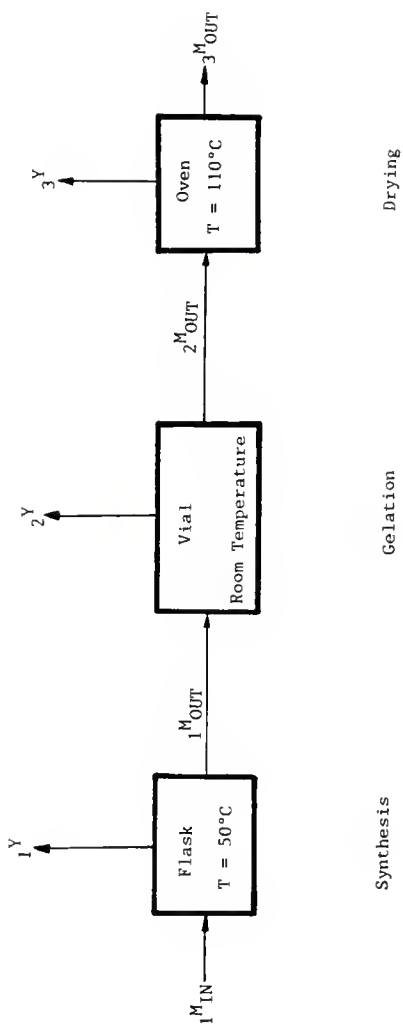


Figure 11.1. Schematic of traditional lyogel synthesis and processing steps.

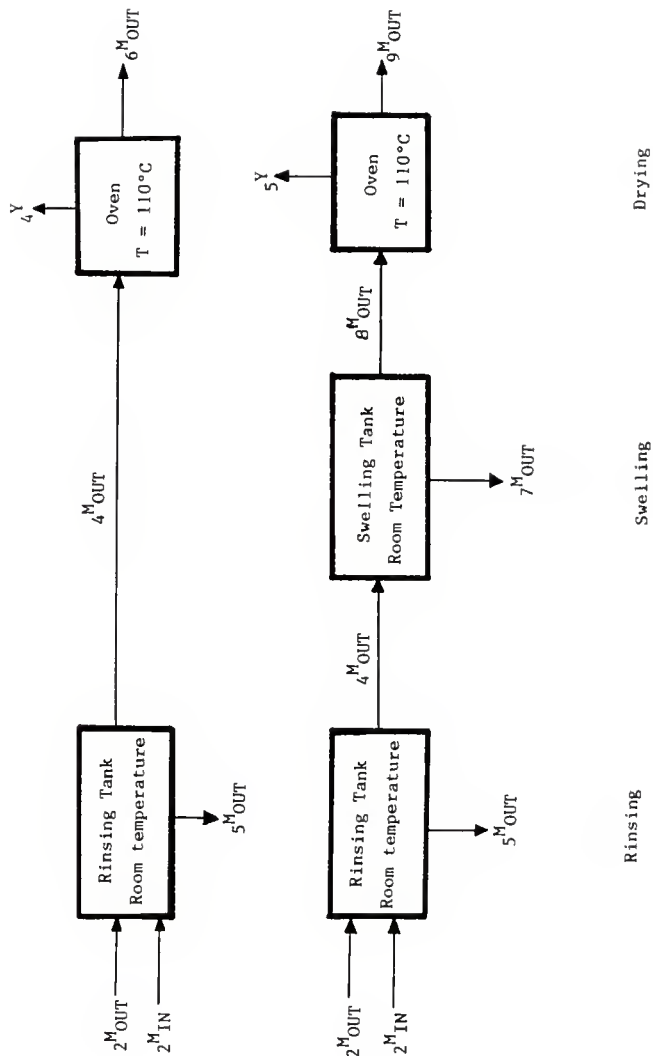


Figure 11.2. Schematic of post-gelation lyogel processing steps.

$$2^M_{out} = 2^m Si(OC_2H_5)_4 + 2^m B(OCH_3)_3 + 2^m SiO_2 + 2^m B_2O_3 \\ + 2^m H_2O + 2^m C_2H_5OH + 2^m CH_3OH + 2^m C$$

$$3^Y = 3^y Si(OC_2H_5)_4 + 3^y SiO_2 + 3^y B(OCH_3)_3 + 3^y B_2O_3 \\ + 3^y H_2O + 3^y CH_3OH + 3^y C_2H_5OH + 3^y C$$

$$3^M_{out} = 3^m Si(OC_2H_5)_4 + 3^m SiO_2 + 3^m H_2O + 3^m C_2H_5OH \\ + 3^m CH_3OH + 3^m C + 3^m B(OCH_3)_3 + 3^m B_2O_3$$

$$2^M_{IN} = z C_2H_5OH + z H_2O$$

$$4^M_{out} = 4^m SiO_2 + 4^m B_2O_3 + 4^m H_2O + 4^m C$$

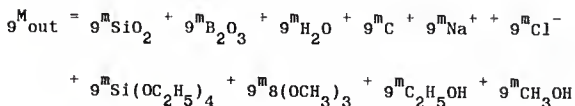
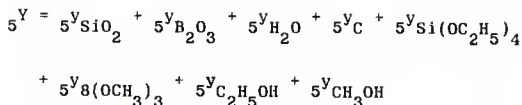
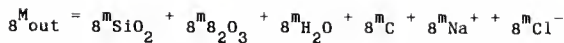
$$5^M_{out} = 5^m Si(OC_2H_5)_4 + 5^m B(OCH_3)_3 + 5^m SiO_2 + 5^m B_2O_3 \\ + 5^m H_2O + 5^m C_2H_5OH + 5^m CH_3OH + 5^m C$$

$$4^Y = 4^y SiO_2 + 4^y B_2O_3 + 4^y H_2O + 4^y C + 4^y Si(OC_2H_5)_4 \\ + 4^y B(OCH_3)_3 + 4^y C_2H_5OH + 4^y CH_3OH$$

$$6^M_{out} = 6^m SiO_2 + 6^m B_2O_3 + 6^m C + 6^m Si(OC_2H_5)_4 + 6^m H_2O \\ + 6^m B(OCH_3)_3 + 6^m C_2H_5OH + 6^m CH_3OH$$

$$4^M_{IN} = z_{NaCl} + w_{H_2O}$$

$$7^M_{out} = 7^m SiO_2 + 7^m B_2O_3 + 7^m H_2O + 7^m C + 7^m Na^+ + 7^m Cl^- \\ + 7^m Si(OC_2H_5)_4 + 7^m B(OCH_3)_3 + 7^m C_2H_5OH + 7^m CH_3OH$$



a^M = total moles at stage "a"

M_i = initial moles of species "i"

a^Y = total moles of vapor at stage "a"

a^y_i = moles of species "i" vaporized at stage "a"

a^m_i = moles of species "i" not vaporized at stage "a"

w_i, z_i = moles of species "i" added

subscript "c" = "attached" carbon, or carbon that remains attached to silicon species after hydrolysis reactions are completed and the samples dried.

Consider the following simplified reactions.



where C(s) is "attached" carbon or carbon that remains attached to silicon species after hydrolysis reactions are completed and the samples dried. For simplicity Reactions (1) and (2) neglect details of the polymerization reactions. X_i is the fractional conversion of species "i" and is defined as

$$X_i = \frac{N_1^{\text{in}} - N_1^{\text{out}}}{N_1^{\text{in}}} \quad (3)$$

where N_1^{in} = moles of reactant i in inlet stream

N_1^{out} = moles of reactant i in outlet stream.

B. Suggested Chemical Analyses

Dr. Steven Hughes and Dr. Robert Fry of the Department of Chemistry at Kansas Ste University, and Dr. John Schlup of the Department of Chemical Engineering at Kansas State University were consulted to determine possible methods of chemical analyses. It should be noted that using reagents during the chemical analyses of borosilicate lyogels changes the nature and make-up of these lyogels. This makes conclusions more difficult. Thus it is desirable to avoid any "destructive" types of analysis.

Samples containing $C_2H_5OH, CH_3OH, Si(OC_2H_5)_4$ and $B(OCH)_3$ can be analyzed by gas chromatography in conjunction with mass spectroscopy or emission spectroscopy. "Attached" carbon can be analyzed via NMR spectroscopy. Boron and silicon in liquid samples can be analyzed by using plasma emission spectroscopy. Silicon, sodium and chlorine in dried solid lyogels can be analyzed via INAA. Sodium in liquid samples can be extracted into aqueous solution and analyzed by flame emission spectroscopy. Chlorine in liquid samples can be extracted into aqueous solution and analyzed by coulometric analysis. OH^-

groups can be analyzed by putting the sample in aqueous solution and performing an acid-base titration using a pH indicator.

C. Material Balance Around Reaction Flask

As indicated in Figure 11.1, the total material balance around the reaction flask is

$$1^M_{IN} = 1^Y + 1^M_{out} \quad (4)$$

The component balances are as follows. The details are given in Section A of Appendix E.

$$1^Y_{Si(OC_2H_5)_4} = M_{Si(OC_2H_5)_4} - 1^m_{Si(OC_2H_5)_4} - 1^m_{SiO_2} \quad (5)$$

$$1^Y_{C_2H_5OH} = \left(\frac{4-a}{2a}\right) 1^m_C - 1^m_{C_2H_5OH} + M_{C_2H_5OH} \quad (6)$$

$$1^Y_{B(OCH_3)_3} = M_{B(OCH_3)_3} - 1^m_{B(OCH_3)_3} - 2 \cdot 1^m_{B_2O_3} \quad (7)$$

$$1^Y_{CH_3OH} = 6 \cdot 1^m_{B_2O_3} - 1^m_{CH_3OH} \quad (8)$$

$$1^Y_{H_2O} = M_{H_2O} - 1^m_{H_2O} - (2-3a) \cdot 1^m_{SiO_2} - \frac{1}{2}(1^m_{CH_3OH} + 1^Y_{CH_3OH}) \quad (9)$$

The recommended methods for complete analysis are summarized in Table 11.2.

D. Material Balance Around Sample Vial

As indicated in Figure 11.1, the total material balance around the sample vial is

$$1^M_{out} = 2^Y + 2^M_{out}$$

The component balances are as follows. The details are given in Section B of Appendix E.

Table 11.2 Summary of Results for Material Balance Around Reaction Flask.

Already measuring	Measurements to make (with recommended method of analysis).	Quantity to be obtained from material balance
M_1 (reactants)	1^mSiO_2 (plasma emission spectroscopy)	$1^y\text{Si}(\text{OC}_2\text{H}_5)_4$ from Eq. (5)
	$1^m\text{B}_2\text{O}_3$ (plasma emission spectroscopy)	$1^y\text{C}_2\text{H}_5\text{OH}$ from Eq. (6)
	$1^m\text{Si}(\text{OC}_2\text{H}_5)_4$ (gas chromatography with mass spectroscopy)	
	$1^m\text{B}(\text{OCH}_3)_3$ (gas chromatography with mass spectroscopy)	
	$1^m\text{H}_2\text{O}$ (acid base titrations using a pH indicator)	$1^y\text{B}(\text{OCH}_3)_3$ from Eq. (7)
	$1^m\text{C}_2\text{H}_5\text{OH}$ (gas chromatography with mass spectroscopy)	$1^y\text{CH}_3\text{OH}$ from Eq. (8)
	$1^m\text{CH}_3\text{OH}$ (gas chromatography with mass spectroscopy)	$1^y\text{H}_2\text{O}$ from Eq. (9)
	1^mC (NMR spectroscopy)	
Assumptions: $1^y\text{SiO}_2 = 0$, $1^y\text{B}_2\text{O}_3 = 0$, $1^y\text{C} = 0$		

$$2^y \text{Si}(\text{OC}_2\text{H}_5)_4 = 1^m \text{Si}(\text{OC}_2\text{H}_5)_4 - 2^m \text{Si}(\text{OC}_2\text{H}_5)_4 - 2^m \text{SiO}_2 + 1^m \text{SiO}_2 \quad (11)$$

$$2^y \text{C}_2\text{H}_5\text{OH} = \frac{4-a}{2a} (2^m \text{C} - 1^m \text{C}) + 1^m \text{C}_2\text{H}_5\text{OH} - 2^m \text{C}_2\text{H}_5\text{OH} \quad (12)$$

$$2^y \text{B}(\text{OCH}_3)_3 = 1^m \text{B}(\text{OCH}_3)_3 - 2^m \text{B}(\text{OCH}_3)_3 - 2(2^m \text{B}_2\text{O}_3 - 1^m \text{B}_2\text{O}_3) \quad (13)$$

$$2^y \text{CH}_3\text{OH} = 6(2^m \text{B}_2\text{O}_3 - 1^m \text{B}_2\text{O}_3) - 2^m \text{CH}_3\text{OH} + 1^m \text{CH}_3\text{OH} \quad (14)$$

$$2^y \text{H}_2\text{O} = 1^m \text{H}_2\text{O} - (2-3a)(2^m \text{SiO}_2 - 1^m \text{SiO}_2) - \frac{1}{2}(2^m \text{C}_2\text{H}_5\text{OH} + 2^y \text{CH}_3\text{OH} - 1^m \text{CH}_3\text{OH}) \quad (15)$$

The recommended methods for complete analysis are summarized in Table 11.3.

E. Material Balance Around Dryer For an Unrlnsed Lyogel

As indicated in Figure 11.1, the total material balance around the dryer for an unrlnsed lyogel ls

$$2^M_{\text{OUT}} = 3^Y + 3^M_{\text{OUT}} \quad (16)$$

The component balances are as follows. The details are given in Section C of Appendix E.

$$3^y \text{Si}(\text{OC}_2\text{H}_5)_4 = 2^m \text{Si}(\text{OC}_2\text{H}_5)_4 - 3^m \text{Si}(\text{OC}_2\text{H}_5)_4 - 3^m \text{SiO}_2 - 3^y \text{SiO}_2 + 2^m \text{SiO}_2 \quad (17)$$

$$3^y \text{C}_2\text{H}_5\text{OH} = \frac{4-a}{2a} (3^m \text{C} + 3^y \text{C} - 2^m \text{C}) - 3^m \text{C}_2\text{H}_5\text{OH} + 2^m \text{C}_2\text{H}_5\text{OH} \quad (18)$$

Table 11.3 Summary of Results for Material Balance Around Sample Vial.

Already measuring	Measurements to make (with recommended method of analysis)	Quantity to be obtained from material balance
No quantities	$1^m, 2^m \text{Si}(\text{OC}_2\text{H}_5)_4$ (g.c. with mass spec.)	$2^v \text{Si}(\text{OC}_2\text{H}_5)_4$ from Eq.(11)
	$1^m, 2^m \text{B}(\text{OCH}_3)_3$ (g.c. with mass spec.)	$2^v \text{C}_2\text{H}_5\text{OH}$ from Eq.(12)
	$1^m, 2^m \text{C}_2\text{H}_5\text{OH}$ (gas chromatography with mass spectroscopy)	
	$1^m, 2^m \text{CH}_3\text{OH}$ (g.c. with mass spec.)	
	$1^m, 2^m \text{H}_2\text{O}$ (acid base titration using a pH indicator)	$2^v \text{B}(\text{OCH}_3)_3$ from Eq.(13)
	$1^m, 2^m \text{C}$ (NMR spectroscopy)	$2^v \text{CH}_3\text{OR}$ from Eq.(14)
	1^mSiO_2 (plasma emission spectroscopy)	$2^v \text{H}_2\text{O}$ from Eq.(15)
	2^mSiO_2 (INAA)	
	$1^m \text{B}_2\text{O}_3$ (plasma emission spectroscopy)	
	$2^m \text{B}_2\text{O}_3$ (by difference)	
Assumptions: $2^v \text{SiO}_2 = 0$, $2^v \text{B}_2\text{O}_3 = 0$, $2^v \text{C} = 0$		

$$3^y_{B(OCH_3)_3} = 2^m_{B(OCH_3)_3} - 3^m_{B(OCH_3)_3} - 2(3^m_{B_2O_3}) - 2(3^y_{B_2O_3} - 2^m_{B_2O_3}) \quad (19)$$

$$3^y_{CH_3OH} = 6(3^m_{B_2O_3} + 3^y_{B_2O_3} - 2^m_{B_2O_3}) - 3^m_{CH_3OH} + 2^m_{CH_3OH} \quad (20)$$

$$3^y_{H_3O} = 2^m_{H_2O} - 3^m_{H_2O} - (2-3a)(3^m_{SiO_2} + 3^y_{SiO_2} - 2^m_{SiO_2}) - \frac{1}{2}(3^m_{CH_3OH} + 3^y_{CH_3OH} - 2^m_{CH_3OH}) \quad (21)$$

The recommended methods for complete analysis are summarized in Table 11.4

F. Material Balance Around Rinsing Tank

As indicated in Figure 11.2 the total material balance around the rinsing tank is

$$2^M_{OUT} + 2^M_{IN} = 4^M_{OUT} + 5^M_{OUT} \quad (22)$$

The component balances are below, assuming that all $Si(OC_2H_5)_4$, $B(OCH_3)_3$, CH_3OH and C_2H_5OH have been rinsed out of the lyogel at the completion of the rinsing process. The details are given in Section D of Appendix E.

$$5^m_{Si(OC_2H_5)_4} = 2^m_{Si(OC_2H_5)_4} - 4^m_{SiO_2} - 5^m_{SiO_2} + 2^m_{SiO_2} \quad (23)$$

$$5^m_{C_2H_5OH} = \frac{4-a}{2a} (4^m_C + 5^m_C - 2^m_C) + 2^m_{C_2H_5OH} \quad (24)$$

Table 11.4. Summary of Results for Material Balance Around Dryer for an Unrinsed Lyogel.

Already measuring	Measurements to make (with recommended method of analysis)	Quantity to be obtained from material balance
3^mSiO_2 (by INAA)	$2^m, 3^m\text{Si}(\text{OC}_2\text{H}_5)_4$ (g.c. with mass spec.)	$3^y\text{Si}(\text{OC}_2\text{H}_5)_4$ from Eq.(17)
$3^m\text{B}_2\text{O}_3$ (by difference)	$2^m, 3^m\text{B}(\text{OCH}_3)$ (gas chromatography with mass spectroscopy)	$3^y\text{C}_2\text{H}_5\text{OH}$ from Eq. (18)
	$2^m, 3^m\text{C}_2\text{H}_5\text{OH}$ (g.c. with mass spec.)	
	$2^m, 3^m\text{CH}_3\text{OH}$ (g.c. with mass spec.)	
	$2^m, 3^m\text{H}_2\text{O}$ (acid base titration using a pH indicator)	$3^y\text{B}(\text{OCH}_3)_3$ from Eq.(19)
	$2^m, 3^m\text{C}$ (NMR spectroscopy)	$3^y\text{CH}_3\text{OH}$ from Eq. (20)
	2^mSiO_2 (INAA)	$3^y\text{H}_2\text{O}$ from Eq. (21)
	$2^m\text{B}_2\text{O}_3$ (by difference)	
	3^ySiO_2	
	$3^y\text{B}_2\text{O}_3$ (plasma emission spectroscopy)	
	3^yC (gas chromatography with mass spectroscopy)	

$${}^5\text{mB}(\text{OCH}_3)_3 = 2{}^{\text{m}}\text{B}(\text{OCH}_3)_3 - 2({}^4\text{mB}_2\text{O}_3 + {}^5\text{mB}_2\text{O}_3) + 2({}^2\text{mB}_2\text{O}_3) \quad (25)$$

$${}^5\text{mCH}_3\text{OH} = 6({}^4\text{mB}_2\text{O}_3 + {}^5\text{mB}_2\text{O}_3 - {}^2\text{mB}_2\text{O}_3) + 2{}^{\text{m}}\text{CH}_3\text{OH} \quad (26)$$

$$\begin{aligned} {}^5\text{mH}_2\text{O} = & 2{}^{\text{m}}\text{H}_2\text{O} - 4{}^{\text{m}}\text{H}_2\text{O} - (2-3a)({}^4\text{mSiO}_2 + {}^5\text{mSiO}_2) + Z{}^{\text{m}}\text{H}_2\text{O} \quad (27) \\ & + (2-3a)2{}^{\text{m}}\text{SiO}_2 - \frac{1}{2}({}^5\text{mCH}_3\text{OH} - 2{}^{\text{m}}\text{CH}_3\text{OH}) \end{aligned}$$

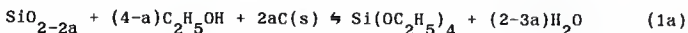
The recommended methods for complete analysis are summarized in Table 11.5

G. Material Balance Around Dryer For a Rinsed Lyogel

As indicated in Figure 11.2 the total material balance around the dryer for an unrinsed lyogel is

$$4{}^{\text{M}}\text{OUT} = 4{}^{\text{Y}} + 6{}^{\text{M}}\text{OUT} \quad (28)$$

The chemical reactions are taken to be the reverse of Reactions (1) and (2) since all $\text{Si}(\text{OC}_2\text{H}_5)_4$ and $\text{B}(\text{OCH}_3)_3$ is assumed to be rinsed out of the lyogel at the completion of the rinsing process.



The component balances are as follows. The details are given in Section E of Appendix E.

$$4{}^{\text{Y}}\text{Si}(\text{OC}_2\text{H}_5)_4 = 4{}^{\text{M}}\text{SiO}_2 - 4{}^{\text{Y}}\text{SiO}_2 - 6{}^{\text{M}}\text{SiO}_2 - 6{}^{\text{M}}\text{Si}(\text{OC}_2\text{H}_5)_4 \quad (29)$$

$$4{}^{\text{Y}}\text{C}_2\text{H}_5\text{OH} = \frac{4-a}{2a} (4{}^{\text{M}}\text{C} - 4{}^{\text{Y}}\text{C} - 6{}^{\text{M}}\text{C}) - 6{}^{\text{M}}\text{C}_2\text{H}_5\text{OH} \quad (30)$$

$$4{}^{\text{Y}}\text{B}(\text{OCH}_3)_3 = 2({}^4\text{mB}_2\text{O}_3 - 4{}^{\text{Y}}\text{B}_2\text{O}_3 - 6{}^{\text{M}}\text{B}_2\text{O}_3) - 6{}^{\text{M}}\text{B}(\text{OCH}_3)_3 \quad (31)$$

Table 11.5. Summary of Results for Material Balance Around Rinsing Tank.

Already measuring	Measurements to make (with recommended method of analysis)	Quantity to be obtained from material balance
${}^z\text{C}_2\text{H}_5\text{OH}$ input to rinsing tank	${}^m\text{Si}(\text{OC}_2\text{H}_5)_4$ (g.c. with mass spec.)	${}^m\text{Si}(\text{OC}_2\text{H}_5)_4$ from Eq. (23)
${}^z\text{H}_2\text{O}$ input to rinsing tank	${}^m\text{B}(\text{OCH}_3)_3$ (gas chromatography with mass spectroscopy)	${}^m\text{C}_2\text{H}_5\text{OH}$ from Eq. (24)
	${}^m\text{C}_2\text{H}_5\text{OH}$ (g. c. with mass spec.)	
	${}^m\text{CH}_3\text{OH}$ (g.c. with mass spec.)	
	${}^m, {}^m\text{H}_2\text{O}$ (acid base titration using a pH indicator)	${}^m\text{B}(\text{OCH}_3)_3$ from Eq. (25)
	${}^m, {}^m\text{C}$ (NMR spectroscopy)	${}^m\text{CH}_3\text{OH}$ from Eq. (26)
	${}^m, {}^m\text{SiO}_2$ (INAA)	${}^m\text{H}_2\text{O}$ from Eq. (27)
	${}^m\text{SiO}_2$ (plasma emission spectroscopy)	
	${}^m, {}^m\text{B}_2\text{O}_3$ (by difference)	
	${}^m\text{B}_2\text{O}_3$ (plasma emission spec.)	
	${}^m\text{C}$ (gas chromatography with mass spectroscopy)	

Assumptions: ${}^m\text{Si}(\text{OC}_2\text{H}_5)_4 = 0$, ${}^m\text{B}(\text{OCH}_3)_3 = 0$,

${}^m\text{CH}_3\text{OH} = 0$, ${}^m\text{C}_2\text{H}_5\text{OH} = 0$

(Assumed to be rinsed out of lyogel after completion of the rinsing process.)

$$4^y \text{CH}_3\text{OH} = 6(4^m \text{B}_2\text{O}_3 - 4^y \text{B}_2\text{O}_3 - 6^m \text{B}_2\text{O}_3) - 6^m \text{CH}_3\text{OH} \quad (32)$$

$$4^y \text{H}_2\text{O} = 4^m \text{H}_2\text{O} - 6^m \text{H}_2\text{O} + (2+3a)(4^m \text{SiO}_2 - 6^m \text{SiO}_2 - 4^y \text{SiO}_2) \\ + \frac{1}{2} (6^m \text{CH}_3\text{OH} + 4^y \text{CH}_3\text{OH}) \quad (33)$$

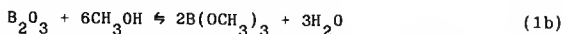
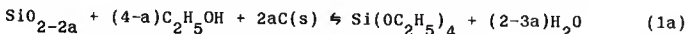
The results and suggested methods of chemical analysis are summarized in Table 11.6.

H. Material Balance Around Swelling Solution Tank

As indicated in Figure 11.2 the total material balance around the swelling solution tank is

$$4^M \text{OUT} + 4^M \text{IN} = 7^M \text{OUT} + 8^M \text{OUT} \quad (34)$$

The chemical reactions are taken to be the following.



The component balances are as follows, assuming that all $\text{Si}(\text{OC}_2\text{H}_5)_4$, $\text{B}(\text{OCH}_3)_3$, CH_3OH and $\text{C}_2\text{H}_5\text{OH}$ have been removed from the lyogel by the swelling solution. The details are given in Section F of Appendix E.

$$7^m \text{Si}(\text{OC}_2\text{H}_5)_4 = 4^m \text{SiO}_2 - 7^m \text{SiO}_2 - 6^m \text{SiO}_2 \quad (35)$$

$$7^m \text{C}_2\text{H}_5\text{OH} = \frac{4-a}{2a} (4^m \text{C} - 7^m \text{C} - 8^m \text{C}) \quad (36)$$

$$7^m \text{B}(\text{OCH}_3)_3 = 2(4^m \text{B}_2\text{O}_3 - 7^m \text{B}_2\text{O}_3 - 8^m \text{B}_2\text{O}_3) \quad (37)$$

$$7^m \text{CH}_3\text{OH} = 6(4^m \text{B}_2\text{O}_3 - 7^m \text{B}_2\text{O}_3 - 8^m \text{B}_2\text{O}_3) \quad (38)$$

Table 11.6. Summary of Results for Material Balance Around Dryer for a Rinsed Lyogel.

Already measuring	Measurements to make (with recommended method of analysis)	Quantity to be obtained from material balance
6^mSiO_2 (by INAA)	$6^m\text{Si}(\text{OC}_2\text{H}_5)_4$ (g.c. with mass spec.)	$4^y\text{Si}(\text{OC}_2\text{H}_5)_4$ from Eq. (29)
$6^m\text{B}_2\text{O}_3$ (by difference)	$6^m\text{B}(\text{OCH}_3)_3$ (gas chromatography with mass spectrometry)	$4^y\text{C}_2\text{H}_5\text{OH}$ from Eq. (30)
	$6^m\text{C}_2\text{H}_5\text{OH}$ (g.c. with mass spec.)	
	$6^m\text{CH}_3\text{OH}$ (g.c. with mass spec.)	
	$4^m, 6^m\text{H}_2\text{O}$ (acid base titration using a pH indicator)	$4^y\text{B}(\text{OCH}_3)_3$ from Eq. (31)
	$4^m, 6^m\text{C}$ (NMR spectroscopy)	$4^y\text{CH}_3\text{OH}$ from Eq. (32)
	4^mSiO_2 (INAA)	$4^y\text{H}_2\text{O}$ from Eq. (33)
	$4^y\text{B}_2\text{O}_3$ (by difference)	
	4^ySiO_2 (plasma emission spectroscopy)	
	$4^y\text{B}_2\text{O}_3$ (plasma emission spectroscopy)	
	4^yC (gas chromatography with mass spectrometry)	

$$7^m \text{H}_2\text{O} = 4^m \text{H}_2\text{O} - 8^m \text{H}_2\text{O} + \frac{1}{2} 7^m \text{CH}_3\text{OH} + W \text{H}_2\text{O} \\ + (2+3a)(4^m \text{SiO}_2 - 7^m \text{SiO}_2 - 8^m \text{SiO}_2) \quad (39)$$

$$7^m \text{Na}^+ = Z \text{Na}^+ - 8^m \text{Na}^+ \quad (40)$$

$$7^m \text{Cl}^- = Z \text{Cl}^- - 8^m \text{Cl}^- \quad (41)$$

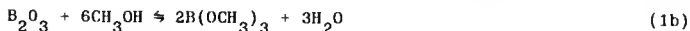
The recommended methods for complete analysis are summarized in Table 11.7.

I. Material Balance Around Dryer For a Swelled Lyogel

As indicated in Figure 11.2 the total material balance around the swelling solution tank is

$$8^M \text{OUT} = 5^Y + 9^M \text{OUT} \quad (42)$$

The chemical reactions are taken to be the following.



The component balances are as follows. The details are given in Section G of Appendix E.

$$5^Y \text{Si}(\text{OC}_2\text{H}_5)_4 = 8^m \text{SiO}_2 - 5^Y \text{SiO}_2 - 9^m \text{SiO}_2 - 9^m \text{Si}(\text{OC}_2\text{H}_5)_4 \quad (43)$$

$$5^Y \text{C}_2\text{H}_5\text{OH} = \frac{4-a}{2a} (8^m \text{C} - 5^Y \text{C} - 9^m \text{C}) - 9^m \text{C}_2\text{H}_5\text{OH} \quad (44)$$

$$5^Y \text{B}(\text{OCH}_3)_3 = 2(8^m \text{B}_2\text{O}_3 - 5^Y \text{B}_2\text{O}_3 - 9^m \text{B}_2\text{O}_3) - 9^m \text{B}(\text{OCH}_3)_5 \quad (45)$$

Table 11.7. Summary of Results for Material Balance Around Swelling Solution Tank.

Already measuring	Measurements to make (with recommended method of analysis)	Quantity to be obtained from material balance
z_{NaCl} input to swelling tank	$4^m, 6^m \text{B}^m \text{H}_2\text{O}$ (acid base titration with pH indicator)	$7^m \text{Si}(\text{OC}_2\text{H}_5)_4$ from Eq. (3S)
$w_{\text{H}_2\text{O}}$ input to swelling tank	$4^m, 6^m \text{C}$ (NMR spectroscopy)	$7^m \text{C}_2\text{H}_5\text{OH}$ from Eq. (36)
	$4^m, 6^m \text{SiO}_2$ (INAA)	$7^m \text{B}(\text{OCH}_3)_3$ from Eq. (37)
	$4^m, 6^m \text{B}_2\text{O}_3$ (by difference)	$7^m \text{CH}_3\text{OH}$ from Eq. (3B)
	6^mNa^+ (INAA)	$7^m \text{H}_2\text{O}$ from Eq. (39)
	6^mCl^- (INAA)	7^mNa^+ from Eq. (40)
	7^mSiO_2 (plasma emission spec.)	7^mCl^- from Eq. (41)
	$7^m \text{B}_2\text{O}_3$ (plasma emission spec.)	
	7^mC (gas chromatography with mass spectroscopy)	

Assumptions: Swelled lyogel contains no $\text{Si}(\text{OC}_2\text{H}_5)_4$, $\text{B}(\text{OCH}_3)_3$, $\text{C}_2\text{H}_5\text{OH}$ or CH_3OH .

$${}^5\text{YCH}_3\text{OH} = 6({}^8\text{m}_8\text{O}_3 - {}^5\text{Y}_8\text{O}_3 - {}^9\text{m}_8\text{O}_3) - {}^9\text{m}_8(\text{OCH}_3)_3 \quad (46)$$

$${}^5\text{YH}_2\text{O} = {}^8\text{m}_\text{H}_2\text{O} - {}^9\text{m}_\text{H}_2\text{O} + (2-3a)({}^8\text{m}_\text{SiO}_2 - {}^5\text{Y}_\text{SiO}_2 - {}^9\text{m}_\text{SiO}_2) \\ + \frac{1}{2}({}^9\text{m}_\text{CH}_3\text{OH} + {}^5\text{Y}_\text{CH}_3\text{OH}) \quad (47)$$

$${}^9\text{m}_\text{Na}^+ = {}^8\text{m}_\text{Na}^+ \quad (48)$$

$${}^9\text{m}_\text{Cl}^- = {}^8\text{m}_\text{Cl}^- \quad (49)$$

Assumptions: Na^+ and Cl^- does not vaporize at 110°C .

The recommended methods for complete analysis are summarized in Table 11.8.

J. Data Acquisition

The data required to close the material balance for the entire synthetic process shown in Figures 11.1 and 11.2 may be obtained as follows. Borosilicate lyogels are synthesized following the procedure modified by Angell [8] and stated in Chapter VIII, Section A. A liquid nitrogen cold trap is to be attached to the glass condenser at the top of the reaction vessel to collect vapors designated as ${}_1\text{Y}$ in Figure 11.1. After reacting at 50°C for the required length of time, the solution in the flask, ${}_1\text{M}_{\text{OUT}}$, is placed in a closed vessel with a liquid nitrogen cold trap attached to a side arm. The vapors collected are ${}_2\text{Y}$. Then the solution is allowed to gel and ${}_2\text{M}_{\text{OUT}}$ is obtained.

Table 11.8. Summary of Results for Material Balance Around Dryer for a Swelled Lyogel.

Already measuring	Measurements to make (with recommended method of analysis)	Quantity to be obtained from material balance
9^mSiO_2 (by INAA)	$9^m\text{Si}(\text{OC}_2\text{H}_5)_4$ (g.c. with mass spec.)	$5^y\text{Si}(\text{OC}_2\text{H}_5)_4$ from Eq. (43)
9^mNa^+ (by INAA)	$9^m\text{B}(\text{OCH}_3)_3$ (gas chromatography and mass spectroscopy)	$5^y\text{C}_2\text{H}_5\text{OH}$ from Eq. (44)
9^mCl^- (by INAA)	$9^m\text{C}_2\text{H}_5\text{OH}$ (g.c. with mass spec.) $9^m\text{CH}_3\text{OH}$ (g.c. with mass spec.)	
$9^m\text{B}_2\text{O}_3$ (by difference)	$8^m, 9^m\text{H}_2\text{O}$ (acid base titration with pH indicator) $8^m, 9^m\text{C}$ (NMR spectroscopy)	$5^y\text{B}(\text{OCH}_3)_3$ from Eq. (45) $5^y\text{CH}_3\text{OH}$ from Eq. (46)
	8^mSiO_2 (INAA)	$5^y\text{H}_2\text{O}$ from Eq. (47)
	$8^m\text{B}_2\text{O}_3$ (by difference)	8^mNa^+ from Eq. (48)
	5^ySiO_2 (plasma emission spectroscopy)	8^mCl^- from Eq. (49)
	$5^y\text{B}_2\text{O}_3$ (plasma emission spec.)	
	5^yC (gas chromatography with mass spectroscopy)	

Assumptions: Swelled lyogel contains no $\text{Si}(\text{OC}_2\text{H}_5)_4$, $\text{B}(\text{OCH}_3)_3$, $\text{C}_2\text{H}_5\text{OH}$ or CH_3OH .

Na^+ and Cl^- does not vaporize at 110°C .

All drying of samples is to be done in a heated chamber with a vacuum line attached. The chamber is purged with nitrogen and the sample is heated in dry air. The vapors are collected via the vacuum line and condensed by using a dry ice/acetone cold trap.

The first sample is weighed, $2^{M_{OUT}}$, and dried at $110^{\circ}C$ until constant weight. This gives $3^{M_{OUT}}$ and the condensed vapors are 3^Y . The second sample is weighed, $2^{M_{OUT}}$, rinsed until the rinsing solution is no greater than 1 percent ethanol, weighed again, $4^{M_{OUT}}$, and dried at $110^{\circ}C$ until constant weight. $6^{M_{OUT}}$ is obtained and the condensed vapors are 4^Y . The rinsing solution, $5^{M_{OUT}}$, is kept for subsequent analysis. The third sample is weighed, rinsed until the rinsing solution is no greater than 1 percent ethanol, swelled in 0.0 N NaCl solution for 28 days, weighed again, $8^{M_{OUT}}$, and dried at $110^{\circ}C$ until constant weight. $9^{M_{OUT}}$ is obtained and the condensed vapors are 5^Y . The rinsing solution and swelling solution, $7^{M_{OUT}}$, are kept for analysis. The fourth sample is processed as the third sample except that it is swelled in 1.0 N NaCl solution. The fifth sample is processed as the fourth sample except that it is swelled in 2.0 N NaCl solution.

K. Modification of INAA Method

As discussed in Chapter IV, Sections C and D, the mass of NaCl in a sample computed from INAA is less than the actual mass of NaCl in

the sample. Thus the estimates for boron content are higher than the actual boron content because the mass of boron is obtained by difference. This situation can probably be corrected by modifying the standards as follows [66]. Keeping the boron content constant, for example using 0.120 grams H_3BO_3 , vary the masses of SiO_2 and NaCl and obtain calibration lines similar to those discussed in Chapter IV, Section B. A series of samples will be needed, starting with no boron and increasing the boron content with each new calibration. The percentage of silicon in samples of unknown composition then can be used as an indicator for the selection of calibration lines. Two calibration lines can be used and the calculated mass values averaged. This modification should make the standards resemble more closely the borosilicate lyogels and hence give a better estimate of the boron content of these lyogels.

APPENDIX A.

Derivation of Model Used For Instrumental Neutron Activation Analysis

[24]

The derivation of the model developed by Higginbotham [24] to determine the amount of a particular element in an unknown sample is presented herein. All equations apply to the l^{th} element in the sample. It is assumed that this element activates to a daughter product that emits gamma rays, with only one particular energy being used for analysis.

The number of activated daughter products at a time, t , during irradiation is found by solving the rate equation which describes the change in those atoms. Let N represent the number of daughter product atoms at time t . Then

$$\{\text{Change in } N\} = \{\text{production of } N\} - \{\text{loss of } N\}. \quad (1)$$

The production of N is the number of parent atoms present at time t , $p(t)$, multiplied by the product of the probability of activation of the parent atom upon interaction with a neutron, σ , and the flux of neutrons striking the target, ϕ . It is assumed that the flux varies so slowly with time that it is essentially constant. Also, any energy or scattering angle dependence in the cross section is applied as required by the neutron flux; i.e., $\sigma\phi$ is constant. Self-shielding effects, or material resistance to neutron capture, are neglected. Thus, the production of N is expressed as the product $p(t)\sigma_p\phi$, where σ_p is the absorption cross section of the parent isotope. The number

of parent atoms at time t is the initial number, N_0 , minus the numbers that become activated;

$$p(t) = N_0 - \int_0^t N(z) dz.$$

Upon substitution one finds that

$$\{\text{production of } N\} = \sigma_p \phi \left[N_0 - \int_0^t N(z) dz \right]. \quad (2)$$

The loss of N is the number of daughter product atoms that decay plus the number that are converted to another isotope. The decay of N is the number of daughter product atoms multiplied by the probability of decay, λ .

$$\{\text{decay of } N\} = \lambda N \quad (3)$$

$$\text{The number of } N \text{ lost by activation is } N \sigma_d \phi. \quad (4)$$

where σ_d is the cross section of the daughter. Therefore,

$$\{\text{loss of } N\} = \lambda N + N \sigma_d \phi. \quad (5)$$

Combining Eqs. (5), (2) and (1) yields

$$\frac{dN}{dt} = \sigma_p \phi \left[N_0 - \int_0^t N(z) dz \right] - \lambda N - N \sigma_d \phi. \quad (6)$$

Taking the Laplace transform of Eq. (6) with an initial condition of $N(0) = 0$ yields

$$s \bar{N}(s) = \frac{\sigma_p \phi N_0}{s} - \frac{\sigma_p \phi \bar{N}(s)}{s} - \lambda \bar{N}(s) - \sigma_d \phi \bar{N}(s)$$

Solving for $\bar{N}(s)$ gives

$$\bar{N}(s) = \frac{N_0 \sigma_p \phi}{s^2 + [\lambda + \sigma_d \phi] s + \sigma_p \phi}$$

$$s = \frac{-(\lambda + \sigma_d \phi) + \left[(\lambda + \sigma_d \phi)^2 - 4\sigma_p \phi \right]^{1/2}}{2}$$

$$\bar{N}(s) = \frac{N_0 \sigma_p \phi}{(s - R_1)(s - R_2)}$$

$$\text{where } R_1 = \frac{-(\lambda + \sigma_d \phi) - \left[(\lambda + \sigma_d \phi)^2 - 4\sigma_p \phi \right]^{1/2}}{2}$$

$$R_2 = \frac{-(\lambda + \sigma_d \phi) + \left[(\lambda + \sigma_d \phi)^2 - 4\sigma_p \phi \right]^{1/2}}{2}$$

The time dependent solution is given by the inverse Laplace transform of the above equation,

$$N(t) = \frac{N_0 \sigma_p \phi}{(R_1 - R_2)} \left[e^{R_1 t} - e^{R_2 t} \right]. \quad (7)$$

Assuming there are no significant losses due to the activation of the daughter product, i.e., $\sigma_d \phi \ll \lambda$, Eq. (7)

becomes

$$N(t) = \frac{-N_0 \sigma_p \phi}{\left[\lambda^2 - 4\sigma_p \phi \right]^{1/2}} \exp \left[\frac{-\lambda - \left[\lambda^2 - 4\sigma_p \phi \right]^{1/2}}{2} t \right] \quad (8)$$

$$- \exp \left[\frac{-\lambda + \left[\lambda^2 - 4\sigma_p \phi \right]^{1/2}}{2} t \right].$$

Further, if depletion of the parent isotope during activation is neglected, i.e., $4\sigma_p \phi \ll \lambda^2$, then

$$N(t) = \frac{N_0 \sigma_p \phi}{\lambda} (1 - e^{-\lambda t}). \quad (9)$$

It is advantageous to express the number of parent atoms in terms of the mass of the parent element initially present.

$$N_0 = \frac{MA_b N_A}{A}, \quad (10)$$

where M is the mass of the parent element, A_b is the natural abundance of the parent isotope, N_A is Avogadro's number and A is the isotope atomic weight. Substituting Eq. (10) into Eq. (9),

$$N(t) = \frac{MA_b N_A \sigma_p \phi}{A\lambda} (1 - e^{-\lambda t}). \quad (11)$$

Hence, the number of daughter atoms at the end of the irradiation time, t_r , is

$$N_R = N(t_r) = \frac{MA_b N_A \sigma_p \phi}{A\lambda} (1 - e^{-\lambda t_r}). \quad (12)$$

After irradiation there is no production of N and Eq. (1) simplifies to

$$\{\text{change in } N\} = - \text{loss of } N \quad (13)$$

Since the only loss is due to radioactive decay,

$$\frac{dN}{dt} = -\lambda N, \text{ for } t > t_r.$$

Solving this equation for N , one finds

$$N = Ce^{-\lambda t}. \quad (14)$$

To determine the constant of integration, C , one applies the initial condition given by Eq. (12). Letting $N_R = N(t_r)$, one obtains

$$C = N_R e^{\lambda t_r}$$

Substitution into Eq. (14) yields

$$N(t) = N_R e^{\lambda(t_r - t)} \quad (15)$$

At this point in the experiment, the sample is placed adjacent to a gamma ray detector. At time t_s the detector system begins to count the number of gamma-ray detector interactions. These counts are stored as a function of energy. At time t_e the detector system stops collecting.

The number of atoms that decay during this interval, N_D , is given by

$$N_D = N(t_s) - N(t_e). \quad (16)$$

Substituting Eq. (15) into Eq. (16) one finds

$$N_D = N_R \left[e^{\lambda(t_r - t_s)} - e^{\lambda(t_r - t_e)} \right]. \quad (17)$$

The number of gamma rays emitted by the decayed atoms during the counting interval is the number of atoms that decay multiplied by the gamma-ray yield, i.e., gamma rays of each energy per disintegration,

Y. The number of counts recorded by the detector system is the number of gamma rays emitted multiplied by the absolute efficiency of the detector, E_f . E_f is the number of counts recorded in a certain channel divided by the number of counts actually occurring. The total number of counts recorded during the time interval is the peak area, P_a .

$$P_a = N_D E_f Y \quad (18)$$

Substituting Eq. (17) for N_D and Eq. (12) for N_R into Eq. (18)

and solving for M, the mass of the parent element, one finds

$$M = \frac{P_a A \lambda}{A_b N_A \sigma_p \phi E_f Y \left[1 - e^{-\lambda t_r} \right] \left[e^{\lambda(t_r - t_s)} - e^{\lambda(t_r - t_e)} \right]} \quad (19)$$

The peak area for each energy gamma ray is calculated from the measured pulse height distribution (plot of the number of counts versus channel number) and the time values for t_r , t_s , and t_e are recorded for each sample measured. The values of the neutron flux, ϕ , and the cross section, σ_p , are difficult to determine. Also, the detector efficiency, E_f , is a strong function of the energy of the incident gamma rays. However, if Eq. (19) is to be utilized, ϕ , σ_p , and E_f must be known.

To circumvent this problem, standard samples and fluence monitors are used. The standard sample is encapsulated separately from the unknown sample and the mass of each parent element in the standard must be known. The fluence monitors are metal wires of known mass

wrapped separately around the sample and the standards containers.

They are used to measure the value of $\int \phi dt$.

APPENDIX B.

EXAMPLE OF DATA REDUCTION

A. Calculation of P_a^C For Known Sample Composition

The data for 0.061g of SiO_2 irradiated for 6 minutes at a reactor power of 225 kW is given below.

P_a^P = peak area for sample = 10,570

W_M = mass of tungsten wire fluence monitor = 0.015 g.

$t_{s_r}^W, t_{e_r}^W$ = irradiation time = 6.0 min.

$t_{s_s}^W$ = time starting counts for tungsten wire = 324.417 min.

$t_{e_s}^W$ = time counting ends for tungsten wire = 331.417 min.

P_a^W = peak area for tungsten wire = 43,725

t_{s_s} = time starting counts for sample = 9.0 min.

t_{e_s} = time starting ends for sample = 26.0 min.

P_a^C is calculated from Eq. (6) of Chapter II.

$$P_a^C = \frac{P_a^P (W_M) [e^{\lambda_w (t_{s_r}^W - t_{s_s}^W)} - e^{\lambda_w (t_{e_r}^W - t_{e_s}^W)}]}{P_a^W [e^{\lambda_s (t_{s_r} - t_{s_s})} - e^{\lambda_s (t_{e_r} - t_{e_s})}]} \quad (\text{B-II.6})$$

$$\lambda_i = \ln 2 / (\text{half-life of } i)$$

$$\lambda_w = \ln 2 / 1428 = 4.8540 \times 10^{-4}$$

$$\lambda_s = \ln 2 / 2.241 = 0.3093$$

Thus P_a^C is given by

$$P_a^C = \frac{10,570(0.015) \left[e^{4.8540 \times 10^{-4}(6-324.417)} - e^{4.8540 \times 10^{-4}(6-331.417)} \right]}{43,725 \left(e^{0.3093(6-9)} - e^{0.3093(6-26)} \right)}$$

$$P_a^C = 2.6793 \times 10^{-5}$$

B. Calculation of The Mass of Species "i" in a Sample of Unknown Composition

The mass of species "i", \hat{M}_i , in an unknown sample is given by Eq.

(6) of Chapter II.

$$\hat{M}_i = X P_a^C + b \quad (\text{B-II.6a})$$

where X = slope of the mass line for the standard

b = intercept.

Now consider an $\text{SiO}_2 \cdot \text{B}_2\text{O}_3$ lyogel that had equilibrated with a 2.0N NaCl solution and had been dried at 110°C (i.e., Sample Tagword #126). P_a^C was calculated for SiO_2 , Na and Cl using Eq. (B-II.6) and are given below.

$$\text{SiO}_2 P_a^C = 3.316554 \times 10^{-5}$$

$$\text{Na} P_a^C = 1.310227 \times 10^{-3}$$

$$\text{Cl} P_a^C = 6.146406 \times 10^{-5}$$

The calibration lines for the three species of interest are listed in Table 4.2 and are as follows.

$$\hat{M}_{\text{SiO}_2} = 2543.88 \text{ SiO}_2^{\text{P}_a^{\text{C}}} - 0.005315 \quad (\text{B-1})$$

$$\hat{M}_{\text{Na}} = 9.2022 \text{ Na}^{\text{P}_a^{\text{C}}} - 0.0004428 \quad (\text{B-2})$$

$$\hat{M}_{\text{Cl}} = 322.85 \text{ Cl}^{\text{P}_a^{\text{C}}} - 0.0006072 \quad (\text{B-3})$$

Substituting $i^{\text{P}_a^{\text{C}}}$ into Eqs (1) to (3) yields

$$\hat{M}_{\text{SiO}_2} = 0.0791 \text{ g}$$

$$\hat{M}_{\text{Na}} = 0.0116 \text{ g}$$

$$\hat{M}_{\text{Cl}} = 0.0192 \text{ g}$$

C. Calculation of Lyogel Composition

The composition for the dried lyogel, $\text{SiO}_2 \cdot x\text{B}_2\text{O}_3$, will be computed.

$$\begin{aligned} \text{Mass B}_2\text{O}_3 &= \text{Sample mass} - \text{Mass SiO}_2 - \text{Mass Na} \\ &\quad - \text{Mass Cl} \quad (\text{B-4}) \\ &= 0.127 - 0.0791 - 0.0116 - 0.0192 \text{ g} \\ &= 0.0171 \text{ g} \end{aligned}$$

$$\begin{aligned} \text{Mass of dried lyogel} &= \text{Sample mass} - \text{Mass Na} - \text{Mass Cl} \quad (\text{B-5}) \\ &= 0.127 - 0.0116 - 0.0192 \text{ g} \\ &= 0.0962 \text{ g} \end{aligned}$$

$$\begin{aligned} \text{Fraction B}_2\text{O}_3 &= \frac{\text{Mass B}_2\text{O}_3}{\text{Mass of dried lyogel}} \quad (\text{B-6}) \\ &= \frac{0.0171\text{g}}{0.0962\text{g}} \\ &= 0.1778 \end{aligned}$$

The ratio of the moles of B_2O_3 per mole of SiO_2 is desired. The molecular weight of SiO_2 is 60.09 g/mole, and the molecular weight of B_2O_3 is 69.62 g/mole.

Let X = number of moles of B_2O_3

$$\text{Fraction } B_2O_3 = \frac{X(69.62)}{60.09 + X(69.62)} = 0.1178 \quad (B-7)$$

Solving for X in Eq. (B-7) gives

$$X = 0.1866. \quad (B-8)$$

Thus, the dried lyogel composition is $SiO_2 \cdot 0.1866B_2O_3$. The lyogel had been batched as $SiO_2 \cdot B_2O_3$, and a large difference in the boron content between the as-batched and dried lyogel compositions is noticed.

APPENDIX C

EXAMPLE OF MAXIMUM EXPERIMENTAL ERROR CALCULATION [67]

A. Calculation of Probable Error For P_a^C

An estimate of the error associated with P_a^C is desired. The probable error, ϵ , will be used as this estimate. Consider the following set of P_a^C data for 0.101 g irradiated for 6 minutes at 225 kW.

Trial	P_a^C (x_i)	$r_i = \bar{x} - x_i$	r_i^2
1	4.040961×10^{-5}	1.35380×10^{-6}	$1.8327744 \times 10^{-12}$
2	4.328929×10^{-5}	-1.52588×10^{-6}	$2.3283098 \times 10^{-12}$
3	4.264812×10^{-5}	-8.84710×10^{-7}	$7.8271178 \times 10^{-13}$
4	4.070662×10^{-5}	1.05679×10^{-6}	$1.1168051 \times 10^{-12}$

$$\Sigma x_i = 1.6705364 \times 10^{-4}$$

$$\text{mean} = \bar{x} = \Sigma x_i / 4 = 4.176341 \times 10^{-5}$$

$$\Sigma r_i^2 = 6.0606011 \times 10^{-12}$$

$$n = \text{number of data points} = 4$$

$$\text{degrees of freedom} = (n-1) = 4-1 = 3$$

$$\text{standard deviation} = \sigma = \sqrt{\Sigma r_i^2 / (n-1)} \quad (C-1)$$

$$\begin{aligned}
&= \sqrt{6.0606011 \times 10^{-12} / 3} \\
&= 1.4213375 \times 10^{-6}
\end{aligned}$$

The probable error for "i" is

$$\epsilon_i = t\sigma \quad (\text{C-2})$$

where t = Student's t value.

For 3 degrees of freedom t = 0.765.

Substituting values for t and σ in Eq. (C-2) gives

$$\begin{aligned}
\epsilon_{\text{SiO}_2} &= 0.765(1.4213375 \times 10^{-6}) \\
&= \pm 1.0873232 \times 10^{-6}
\end{aligned}$$

Thus, the error associated with P_a^C for SiO_2 is

$$\text{SiO}_2 P_a^C \pm 1.0873232 \times 10^{-6}$$

Similar calculations for 0.017g NaCl irradiated for 6 minutes at 225 kW gives

$$\text{Na} P_a^C \pm 3.5502473 \times 10^{-5}$$

$$\text{Cl} P_a^C \pm 1.0631543 \times 10^{-6}$$

B. Calculation of Probable Error For Slope and Intercept

The mass of species "i", \hat{M}_i , in an unknown sample is given by Eq.

(6) of Chapter II.

$$\hat{M}_i = XP_a^C + b \quad (\text{C-II.6})$$

where X = slope of the mass line for the standard

b = intercept.

The probable errors for the slope and the intercept, ϵ_X and ϵ_b , respectively, are

$$\epsilon_X = t \sqrt{\frac{n(\Sigma r_i^2)}{(n-2)[n(\Sigma x_i^2) - (\Sigma x_i)^2]}} \quad (C-3)$$

= probable error of slope, X.

$$\epsilon_b = t \sqrt{\frac{(\Sigma x_i^2)(\Sigma r_i^2)}{(n-2)[n(\Sigma x_i^2) - (\Sigma x_i)^2]}} \quad (C-4)$$

= probable error of intercept, b.

where n = number of data points

$r = \hat{M}_i$ - actual mass of i

$$(\Sigma x_i^2) = (\Sigma (P_a^C)^2)$$

$$(\Sigma x_i)^2 = (\Sigma P_a^C)^2$$

t = Student's t value.

Consider the following set of data for SiO_2 irradiated for 6 minutes at 225 kW. Let \hat{M}_{SiO_2} be given by

$$\hat{M}_{\text{SiO}_2} = 2626.37 \text{ SiO}_2 P_a^C - 0.00684. \quad (C-5)$$

P_a^C	$(P_a^C)^2$	M_{S10_2}	\hat{M}_{S10_2}	r_1	r_1^2
(x_1)	(x_1^2)	(y_1)	$Y(x_1)$	$Y(x_1)-y_1$	
5.26170×10^{-6}	$2.7685487 \times 10^{-11}$	0.010	0.00698	-3.02×10^{-3}	9.1204×10^{-6}
1.54923×10^{-5}	$2.4001346 \times 10^{-10}$	0.033	0.03385	8.50×10^{-4}	7.225×10^{-7}
2.67930×10^{-5}	$7.1786485 \times 10^{-10}$	0.081	0.08353	2.53×10^{-3}	6.4009×10^{-7}
4.99909×10^{-5}	2.4990901×10^{-9}	0.131	0.12446	-6.54×10^{-3}	4.27718×10^{-5}
3.48687×10^{-5}	1.2158262×10^{-9}	0.086	0.06474	-1.26×10^{-3}	1.5876×10^{-6}
3.89965×10^{-5}	1.520727×10^{-9}	0.089	0.09558	6.58×10^{-3}	4.32964×10^{-5}
4.15637×10^{-5}	1.7275412×10^{-9}	0.105	0.102325	-2.675×10^{-3}	7.155625×10^{-6}
4.54474×10^{-5}	2.0654662×10^{-9}	0.109	0.112525	3.525×10^{-3}	1.24256×10^{-5}

$$(\Sigma x_1^2) = 1.0014215 \times 10^{-8}$$

n = 8, degrees of freedom = n-2 = 6

$$\Sigma x_1 = 2.584143 \times 10^{-4}$$

$$(\Sigma r_1^2) = 1.2348065 \times 10^{-4}$$

$$(\Sigma x_1)^2 = 8.877795 \times 10^{-8}$$

For 6 degrees of freedom, $t = 0.718$. Substituting into Eqs. (C-3) and (C-4) gives the following.

$$\text{SiO}_2 \epsilon_X = 0.718 \sqrt{\frac{8(1.2348065 \times 10^{-4})}{6[8(1.0014215 \times 10^{-8}) - 6.677795 \times 10^{-8}]}}$$

$$= 79.7782$$

$$\text{SiO}_2 \epsilon_X = \pm 79.8$$

$$\text{SiO}_2 \epsilon_b = 0.718 \sqrt{\frac{(1.0014215 \times 10^{-8})(1.2348085 \times 10^{-4})}{6[8(1.0014215 \times 10^{-8}) - 6.677795 \times 10^{-8}]}}$$

$$= 0.00282259$$

$$\text{SiO}_2 \epsilon_b = \pm 0.0028$$

Similar calculations for masses of NaCl, irradiated for 6 minutes at 225 kW, gives the following probable errors.

$$\text{Na} \epsilon_X = \pm 0.154$$

$$\text{Na} \epsilon_b = \pm 0.0004$$

$$\text{Cl} \epsilon_X = \pm 11.23$$

$$\text{Cl} \epsilon_b = \pm 0.00125$$

C. Calculation of The Maximum Experimental Error of \hat{M}_i

\hat{M}_i is given by the following relationship.

$$\hat{M}_i = X P_a^C + b \quad (\text{C-II.6})$$

where X = slope of the mass line for the standard

b = intercept.

Thus \hat{M}_i is a function of X , P_a^C and b , and

$$d(\hat{M}_i) = \left[\frac{\partial \hat{M}_i}{\partial X} \right] dX + \left[\frac{\partial \hat{M}_i}{\partial P_a^C} \right] dP_a^C + \left[\frac{\partial \hat{M}_i}{\partial b} \right] db \quad (C-6)$$

or

$$\Delta \hat{M}_i = \left[\frac{\partial \hat{M}_i}{\partial X} \right] \Delta X + \left[\frac{\partial \hat{M}_i}{\partial P_a^C} \right] \Delta P_a^C + \left[\frac{\partial \hat{M}_i}{\partial b} \right] \Delta b \quad (C-7)$$

where $\Delta \hat{M}_i$ is the maximum experimental error of \hat{M}_i due to experimental errors ΔX , ΔP_a^C and Δb . The partial derivatives (calculated from Eq. (C-II.6)) are as follows.

$$\left[\frac{\partial \hat{M}_i}{\partial X} \right] = P_a^C$$

$$\left[\frac{\partial \hat{M}_i}{\partial P_a^C} \right] = X$$

$$\left[\frac{\partial \hat{M}_i}{\partial b} \right] = 1$$

Recall from Sections A and B that the experimental errors are as follows.

	ΔP_a^C	ΔX	Δb
SiO ₂	$\pm 1.087 \times 10^{-6}$	± 79.8	± 0.0028
Na	$\pm 3.550 \times 10^{-5}$	± 0.154	± 0.0004
Cl	$\pm 1.063 \times 10^{-6}$	± 11.23	± 0.00125

Thus $\hat{\Delta M}_i$ is given by

$$\hat{\Delta M}_i = \sum_a P_a^C \Delta X_i + X_i \Delta_i P_a^C + \Delta b_i. \quad (C-8)$$

The mass of species "i" in an unknown sample is reported as

$$\hat{M}_i \pm \hat{\Delta M}_i.$$

D. Calculation of The Maximum Experimental Error For The Mass of B_2O_3

In A Sample of Unknown Composition

The mass of B_2O_3 for a sample is calculated from the following.

$$\hat{M}_{B_2O_3} = M_{\text{sample}} - \hat{M}_{SiO_2} - \hat{M}_{Na} - \hat{M}_{Cl} \quad (C-9)$$

Thus $\hat{M}_{B_2O_3}$ is a function of M_{sample} , \hat{M}_{SiO_2} , \hat{M}_{Na} and \hat{M}_{Cl} , and

$$\begin{aligned} d(\hat{M}_{B_2O_3}) &= \left[\frac{\partial \hat{M}_{B_2O_3}}{\partial M_{\text{sample}}} \right] dM_{\text{sample}} + \left[\frac{\partial \hat{M}_{B_2O_3}}{\partial \hat{M}_{SiO_2}} \right] d\hat{M}_{SiO_2} \\ &+ \left[\frac{\partial \hat{M}_{B_2O_3}}{\partial \hat{M}_{Na}} \right] d\hat{M}_{Na} + \left[\frac{\partial \hat{M}_{B_2O_3}}{\partial \hat{M}_{Cl}} \right] d\hat{M}_{Cl} \end{aligned} \quad (C-10)$$

or

$$\begin{aligned} \hat{\Delta M}_{B_2O_3} &= \left[\frac{\partial \hat{M}_{B_2O_3}}{\partial M_{\text{sample}}} \right] \Delta M_{\text{sample}} + \left[\frac{\partial \hat{M}_{B_2O_3}}{\partial \hat{M}_{SiO_2}} \right] \Delta \hat{M}_{SiO_2} \\ &+ \left[\frac{\partial \hat{M}_{B_2O_3}}{\partial \hat{M}_{Na}} \right] \Delta \hat{M}_{Na} + \left[\frac{\partial \hat{M}_{B_2O_3}}{\partial \hat{M}_{Cl}} \right] \Delta \hat{M}_{Cl} \end{aligned} \quad (C-11)$$

where $\hat{\Delta M}_{B_2O_3}$ is the maximum experimental error of $\hat{M}_{B_2O_3}$ due to experimental errors ΔM_{sample} , $\hat{\Delta M}_{Na}$ and $\hat{\Delta M}_{Cl}$. The partial derivatives which follow are calculated from Eq. (C-9).

$$\left[\frac{\partial \hat{M}_{B_2O_3}}{\partial \Delta M_{\text{sample}}} \right] = 1$$

$$\left[\frac{\partial \hat{M}_{B_2O_3}}{\partial \hat{M}_{SiO_2}} \right] = -1$$

$$\left[\frac{\partial \hat{M}_{B_2O_3}}{\partial \hat{M}_{Na}} \right] = -1$$

$$\left[\frac{\partial \hat{M}_{B_2O_3}}{\partial \hat{M}_{Cl}} \right] = -1$$

$\Delta M_{\text{sample}} = \pm 0.001g$ and $\hat{\Delta M}_I$ are calculated from Eq. (C-B). Thus

$\hat{\Delta M}_{B_2O_3}$ is given by

$$\hat{\Delta M}_{B_2O_3} = 0.001 + \hat{\Delta M}_{SiO_2} + \hat{\Delta M}_{Na} + \hat{\Delta M}_{Cl}. \quad (C-12)$$

Note that all the minus signs have been changed to plus signs in order to obtain the largest possible experimental error. It is desirable to assume that all the experimental errors are working in the same direction when computing such an error in the final quantity.

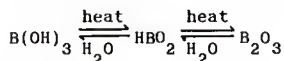
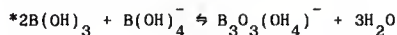
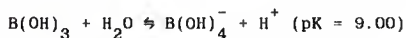
The mass of B_2O_3 is reported as $\hat{M}_{B_2O_3} \pm \Delta\hat{M}_{B_2O_3}$.

APPENDIX O.

COMPENIUM of BORON and BOROSILICATE CHEMISTRY

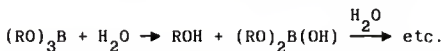
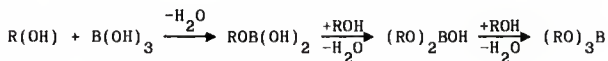
A summary of boron and borosilicate chemistry references with associated chemical reactions is presented herein.

1. Advanced Inorganic Chemistry, 4th ed., F.A. Cotton and G. Wilkinson, Wiley-Interscience, 1980, pp. 297-299, New York.

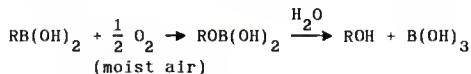
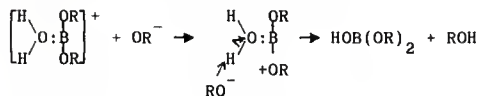


*R.E. Mesmer, C.F. Baes, Jr. and F.H. Sweeton, "Inorg. Chem.", 11, 537 (1972); H.O. Smith, Jr., and R.W. Wiersema, Inorg. Chem., 11, 1152 (1972).

2. Comprehensive Inorganic Chemistry, Vol. 1, A. F. Trotman-Dickenson, Executive Editor, p. B97, Pergamon Press Ltd., New York, 1973.



3. The Organic Chemistry of Boron, W. Gerrard, pp. 12, 7B, Academic Press, New York, 1961.



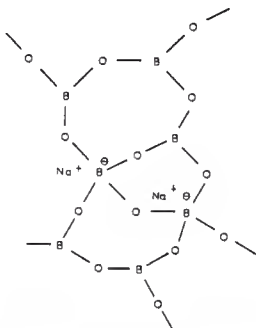
"On the other hand, alkylboronic acids are much more susceptible to oxidative cleavage than their aryl analogues, and are readily autoxidized in air, although they appear to be more stable when moist." (Snyder *et al.*, 1938; Johnson *et al.*, 1938).*

*Snyder, H.R., Kuck, J.A., and Johnson, J.R., J. Amer. Chem. Soc., 60, 105 (1938).

*Johnson, J.R., Snyder, H.R., and Van Campen, M.G., J. Amer. Chem. Soc., 60, 115 (1938).

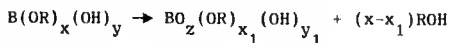
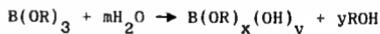
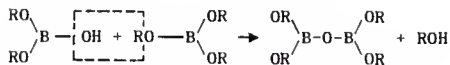
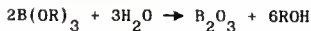
*Johnson, J.R., and Van Kampen, M.G., J. Amer. Chem. Soc., 60, 121 (1938).

4. Inorganic Polymers, N.H. Ray, pp. 73-75, Academic Press, New York, 1978.



Change in connectivity of a boronic oxide network produced by introduction of cations.

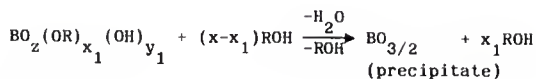
5. "Monolithic Glass Formation by Chemical Polymerization," B.E. Yoldas, J. Mat. Sci., 14, 1B43-1B49 (1979).



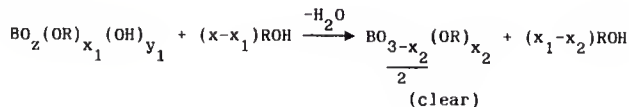
where $x+y=3$

$$z = \frac{1}{2}[3 - (x_1 + y_1)]$$

(if $x_1 < y_1$):



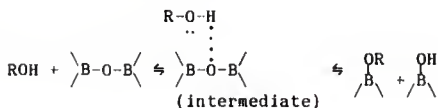
(if $x_1 > y_1$):



if $m > 1.5$: $x_2 < 0$ (does not exist)

if $m < 1.5$: $x_2 > 0$

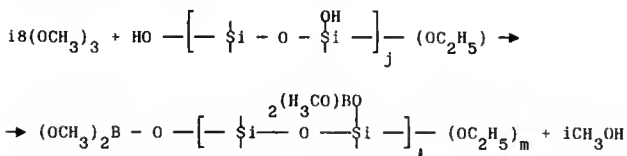
6. "Solution Chemistry of Silicate and Borate Materials," B.C. Bunker, in Better Ceramics Through Chemistry II, Vol. 73, Brinker, C.J., Clark, D.E., and Ulrich, D.R. editors, pp. 57-68, MRS, Pittsburgh, 1986.



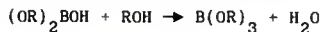
7. "Sol-Gel Processing of SiO_2 - B_2O_3 Glasses", B. Kumar, Mat. Res. Bull., 19, 31-338 (1984).



8. "Glass Formation of the SiO_2 - B_2O_3 System by the Gel Process from Metal Alkoxides," M. Nogami, and Y. Moriya, J. Non-Cryst. Solids, 48, 359-366 (1982).



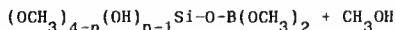
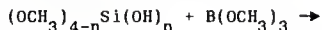
9. "Stronger Glass Via Sol-Gel Coatings," 8.D. Fabes, et al., Science of Ceramic Chemical Processing, L.L. Hench and D.R. Ulrich editors, pp. 217-23, John Wiley & Sons, Inc., New York, 1986.



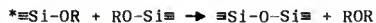
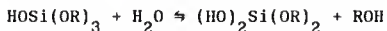
14. "Physical-Chemical Variables in Processing $\text{Na}_2\text{O}-\text{B}_2\text{O}_3-\text{SiO}_2$ Gel Monoliths," G. Orcel and L.L. Hench, Mat. Res. Symp. Proc., **32**, Elsevier 79-84 (1984).



15. "Monolithic Aerogels in the Systems $\text{SiO}_2-\text{B}_2\text{O}_3$, $\text{SiO}_2-\text{P}_2\text{O}_5$, $\text{SiO}_2-\text{B}_2\text{O}_3-\text{P}_2\text{O}_5$," T. Woinier et al., J. Non-Cryst. Solids, **63**, 117-130 (1984).



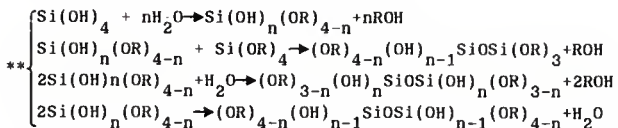
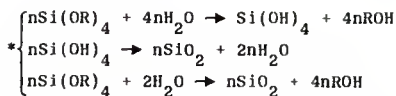
16. "Principles of Hydrolysis and Condensation Reaction of Alkoxyxilanes," H. Schmidt et al., J. Non-Cryst. Solids, **63**, 1-11 (1984).



*W. Noll, Chemie und Technologie der Silicone, Z. Auflage (Verlag Chemie, Weinheim, 1968).

*M.G. Voronkov et al., The Siloxane Bond (Plenum, New York, London, 1978).

17. "Sol-Gel Transition In The Hydrolysis of Silicon Methoxide," M. Yamane *et al.*, J. Non-Cryst. Solids, **63**, 13-21 (1984).



*H. Dishlish and P. Hinz, J. Non-Cryst. Solids, **48**, 11 (1982).

* and ** S. Sakka and K. Kamiya, J. Non-Cryst. Solids, **48**, 31 (1982).

8.E. Yoldas, J. Non-Cryst. Solids, **81, 38-39 (1980).

C.J.R. Gonzalez-Oliver *et al.*, J. Non-Cryst. Solids, **48, 129 (1982).

APPENDIX E.

SIMPLIFICATION OF COMPONENT MATERIAL BALANCES

A. Material Balance Around Reaction Flask

The overall material balance around the reaction flask is given by Eq. (4) of Chapter XI.

$$1^M_{IN} = 1^Y + 1^M_{OUT} \quad (11-4)$$

The component balances are as follows.

$$1^m_{Si(OC_2H_5)_4} = M_{Si(OC_2H_5)_4} - 1^Y_{Si(OC_2H_5)_4} - X_{h,TEOS} M_{Si(OC_2H_5)_4} \quad (5)$$

where $X_{h,TEOS}$ = extent of $Si(OC_2H_5)_4$ hydrolysis

Rearranging and solving for $X_{h,TEOS}$ yields

$$X_{h,TEOS} = \frac{1}{M_{Si(OC_2H_5)_4}} (M_{Si(OC_2H_5)_4} - 1^Y_{Si(OC_2H_5)_4} - 1^m_{Si(OC_2H_5)_4}) \quad (5a)$$

$$1^m_{B(OCH_3)_3} = M_{B(OCH_3)_3} - 1^Y_{B(OCH_3)_3} - X_{h,TMB} M_{B(OCH_3)_3} \quad (6)$$

Rearranging and solving for $X_{h,TMB}$ gives

$$X_{h,TMB} = \frac{1}{M_{B(OCH_3)_3}} (M_{B(OCH_3)_3} - 1^Y_{B(OCH_3)_3} - 1^m_{B(OCH_3)_3}) \quad (6a)$$

$$1^m_{SiO_2} = X_{h,TEOS} M_{Si(OC_2H_5)_4} - 1^Y_{SiO_2} \quad (7)$$

$$X_{h,TEOS} = \frac{1}{M_{Si(OC_2H_5)_4}} (1^m_{SiO_2} + 1^Y_{SiO_2}) \quad (7a)$$

$$1^m B_2O_3 = \frac{1}{2} X_{h, TMB} M_B(OCH_3)_3 - 1^y B_2O_3 \quad (B)$$

$$X_{h, TMB} = \frac{2}{M_B(OCH_3)_3} (1^m B_2O_3 + 1^y B_2O_3) \quad (Ba)$$

$$1^m H_2O = M_{H_2O} - 1^y H_2O - (2 - 3a) X_{h, TEOS} M_{Si(OC_2H_5)_4} - \frac{3}{2} X_{h, TMB} M_B(OCH_3) \quad (9)$$

$$X_{h, TMB} = \frac{2}{3M_B(OCH_3)_3} [M_{H_2O} - 1^y H_2O - 1^m H_2O - (2 - 3a) X_{h, TEOS} M_{Si(OC_2H_5)_4}] \quad (9a)$$

$$1^m C_2H_5OH = M_{C_2H_5OH} - 1^y C_2H_5OH + (4 - a) X_{h, TEOS} M_{Si(OC_2H_5)_4} \quad (10)$$

$$X_{h, TEOS} = \frac{1}{(4 - a)M_{Si(OC_2H_5)_4}} (1^m C_2H_5OH - M_{C_2H_5OH} + 1^y C_2H_5OH) \quad (10a)$$

$$1^m CH_3OH = \frac{6}{2} X_{h, TMB} M_B(OCH_3)_3 - 1^y CH_3OH \quad (11)$$

$$X_{h, TMB} = \frac{1}{3M_B(OCH_3)_3} (1^m CH_3OH + 1^y CH_3OH) \quad (11a)$$

$$1^m C = 2aX_{h, TEOS} M_{Si(OC_2H_5)_4} - 1^y C \quad (12)$$

$$X_{h, TEOS} = \frac{1}{2aM_{Si(OC_2H_5)_4}} (1^m C + 1^y C) \quad (12a)$$

Equating Eq. (5a) to Eq. (7a) and simplifying gives

$$1^y Si(OC_2H_5)_4 = M_{Si(OC_2H_5)_4} - 1^m Si(OC_2H_5)_4 - 1^m SiO_2 - 1^y SiO_2 \quad (13)$$

Equating Eq. (10a) to Eq. (12a) and simplifying gives

$$1^y_{C_2H_5OH} = \frac{4-a}{2a} (1^m_C + 1^y_C) - 1^m_{C_2H_5OH} + M_{C_2H_5OH} \quad (14)$$

Equating Eq. (6a) to Eq. (8a) and simplifying gives

$$1^y_{B(OCH_3)_3} = M_{B(OCH_3)_3} - 1^m_{B(OCH_3)_3} - 2(1^m_{B_2O_3} + 1^y_{B_2O_3}) \quad (15)$$

Equating Eq. (8a) to Eq. (11a) and simplifying gives

$$1^y_{CH_3OH} = 6(1^m_{B_2O_3} + 1^y_{B_2O_3}) - 1^m_{CH_3OH} \quad (16)$$

Substituting Eqs. (7a) and (11a) into Eq. (9) yields

$$1^y_{H_2O} = M_{H_2O} - 1^m_{H_2O} - (2 - 3a)(1^m_{SiO_2} + 1^y_{SiO_2}) - \frac{1}{2}(1^m_{CH_3OH} + 1^y_{CH_3OH}) \quad (17)$$

$1^y_{SiO_2}$, $1^y_{B_2O_3}$ and 1^y_C are assumed to be negligible.

B. Material Balance Around Sample Vial

The overall material balance around the sample vial is given by Eq. (1B) of Chapter XI.

$$1^M_{OUT} = 2^Y + 2^M_{OUT} \quad (11-1B)$$

Using procedures similar to those in Section A, the component balances are as follows.

$$X'_{h,TEOS} = \frac{1}{1^m_{Si(OC_2H_5)_4}} \left[1^m_{Si(OC_2H_5)_4} - 2^y_{Si(OC_2H_5)_4} - 2^m_{Si(OC_2H_5)_4} \right] \quad (19)$$

$$X'_{h,TMB} = \frac{1}{1^m_{B(OCH_3)_3}} \left(1^m_{B(OCH_3)_3} - 2^y_{B(OCH_3)_3} - 2^m_{B(OCH_3)_3} \right) \quad (20)$$

$$X'_{h,TEOS} = \frac{1}{1^m_{Si(OC_2H_5)_4}} \left(2^m_{SiO_2} + 2^y_{SiO_2} - 1^m_{SiO_2} \right) \quad (21)$$

$$X'_{h,TMB} = \frac{2}{1^m_{B(OCH_3)_3}} \left(2^m_{B_2O_3} + 2^y_{B_2O_3} - 1^m_{B_2O_3} \right) \quad (22)$$

$$2^m_{H_2O} = 1^m_{H_2O} - 2^y_{H_2O} - (2-3a) X'_{h,TEOS} 1^m_{Si(OC_2H_5)_4} - \frac{3}{2} X'_{h,TMB} 1^m_{B(OCH_3)_3} \quad (23)$$

$$X'_{h,TEOS} = \frac{1}{(4-a) 1^m_{Si(OC_2H_5)_4}} \left(2^m_{C_2H_5OH} - 1^m_{C_2H_5OH} + 2^y_{C_2H_5OH} \right) \quad (24)$$

$$X'_{h,TMB} = \frac{1}{3 1^m_{B(OCH_3)_3}} \left(2^m_{CH_3OH} + 2^y_{CH_3OH} - 1^m_{CH_3OH} \right) \quad (25)$$

$$X'_{h,TEOS} = \frac{1}{2a 1^m_{Si(OC_2H_5)_4}} \left(2^m_C + 2^y_C - 1^m_C \right) \quad (26)$$

Equating Eq. (19) to Eq. (21) and simplifying gives

$$2^y \text{Si}(\text{OC}_2\text{H}_5)_4 = 1^m \text{Si}(\text{OC}_2\text{H}_5)_4 - 2^m \text{Si}(\text{OC}_2\text{H}_5)_4 - 2^m \text{SiO}_2 - 2^y \text{SiO}_2 + 1^m \text{SiO}_2 \quad (27)$$

Equating Eq. (24) to Eq. (26) and simplifying yields

$$2^y \text{C}_2\text{H}_5\text{OH} = \frac{4-a}{2a} (2^m \text{C} + 2^y \text{C} - 1^m \text{C}) + 1^m \text{C}_2\text{H}_5\text{OH} - 2^m \text{C}_2\text{H}_5\text{OH} \quad (28)$$

Equating Eq. (20) to Eq. (22) and simplifying gives

$$2^y \text{B}(\text{OCH}_3)_3 = 1^m \text{B}(\text{OCH}_3)_3 - 2^m \text{B}(\text{OCH}_3)_3 - 2(2^m \text{B}_2\text{O}_3 + 2^y \text{B}_2\text{O}_3 - 1^m \text{B}_2\text{O}_3) \quad (29)$$

Equating Eq. (22) to Eq. (25) and simplifying yields

$$2^y \text{CH}_3\text{OH} = 6(2^m \text{B}_2\text{O}_3 + 2^y \text{B}_2\text{O}_3 - 1^m \text{B}_2\text{O}_3) - 2^m \text{CH}_3\text{OH} + 1^m \text{CH}_3\text{OH} \quad (30)$$

Substituting Eqs. (21) and (25) into Eq. (23) gives

$$2^y \text{H}_2\text{O} = 1^m \text{H}_2\text{O} - 2^m \text{H}_2\text{O} - (2-3a)(2^m \text{SiO}_2 + 2^y \text{SiO}_2 - 1^m \text{SiO}_2) - \frac{1}{2} (2^m \text{C}_2\text{H}_5\text{OH} + 2^y \text{CH}_3\text{OH} - 1^m \text{CH}_3\text{OH}) \quad (31)$$

2^ySiO_2 , $2^y \text{B}_2\text{O}_3$ and 2^yC are assumed to be negligible.

C. Material Balance Around Dryer For an Unrinsed Lyogel

The overall material balance around the dryer for an unrinsed lyogel is given by Eq. (16) of Chapter XI.

$$2^M \text{OUT} = 3^Y + 3^M \text{OUT} \quad (11-16)$$

Using procedures similar to those in Section A, the component balances are as follows.

$$X_{h,TEOS}^{//} = \frac{1}{2^m Si(OC_2H_5)_4} (2^m Si(OC_2H_5)_4 - 3^y Si(OC_2H_5)_4 - 3^m Si(OC_2H_5)_4) \quad (32)$$

$$X_{h,TMB}^{//} = \frac{1}{2^m B(OCH_3)_3} (2^m B(OCH_3)_3 - 3^y B(OCH_3)_3 - 3^m B(OCH_3)_3) \quad (33)$$

$$X_{h,TEOS}^{//} = \frac{1}{2^m Si(OC_2H_5)_4} (3^m SiO_2 + 3^y SiO_2 - 2^m SiO_2) \quad (34)$$

$$X_{h,TMB}^{//} = \frac{1}{2^m B(OCH_3)_3} (3^m B_2O_3 + 3^y B_2O_3 - 2^m B_2O_3) \quad (35)$$

$$3^m H_2O = 2^m H_2O - 3^y H_2O - (2-3a) X_{h,TEOS}^{//} 2^m Si(OC_2H_5)_4 - \frac{3}{2} X_{h,TMB}^{//} 2^m B(OCH_3)_3 \quad (36)$$

$$X_{h,TEOS}^{//} = \frac{1}{(4-a) 2^m Si(OC_2H_5)_4} (3^m C_2H_5OH - 2^m C_2H_5OH + 3^y C_2H_5OH) \quad (37)$$

$$X_{h,TMB}^{//} = \frac{1}{3 2^m B(OCH_3)_3} (3^m CH_3OH + 3^y CH_3OH - 2^m CH_3OH) \quad (38)$$

$$X_{h,TEOS}^{//} = \frac{1}{2a 2^m Si(OC_2H_5)_4} (3^m C + 3^y C - 2^m C) \quad (39)$$

Equating Eq. (32) to Eq. (34) and simplifying gives

$$3^y Si(OC_2H_5)_4 = 2^m Si(OC_2H_5)_4 - 3^m Si(OC_2H_5)_4 - 3^m SiO_2 - 3^y SiO_2 + 2^m SiO_2 \quad (40)$$

Equating Eq. (37) to Eq. (39) and simplifying yields

$$3^y C_2H_5OH = \frac{4-a}{2a} (3^m C + 3^y C - 2^m C) - 3^m C_2H_5OH + 2^m C_2H_5OH \quad (41)$$

Equating Eq. (33) to Eq. (35) and simplifying gives

$$3^y \text{B}(\text{OCH}_3)_3 = 2^m \text{B}(\text{OCH}_3)_3 - 3^m \text{B}(\text{OCH}_3)_3 - 2(3^m \text{B}_2\text{O}_3) - 2(3^y \text{B}_2\text{O}_3 - 2^m \text{B}_2\text{O}_3) \quad (42)$$

Equating Eq. (35) to Eq. (38) and simplifying yields

$$3^y \text{CH}_3\text{OH} = 6(3^m \text{B}_2\text{O}_3 + 3^y \text{B}_2\text{O}_3 - 2^m \text{B}_2\text{O}_3) - 3^m \text{CH}_3\text{OH} + 2^m \text{CH}_3\text{OH} \quad (43)$$

Substituting Eqs. (34) and (38) into Eq. (36) gives

$$2^y \text{H}_2\text{O} = 2^m \text{H}_2\text{O} - 3^m \text{H}_2\text{O} - (2-3a)(3^m \text{SiO}_2 + 3^y \text{SiO}_2 + 2^m \text{SiO}_2) + \frac{1}{2}(3^m \text{CH}_3\text{OH} + 3^y \text{CH}_3\text{OH} - 2^m \text{CH}_3\text{OH}) \quad (44)$$

D. Material Balance Around Rinsing Tank

The overall material balance around the rinsing tank is given by Eq. (22) of Chapter XI.

$$2^M \text{OUT} + 2^M \text{IN} = 4^M \text{OUT} + 5^M \text{OUT} \quad (11-22)$$

The component balances are as follows. It has been assumed that all $\text{Si}(\text{OC}_2\text{H}_5)_4$, $\text{B}(\text{OCH}_3)_3$, CH_3OH and $\text{C}_2\text{H}_5\text{OH}$ have been rinsed out of the lyogel at the completion of the rinsing process.

$$4^m \text{Si}(\text{OC}_2\text{H}_5)_4 = 0 = 2^m \text{Si}(\text{OC}_2\text{H}_5)_4 - 5^m \text{Si}(\text{OC}_2\text{H}_5)_4 - X_{h, \text{TEOS}}^{///} 2^m \text{Si}(\text{OC}_2\text{H}_5)_4 \quad (45)$$

Rearranging and solving for $X_{h, \text{TEOS}}^{///}$ gives

$$X_{h, \text{TEOS}}^{///} = 1 - \frac{5^m \text{Si}(\text{OC}_2\text{H}_5)_4}{2^m \text{Si}(\text{OC}_2\text{H}_5)_4} \quad (45a)$$

$$4^m \text{B}(\text{OCH}_3)_3 = 0 = 2^m \text{B}(\text{OCH}_3)_3 - 5^m \text{B}(\text{OCH}_3)_3 - X_{h, \text{TMB}}^{///} 2^m \text{B}(\text{OCH}_3)_3 \quad (46)$$

$$X_{h, \text{TMB}}^{///} = 1 - \frac{5^m \text{B}(\text{OCH}_3)_3}{2^m \text{B}(\text{OCH}_3)_3} \quad (46a)$$

$$X_{h, \text{TEOS}}^{///} = \frac{1}{2^m \text{Si}(\text{OC}_2\text{H}_5)_3} (4^m \text{SiO}_2 + 5^m \text{SiO}_2 - 2^m \text{SiO}_2) \quad (47)$$

$$X_{h, \text{TMB}}^{///} = \frac{2}{2^m \text{B}(\text{OCH}_3)_3} (4^m \text{B}_2\text{O}_3 + 5^m \text{B}_2\text{O}_3 - 2^m \text{B}_2\text{O}_3) \quad (48)$$

$$4^m \text{H}_2\text{O} = 2^m \text{H}_2\text{O} - 5^m \text{H}_2\text{O} - (2-3a) X_{h, \text{TEOS}}^{///} 2^m \text{Si}(\text{OC}_2\text{H}_5)_4 - \frac{3}{2} X_{h, \text{TMB}}^{///} 2^m \text{B}(\text{OCH}_3)_3 + z \text{H}_2\text{O} \quad (49)$$

$$X_{h, \text{TEOS}}^{///} = \frac{1}{(4-a) 2^m \text{Si}(\text{OC}_2\text{H}_5)_4} (5^m \text{C}_2\text{H}_5\text{OH} - 2^m \text{C}_2\text{H}_5\text{OH}) \quad (50)$$

$$X_{h, \text{TMB}}^{///} = \frac{1}{3 \cdot 2^m \text{B}(\text{OCH}_3)_3} (5^m \text{CH}_3\text{OH} - 2^m \text{CH}_3\text{OH}) \quad (51)$$

$$X_{h, \text{TEOS}}^{///} = \frac{1}{2a \cdot 2^m \text{Si}(\text{OC}_2\text{H}_5)_4} (4^m \text{C} + 5^m \text{C} - 2^m \text{C}) \quad (52)$$

Equating Eq. (45a) to Eq. (47) and simplifying gives

$$5^m \text{Si}(\text{OC}_2\text{H}_5)_4 = 2^m \text{Si}(\text{OC}_2\text{H}_5)_4 - 4^m \text{SiO}_2 - 5^m \text{SiO}_2 + 2^m \text{SiO}_2 \quad (53)$$

Equating Eq. (50) to Eq. (52) and simplifying yields

$$5^m C_2H_5OH = \frac{4-a}{2a} (4^m C + 5^m C - 2^m C) + 2^m C_2H_5OH \quad (54)$$

Equating Eq. (46a) to Eq. (4B) and simplifying gives

$$5^m B(OCH_3)_3 = 2^m B(OCH_3)_3 - 2(4^m B_2O_3 + 5^m B_2O_3 + 2^m B_2O_3) \quad (55)$$

Equating Eq. (4B) to Eq. (51) and simplifying yields

$$5^m CH_3OH = 6(4^m B_2O_3 + 5^m B_2O_3 + 2^m B_2O_3) + 2^m CH_3OH \quad (56)$$

Substituting Eqs. (47) and (51) into Eq. (49) gives

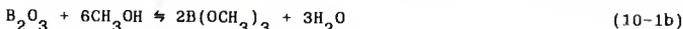
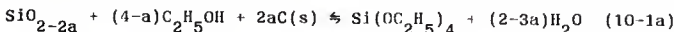
$$5^m H_2O = 2^m H_2O - 4^m H_2O - (2-3a)(4^m SiO_2 + 5^m SiO_2) \\ + (2 - 3a)(2^m SiO_2) - \frac{1}{2}(5^m CH_3OH - 2^m CH_3OH) + z_{H_2O} \quad (57)$$

E. Material Balance Around Dryer For a Rinsed Lyogel

The overall material balance around the dryer for a rinsed lyogel is given by Eq. (2B) of Chapter XI.

$$4^M_{OUT} = 4^Y + 6^M_{OUT} \quad (11-2B)$$

The chemical reactions are taken to be the following.



The component balances are as follows.

$$6^m Si(OC_2H_5)_4 = X_{SiO_2} 4^m SiO_2 - 4^y Si(OC_2H_5)_4 \quad (5B)$$

$$X_{SiO_2} = \frac{1}{4^m SiO_2} [6^m Si(OC_2H_5)_4 + 4^y Si(OC_2H_5)_4] \quad (5Ba)$$

$$6^m B(OCH_3)_3 = 2X_{B_2O_3} 4^m B_2O_3 - 4^y B(OCH_3)_3 \quad (59)$$

$$X_{B_2O_3} = \frac{1}{2 \cdot 4^m B_2O_3} (6^m B(OCH_3)_3 + 4^y B(OCH_3)_3) \quad (59a)$$

$$6^m SiO_2 = 4^m SiO_2 - 4^y SiO_2 - X_{SiO_2} 4^m SiO_2 \quad (60)$$

$$X_{SiO_2} = \frac{1}{4^m SiO_2} (4^m SiO_2 - 4^y SiO_2 - 6^m SiO_2) \quad (60a)$$

$$6^m B_2O_3 = 4^m B_2O_3 - 4^y B_2O_3 - X_{B_2O_3} 4^m B_2O_3 \quad (61)$$

$$X_{B_2O_3} = \frac{1}{4^m B_2O_3} (4^m B_2O_3 - 4^y B_2O_3 - 6^m B_2O_3) \quad (61a)$$

$$6^m H_2O = 4^m H_2O - 4^y H_2O + (2-3a)X_{SiO_2} 4^m SiO_2 + 3X_{B_2O_3} 4^m B_2O_3 \quad (62)$$

$$6^m C_2H_5OH = (4-a) X_{SiO_2} 4^m SiO_2 - 4^y C_2H_5OH \quad (63)$$

$$X_{SiO_2} = \frac{1}{(4-a)4^m SiO_2} (6^m C_2H_5OH + 4^y C_2H_5OH) \quad (63a)$$

$$6^m CH_3OH = 6X_{B_2O_3} 4^m B_2O_3 - 4^y CH_3OH \quad (64)$$

$$X_{B_2O_3} = \frac{1}{6 \cdot 4^m B_2O_3} (6^m CH_3OH + 4^y CH_3OH) \quad (64a)$$

$$6^m C = 4^m C - 4^y C - 2aX_{SiO_2} 4^m SiO_2 \quad (65)$$

$$X_{SiO_2} = \frac{1}{2a \cdot 4^m SiO_2} (4^m C - 4^y C - 6^m C) \quad (65a)$$

Equating Eq. (5Ba) to Eq. (60a) and simplifying gives

$$4^y Si(OC_2H_5)_4 = 4^m SiO_2 - 4^y SiO_2 - 6^m SiO_2 - 6^m Si(OC_2H_5)_4 \quad (66)$$

Equating Eq. (63a) to Eq. (65a) and simplifying yields

$$4^y C_2H_5OH = \frac{4-a}{2a} (4^m C - 4^y C - 6^m C) - 6^m C_2H_5OH \quad (67)$$

Equating Eq. (59a) to Eq. (61a) and simplifying gives

$$4^y B(OCH_3)_3 = 2(4^m B_2O_3 - 4^y B_2O_3 - 6^m B_2O_3) - 6^m B(OCH_3)_3 \quad (68)$$

Equating Eq. (61a) to Eq. (64a) and simplifying yields

$$4^y CH_3OH = 6(4^m B_2O_3 - 4^y B_2O_3 - 6^m B_2O_3) - 6^m CH_3OH \quad (69)$$

Substituting Eqs. (60a) and (64a) into Eq. (62) gives

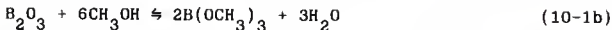
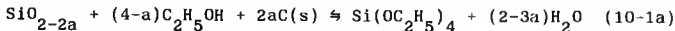
$$4^y H_2O = 4^m H_2O - 6^m H_2O + (2+3a)(4^m SiO_2 - 4^y SiO_2) - (2 + 3a)6^m SiO_2 + \frac{1}{2}(6^m CH_3OH + 4^y CH_3OH) \quad (70)$$

F. Material Balance Around Swelling Solution Tank

The overall material balance around the swelling solution tank is given by Eq. (34) of Chapter XI.

$$4^M_{OUT} + 4^M_{IN} = 7^M_{OUT} + B^M_{OUT} \quad (11-34)$$

The chemical reactions are taken to be the following.



The component balances are as follows. It has been assumed that all $Si(OC_2H_5)_4$, $B(OCH_3)_3$, CH_3OH and C_2H_5OH have been removed from the lyogel by the swelling solution.

$$X'_{SiO_2} = \frac{1}{4^m SiO_2} (8^m Si(OC_2H_5)_4 + 7^m Si(OC_2H_5)_4) \quad (71)$$

$$X'_{B_2O_3} = \frac{1}{2 \cdot 4^m B_2O_3} (B^m B(OCH_3)_3 + 7^m B(OCH_3)_3) \quad (72)$$

$$X'_{\text{SiO}_2} = \frac{1}{4^m \text{SiO}_2} (4^m \text{SiO}_2 - 7^m \text{SiO}_2 - 8^m \text{SiO}_2) \quad (73)$$

$$X'_{\text{B}_2\text{O}_3} = \frac{1}{4^m \text{B}_2\text{O}_3} (4^m \text{B}_2\text{O}_3 - 7^m \text{B}_2\text{O}_3 - 6^m \text{B}_2\text{O}_2) \quad (74)$$

$$8^m \text{H}_2\text{O} = 4^m \text{H}_2\text{O} - 7^m \text{H}_2\text{O} + (2-3a)X'_{\text{SiO}_2} 4^m \text{SiO}_2 + 3X'_{\text{B}_2\text{O}_3} 4^m \text{B}_2\text{O}_3 + {}^w \text{H}_2\text{O} \quad (75)$$

$$X'_{\text{SiO}_2} = \frac{1}{(4-a)4^m \text{SiO}_2} (8^m \text{C}_2\text{H}_5\text{OH} + 7^m \text{C}_2\text{H}_5\text{OH}) \quad (76)$$

$$X'_{\text{B}_2\text{O}_3} = \frac{1}{6^m \text{B}_2\text{O}_3} (8^m \text{CH}_3\text{OH} + 7^m \text{CH}_3\text{OH}) \quad (77)$$

$$X'_{\text{SiO}_2} = \frac{1}{2a 4^m \text{SiO}_2} (4^m \text{C} - 7^m \text{C} - 8^m \text{C}) \quad (78)$$

Equating Eq. (71) to Eq. (73) and simplifying gives

$$7^m \text{Si}(\text{OC}_2\text{H}_5)_4 = 4^m \text{SiO}_2 - 7^m \text{SiO}_2 - 8^m \text{SiO}_2 \quad (79)$$

Equating Eq. (76) to Eq. (78) and simplifying yields

$$7^m \text{C}_2\text{H}_5\text{OH} = \frac{4-a}{2a} (4^m \text{C} - 7^m \text{C} - 8^m \text{C}) \quad (80)$$

Equating Eq. (72) to Eq. (74) and simplifying gives

$$7^m \text{B}(\text{OCH}_3)_3 = 2(4^m \text{B}_2\text{O}_3 - 7^m \text{B}_2\text{O}_3 - 8^m \text{B}_2\text{O}_3) \quad (81)$$

Equating Eq. (74) to Eq. (77) and simplifying yields

$$7^m \text{CH}_3\text{OH} = 6(4^m \text{B}_2\text{O}_3 - 7^m \text{B}_2\text{O}_3 - 8^m \text{B}_2\text{O}_3) \quad (82)$$

Substituting Eqs. (73) and (77) into Eq. (75) gives

$$7^m \text{H}_2\text{O} = 4^m \text{H}_2\text{O} - 8^m \text{H}_2\text{O} + (2+3a)(4^m \text{SiO}_2 - 7^m \text{SiO}_2) - (2+3a)(8^m \text{SiO}_2) \\ + \frac{1}{2} 7^m \text{CH}_3\text{OH} + w \text{H}_2\text{O} \quad (83)$$

$$7^m \text{Na}^+ = z \text{Na}^+ - 8^m \text{Na}^+ \quad (84)$$

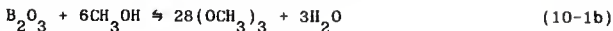
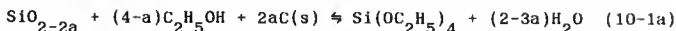
$$7^m \text{Cl}^- = z \text{Cl}^- - 8^m \text{Cl}^- \quad (85)$$

G. Material Balance Around Dryer For a Swelled Lyogel

The overall material balance around the dryer for a swelled lyogel is given by Eq. (42) of Chapter XI.

$$8^M \text{OUT} = 5^Y + 9^M \text{OUT} \quad (11-42)$$

The chemical reactions are taken to be the following.



The component balances are as follows.

$$X_{\text{SiO}_2}^{//} = \frac{1}{8^m \text{SiO}_2} (9^m \text{Si}(\text{OC}_2\text{H}_5)_4 + 5^y \text{Si}(\text{OC}_2\text{H}_5)_4) \quad (86)$$

$$X_{\text{B}_2\text{O}_3}^{//} = \frac{1}{2 \cdot 8^m \text{B}_2\text{O}_3} (9^m \text{B}(\text{OCH}_3)_3 + 5^y \text{B}(\text{OCH}_3)_3) \quad (87)$$

$$X_{\text{SiO}_2}^{//} = \frac{1}{8^m \text{SiO}_2} (8^m \text{SiO}_2 - 5^y \text{SiO}_2 - 9^m \text{SiO}_2) \quad (88)$$

$$X_{\text{B}_2\text{O}_3}^{//} = \frac{1}{8^m \text{B}_2\text{O}_3} (8^m \text{B}_2\text{O}_3 - 5^y \text{B}_2\text{O}_3 - 9^m \text{B}_2\text{O}_3) \quad (89)$$

$$9^m \text{H}_2\text{O} = 8^m \text{H}_2\text{O} - 5^y \text{H}_2\text{O} + (2-3a) X_{\text{SiO}_2}^{//} 8^m \text{SiO}_2 + 3 X_{\text{B}_2\text{O}_3}^{//} 8^m \text{B}_2\text{O}_3 \quad (90)$$

$$X_{\text{SiO}_2}^{//} = \frac{1}{(4-a)8^m \text{SiO}_2} (9^m \text{C}_2\text{H}_5\text{OH} + 5^y \text{C}_2\text{H}_5\text{OH}) \quad (91)$$

$$X_{8_2\text{O}_3}^{//} = \frac{1}{68^m \text{B}_2\text{O}_3} (9^m \text{CH}_3\text{OH} + 5^y \text{CH}_3\text{OH}) \quad (92)$$

$$X_{\text{SiO}_2}^{//} = \frac{1}{2a8^m \text{SiO}_2} (8^m \text{C} - 5^y \text{C} - 9^m \text{C}) \quad (93)$$

Equating Eq. (86) to Eq. (88) and simplifying gives

$$5^y \text{Si}(\text{OC}_2\text{H}_5)_4 = 8^m \text{SiO}_2 - 5^y \text{SiO}_2 - 9^m \text{SiO}_2 - 9^m \text{Si}(\text{OC}_2\text{H}_5)_4 \quad (94)$$

Equating Eq. (91) to Eq. (93) and simplifying yields

$$5^y \text{C}_2\text{H}_5\text{OH} = \frac{4-a}{2a} (8^m \text{C} - 5^y \text{C} - 9^m \text{C}) - 9^m \text{C}_2\text{H}_5\text{OH} \quad (95)$$

Equating Eq. (87) to Eq. (89) and simplifying gives

$$5^y 8(\text{OCH}_3)_3 = 2(8^m 8_2\text{O}_3 - 5^y 8_2\text{O}_3 - 9^m 8_2\text{O}_2) - 9^m 8(\text{OCH}_3)_3 \quad (96)$$

Equating Eq. (89) to Eq. (92) and simplifying yields

$$5^y \text{CH}_3\text{OH} = 6(8^m 8_2\text{O}_3 - 5^y 8_2\text{O}_3 - 9^m 8_2\text{O}_3) - 9^m \text{CH}_3\text{OH} \quad (97)$$

Substituting Eqs. (88) and (92) into Eq. (90) gives

$$\begin{aligned} 5^y \text{H}_2\text{O} &= 8^m \text{H}_2\text{O} - 9^m \text{H}_2\text{O} + (2-3a)(8^m \text{SiO}_2 - 5^y \text{SiO}_2 - 9^m \text{SiO}_2) \\ &\quad + \frac{1}{2}(9^m \text{CH}_3\text{OH} + 5^y \text{CH}_3\text{OH}) \end{aligned} \quad (98)$$

$$9^m \text{Na}^+ = 8^m \text{Na}^+ \quad (99)$$

$$9^m \text{Cl}^- = 8^m \text{Cl}^- \quad (100)$$

It has been assumed the Na^+ and Cl^- does not vaporize at 110°C .

REFERENCES

- [1] Paulson, B.A. Use of Sol-Gels In The Application of Ceramic Oxide Thin Films. Ph.D. dissertation, Iowa State University 1987, Ann Arbor: University Microfilms International, 1988.
- [2] Lackey, W.J., et al. Ceramic Coatings For Heat Engine Materials--Status and Future Needs. Oak Ridge National Laboratory, Oak Ridge, 1984.
- [3] Wymer, R.G. and J.H. Coobs. "Preparation, Coating Evaluation, and Irradiation Testing of Sol-Gel Oxide Microspheres," Proceedings of the British Ceramic Society, 7: 61-79 (1967).
- [4] Cairns, J.A., et al. "The Role of Gel Processing of Catalyst Supports" in Better Ceramics Through Chemistry, edited by C.J. Brinker, et al., New York: Elsevier Science Publishing Co., Inc., 135-138 (1984).
- [5] Komarneni, S. and R. Roy. "Titania Gels Spheres By A New Sol-Gel Process," Materials Letters, 3 (4): 165-167 (1985).
- [6] Ashley, C.S. and S.J. Reed. "Sol-Gel AR Films For Solar Applications," Material Research Society Symposium Proceedings, 73: 671-677 (1986).
- [7] Brinker, C.J., et al. "Structure of Sol-Gel Derived Inorganic Polymers: Silicates and Borates" in Inorganic and Organometallic Polymers, ACS Symposium Series, Vol. 360, edited by M. Zeldin, et al., Washington, D.C.: American Chemical Society, 314-332 (1988).
- [8] Angell, B.L. The Control of Swelling and Syneresis In Sorosilicate Gels Using Colloidal Phenomena. M.S. Thesis, Kansas State University, 1986, unpublished.
- [9] Yamane, M. and T. Kojima, J. Non-Cryst. Solids, 44, 181-190 (1981).
- [10] Uhlmann, D.R., et al. in Science of Ceramic Chemical Processing, edited by D.R. Ulrich, et al., New York: Wiley-Interscience, 173-183 (1986).
- [11] Brinker, C.J., et al. Thin Solid Films, 77: 141-148 (1981).
- [12] Brinker, C.J., et al. in Better Ceramics Through Chemistry, edited by C.J. Brinker, et al., New York: Elsevier Science Publishing Co., Inc., 179-184 (1984).

- [13] Zeilinski, B.J.J. and D.R. Uhlmann. "Gel Technology in Ceramics," Journal of Physical Chemistry and Solids, **45**: 1069-1090 (1984).
- [14] Brinker, C.J., et al. J. Non-Cryst. Solids, **63**, 45-59 (1984).
- [15] Keefer, K.D. in Better Ceramics Through Chemistry, edited by C.J. Brinker, et al., New York: Elsevier Science Publishing Co., Inc., 15-24 (1984).
- [16] Tanaka, T. "Gels," Scientific American, **244**: 124-138 (1981).
- [17] Zarzycki, J., et al. J. Mat. Sci., **17**: 3371-79 (1982).
- [18] Mackenzie, J.D. "Applications of Sol-Gel Methods for Glass and Ceramics Processing" in Ultrastructure Processing of Ceramic, Glass and Composites, Larry L. Hench and Donald R. Ulrich, Eds., New York: John Wiley and Sons, 1984.
- [19] Nogami, M. and K. Moriya. J. Non-Cryst. Solids, **48**, 359 (1982).
- [20] Yoldas, B.E. J. Mater. Sci., **14**. 1843 (1979).
- [21] National Bureau of Standards Certificate Standard Reference Material 4275, Mixed-Radionuclide Point-Source Standard for the Efficiency Calibration of Germanium-Spectrometer Systems.
- [22] Nargolwalla, S.S. and E.P. Przybylowicz. Activation Analysis With Neutron Generators. New York: John Wiley and Sons, 1973.
- [23] "TRIGA Mark II Nuclear Reactor Facility--Kansas State University," Kansas State University Department of Nuclear Engineering, unpublished pamphlet.
- [24] Higginbotham, J.F. Instrumental Neutron Activation Analysis of Coal and Coal Fly Ash. M.S. Thesis, Kansas State University, 1983, unpublished.
- [25] "Canberra Series 8180 Multichannel Analyzer," Kansas State University Department of Nuclear Engineering, unpublished handout.
- [26] "Canberra Series 8641 Multichannel Analyzer," Kansas State University Department of Nuclear Engineering, unpublished handout.

- [27] "Neutron Activation Analysis at Kansas State University," Kansas State University Department of Nuclear Engineering, unpublished handout.
- [28] Higginbotham, J.F., Kansas State University TRIGA Mark II Chief Nuclear Reactor Operator and Ph.D. in nuclear engineering, personal communication.
- [29] Tomberlin, T.A. A Cadmium Filter Technique In Variable-Energy Neutron Activation Analysis, M.S. Thesis, Kansas State University, 1974, unpublished.
- [30] Koch, R.C. Activation Analysis Handbook. New York: Academic Press, Inc. 1960.
- [31] S. Angell, M. Reichwein and J. Schlup. "Control of Gel Densities Using Colloidal Phenomena," presented at the AIChE Conference on Emerging Technologies in Materials, Minneapolis, Minnesota, August, 1987.
- [32] Higginbotham, J.F. Kansas State University TRIGA Mark II Chief Nuclear Reactor Operator and Ph.D. in nuclear engineering, MASCAL BASIC program.
- [33] Stoughton, R.W. and J. Halperin. "Effective Cutoff Energies for boron, Cadmium, Gadolinium, and Samarium Filters," Nucl. Sci. Eng., 15 (1963).
- [34] Stoughton, R.W., et al. "Effective Cadmium Cutoff Energies," Nucl. Sci. Eng., 6 (1959).
- [35] Hickman, C.H. and W.B. Leng. "The Calculation of Effective Cutoff Energies in Cadmium, Samarium, and Gadolinium," Nucl. Sci. Eng., 12 (1962).
- [36] Partlow, D.P. and B.E. Yoldas. J. Non-Cryst. Solids, 46 (1981) 153.
- [37] Yoldas, B.E. J. Mater. Sci. 12 (1977) 103.
- [38] Yoldas, B.E. J. Mater. Sci., 14 (1979) 1843.
- [39] Mazhdyasni, K.S., et al. J. Am. Ceram. Soc., 50 (1967) 537.
- [40] Yoldas, B.E. "Monolithic Glass Formation by Chemical Polymerization," Journal of Materials Science, 14: 1843-1849 (1979).
- [41] "Proceedings of the International Workshop on Glasses and Glass Ceramics from Gels, Oct. 8-9, 1981," J. Non-Cryst. Solids, 48: 1-230 (1982).

- [42] "Proceedings of the Second International Workshop on Glasses and Glass Ceramics from Gels, July 1-2, 1983," J. Non-Cryst. Solids, **63**: 1-300 (1984).
- [43] "Proceedings of the Third International Workshop on Glasses and Glass Ceramics from Gels, Sept. 12-14, 1985," J. Non-Cryst. Solids, **82**: 1-436 (1986).
- [44] Ultrastructure Processing of Ceramics, Glasses and Composites, L.L. Hench and D.R. Ulrich, Eds., New York: John Wiley and Sons, 1984.
- [45] Science of Ceramic Chemical Processing, L.L. Hench and D.R. Ulrich, Eds., New York: Wiley-Interscience, 1986.
- [46] Better Ceramics Through Chemistry, C.J. Brinker, D.E. Clark, and D.R. Ulrich, Eds., New York: Elsevier Science Publishing Co., Inc., 1984.
- [47] Better Ceramics Through Chemistry II, C.J. Brinker, D.E. Clark, and D.R. Ulrich, Eds., Pittsburgh: Mat. Res. Soc., 1986.
- [48] Proceedings of the Third International Conference on Ultrastructure Processing of Glasses, Ceramics and Composites, Feb. 24-27, 1987, to be published.
- [49] "Proceedings of the Fourth International Workshop on Glasses and Glass Ceramics from Gels, July 13-15, 1987," J. Non-Cryst. Solids, **100**: 1-553 (1988).
- [50] Nogami, M. and Y. Moriya. J. Non-Cryst. Solids, **48** (1982) 359.
- [51] Sakka, S. and K. Kamiya. "Glasses From Metal Alcholates," J. Non-Cryst. Solids, **42**: 403-422 (1980).
- [52] Yoldas, B.E. "Effect of Variations in Polymerized Oxides on Sintering and Crystalline Transformations," J. Am. Ceramic Soc., **65** (8): 387-93 (1982).
- [53] Kumar, B. "Sol-Gel Processing of $\text{SiO}_2\text{-B}_2\text{O}_3$ Glasses," Mater. Res. Bull., **19**: 331-338 (1984).
- [54] Nogami, M. and Y. Moriya. "Glass Formation of the $\text{SiO}_2\text{-B}_2\text{O}_3$ System by the Gel Process from Metal Alkoxides," J. Non-Cryst. Solids, **48**: 359-366 (1982).

- [55] Fabes, S.D., et al. "Stronger Glass Via Sol-Gel Coatings" in Science of Ceramic Chemical Processing, edited by L.L. Hench and D.R. Ulrich, New York: Wiley-Interscience, 1986.
- [56] Comprehensive Inorganic Chemistry, A.F. Trotman-Dickenson, Vol. 1, Eds., New York: Pergamon Press Ltd., 1973.
- [57] Gerrard, W. The Organic Chemistry of Boron. New York: Academic Press, 1961.
- [58] Brinker, C.J., et al. "Polymer Growth and Gelation in Borate-Based Systems" in Better Ceramics Through Chemistry II, C.J. Brinker D.E. Clark, and D.R. Ulrich, Eds., Pittsburgh: Mater. Res. Soc., 1986.
- [59] Bray, P.J. and J.G. O'Keefe. Phys. Chem. Glasses, 4 (1963) 37.
- [60] Jellyman, P.E. and J.P. Proctor. Trans., Soc. Glass Tech., 39 (1955) 11T.
- [61] Wong, J. and C.A. Angell. Appl. Spectrosc. Rev., 4 (2), (1971) 155.
- [62] Ray, N.H. Inorganic Polymers. New York: Academic Press, 1978.
- [63] Krough-Moe, J., Phys. Chem. Glasses, 6 (1965) 46.
- [64] Yamane, M., et al., J. Mater. Sci., 13: 865-B70 (197B).
- [65] Scherer, G.W. "Aging and Drying of Gels" in Proceedings of the Fourth International Workshop on Glasses and Glass Ceramics from Gels, J. Non-Cryst. Solids, 100: 77-92 (198B).
- [66] Simons, Gale G., Professor of Nuclear Engineering, Department of Nuclear Engineering, Kansas State University, personal communication.
- [67] Copeland, J.L. "Experimental Errors and Their Treatment," Department of Chemistry, Kansas State University, unpublished handout.
- [6B] Reichwein, M. A. and J. R. Schlup. "Effects of Processing on Borosilicate Gel Compositions," Proceedings of the Southwestern and Rocky Mountain Division of the American Association for the Advancement of Science, 64th Annual Meeting, edited by M. M. Balcomb, Vol. 5, Part 1: 34 (1988).

- [69] Angell, B. L., M. A. Reichwein, and J. R. Schlup. "Control of Borosilicate Lyogel Densities Using Colloidal Phenomena." Submitted to J. Non-Cryst. Solids for publication.
- [70] Brinker, C. J. and G. W. Scherer. "Relationships Between the Sol-to-Gel and Gel-to-Glass Conversions" in Ultrastructure Processing of Ceramics, Glasses, and Composites, Larry L. Hench and Donald R. Ulrich, Eds., New York: John Wiley and Sons, 1984.
- [71] CRC Handbook of Chemistry and Physics, 66th ed. Robert C. Weast, Editor-in-Chief, Boca Raton, Florida: CRC Press, Inc., 1985.
- [72] Purcell, K. F. and J. C. Kotz. Inorganic Chemistry. Philadelphia: W. B. Saunders Co., 1977.
- [73] Cotton, F. A. and G. Wilkinson. Advanced Inorganic Chemistry, 4th ed. New York: John-Wiley and Sons, 1980.

EFFECTS OF PROCESSING ON THE
COMPOSITION OF BOROSILICATE GELS

by

Michael Anthony Reichwein

A.S., Thames Valley State Technical College, 1979
B.S., University of Connecticut, 1981

AN ABSTRACT OF A MASTER'S THESIS

submitted in partial fulfillment of the
requirements for the degree

MASTER OF SCIENCE

College of Engineering
Department of Chemical Engineering

KANSAS STATE UNVIERSITY
Manhattan, Kansas

1989

Abstract

An Instrumental Neutron Activation Analysis (INAA) technique was developed to determine the composition of borosilicate lyogels and the composition of borosilicate lyogels swelled in NaCl solution. The composition of residue formed around the tops of sealed sample vials during gelation was determined by INAA and found to be 99 percent boron containing species. INAA results showed that final lyogel compositions have significantly less boron than the as-batched lyogel composition. B/Si cation ratios were determined for several stages. After gelation and drying they ranged from 0.0 to 0.54, after rinsing and drying (0.0 to 0.92), and after rinsing, swelling and drying (0.0 to 0.37). All these are much smaller than the as-batched B/Si cation ratio.

The chemistry associated with synthesis and swelling of borosilicate lyogels is discussed as well as the chemistry associated with co-precipitation and lyogel formation. A lyogel was formed above a co-precipitate, and these were analyzed by INAA. The lyogel was found to be SiO_2 and the precipitate was found to be $\text{SiO}_2 \cdot 3.2\text{B}_2\text{O}_3$.

Material balances for the entire synthetic process have been derived. Experiments, including suggested analytical techniques, to obtain a closed material balance are proposed.

Abstract

An Instrumental Neutron Activation Analysis (INAA) technique was developed to determine the composition of borosilicate lyogels and the composition of borosilicate lyogels swelled in NaCl solution. The composition of residue formed around the tops of sealed sample vials during gelation was determined by INAA and found to be 99 percent boron containing species. INAA results showed that final lyogel compositions have significantly less boron than the as-batched lyogel composition. B/Si cation ratios were determined for several stages. After gelation and drying they ranged from 0.0 to 0.54, after rinsing and drying (0.0 to 0.92), and after rinsing, swelling and drying (0.0 to 0.37). All these are much smaller than the as-batched B/Si cation ratio.

The chemistry associated with synthesis and swelling of borosilicate lyogels is discussed as well as the chemistry associated with co-precipitation and lyogel formation. A lyogel was formed above a co-precipitate, and these were analyzed by INAA. The lyogel was found to be SiO_2 and the precipitate was found to be $\text{SiO}_2 \cdot 3.2\text{B}_2\text{O}_3$.

Material balances for the entire synthetic process have been derived. Experiments, including suggested analytical techniques, to obtain a closed material balance are proposed.